SAPIENZA UNIVERSITÀ DI ROMA

DOCTORAL THESIS

METAMODEL BASED DESIGN OPTIMIZATION IN INDUSTRIAL TURBOMACHINERY

Author:
Tommaso BONANNI

Supervisor:
Prof. Alessandro CORSINI

*A thesis submitted in fulfilment of the requirements
for the degree of Doctor of Philosophy*

in

Energy and Environment

February 1, 2018

SAPIENZA UNIVERSITÀ DI ROMA

Abstract

Faculty Name
Department of Astronautical, Electrical and Energy Engineering, XXX Cycle

Doctor of Philosophy

**METAMODEL BASED DESIGN OPTIMIZATION IN INDUSTRIAL
TURBOMACHINERY**

by Tommaso BONANNI

Fans and Blowers community is experiencing, during those years, an incredible push in rethinking design approaches and strategies. The change in regulations on minimum efficiency grades and market requirements on even more customized products demand a changing in the way design in fan technology is perceived. In this context, even if synthetic approaches for fan design and analysis are still valuable tools, they need to be flanked by metamodels in order to overcome the limitations and criticism introduced by empirical relationships developed in the past for specific applications. In addition, by replacing computation-intensive functions with approximate surrogate models, it is possible to adopt advanced and nested optimization methods, such as those based on Evolutionary Algorithms, drastically improving the overall optimization computational time. Surrogate-based Optimizations based on Evolutionary Algorithm should become common practice in design optimization because of their capability of find optima in the design space, thanks to their intrinsic balance between exploitation and exploration.

This work proposes methods for interweave elements of metamodeling techniques and multi-objective optimization problems with the synthetic approaches classically developed by the turbomachinery community. The entire Thesis can be ideally divided into two parts; the first gives a brief survey on the classical fan design and analysis approaches and reports two synthetic in-house codes for axial fan performance prediction. The second part present the state-of-the-art in metamodeling and optimization techniques, underlining the role of metamodeling in supporting design optimization and focusing in the more reliable and accurate framework for multi-objective optimization in fans engineering design.

Publications

- G. Angelini, T. Bonanni, A. Corsini, G. Delibra, L. Tieghi, and D. Volponi, "A preliminary investigation on surrogate-based optimization of truly reversible profile family for axial fans", *Currently under review on: Journal of Power and Energy*,

- G. Angelini, T. Bonanni, A. Corsini, G. Delibra, L. Tieghi, and D. Volponi, "A metamodel for deviation in 2d cascade with variable stagger, solidity and reversible profiles", in *ASME Turbo Expo 2018: Turbomachinery Technical Conference and Exposition*, American Society of Mechanical Engineers, 2018

- G. Angelini, T. Bonanni, A. Corsini, G. Delibra, L. Tieghi, and D. Volponi, "Effects of fan inflow distortion on heat exchange in air-cooled condenser. unsteady computations with synthetic blade mode", in *ASME Turbo Expo 2018: Turbomachinery Technical Conference and Exposition*, American Society of Mechanical Engineers, 2018

- T. Bonanni, A. Corsini, G. Delibra, D. Volponi, A. G. Sheard, and M. Bublitz, "Design of a single stage variable pitch axial fan", in *ASME Turbo Expo 2017: Turbomachinery Technical Conference and Exposition*, American Society of Mechanical Engineers, 2017, V001T09A011–V001T09A011

- G. Angelini, T. Bonanni, A. Corsini, G. Delibra, L. Tieghi, and D. Volponi, "Optimization of an axial fan for air cooled condensers", *Energy Procedia*, vol. 126, no. Supplement C, pp. 754 –761, 2017, ATI 2017 - 72nd Conference of the Italian Thermal Machines Engineering Association, ISSN: 1876-6102

- T. Bonanni, A. Corsini, G. Delibra, D. Volponi, and A. G. Sheard, "Modelling of axial fan and anti-stall ring on a virtual test rig for air performance evaluation", in *ASME Turbo Expo 2016: Turbomachinery Technical Conference and Exposition*, American Society of Mechanical Engineers, 2016, V001T09A005–V001T09A005

- T. Bonanni, L. Cardillo, A. Corsini, G. Delibra, A. G. Sheard, and D. Volponi, "Derivative design of axial fan range: From academia to industry", V006T07A006–V006T07A006, 2016

Contents

List of Abbreviations

AD	Actuator Disk
Adj R^2	Adjusted coefficient of determination
AEC	Adaptive Evolution Control
AxLab	Axial Laboratory
AMCA	Air Movement and Control Association
ANN	Artificial Neural Network
ANOVA	ANalysis Of VAriance
CCD	Central Composite Design
CFD	Computer Fluid Dynamics
DF	Diffusion Factor, Degree of Freedom
DFR	Direct Fitness Replacement
DOE	Design Of Experiments
EA	Evolutionary Algorithm
ErP	Energy related Product
ESS	Explained Sum of Square
FEA	Finite Element Analysis
FEC	Fixed Evolution Control
FNN	Feedforward Neural Network
FMEG	Fan and Motor Efficiency Grades
GA	Genetic Algorithm
i4.0	Industry 4.0
IFR	Indirect Fitness Replacement
ISO	International Organization for Standards
LFSS	Lack-of-Fit Sum of Square
LSM	Last Square Method
MLP	Multi-Layer Perceptron
MOEA	Multi-Objective Evolutionary Algorithm
MOOP	Multi-Objective Optimization Problem
MS	Mean Square
NEC	No Evolution Control
NSGA	Non-dominated Sorting Genetic Algorithm
Part R^2	Partial coefficient of determination
PESS	Pure Error Sum of Square
Pred R^2	Predicted coefficient of determination
RANS	Reynolds Averaged Navier Stokes
RE	Residual Error
RSM	Response Surface Methodology
SDS	Search-Driven Sampling
SM	Surrogate Model
SS	Sum of Square
SSR	Sum of Squared Residual
SV	Source of Variation
TSS	Total Sum of Square

List of Symbols

Latin

AoA	Blade angle of attack	deg
c	Absolute velocity component	m/s
C_D	Drag coefficient	$-$
C_L	Lift coefficient	$-$
D	Drag force, fan diameter	N,m
F	Force, F-test	N
f	Source term	N
H_0	Null hypothesis	
H_1	Alternative hypothesis	
i	Incidence angle	deg
k	Number of regressors	$-$
L	Lift force	N
l	Chord length	m
L_e	Specific work	m^2/s^2
m	Incidence coefficient or number of unique tests	$-$
n	Number of tests	$-$
p	Static pressure, p-value	$Pa, -$
p_o	Total pressure	Pa
Q	Volumetric flow rate	m^3/s
r	Fan radius	m
R^2	Coefficient of determination	$-$
Re	Reynolds number	$-$
t	Blade spacing	m
U	Reference frame velocity	m/s
w	Relative velocity component	m/s
X	Force, projection on x axis	N
x,y,z	Coordinates of reference system	$-$
Y	Force, projection on y axis	N
z	Blade count	

Symbols

α	Absolute flow angle	deg
β	Relative flow angle	deg
ρ	Flow density	kg/m^3
θ	Camber	deg
σ	Solidity	$-$
δ	Deviation	deg
ξ	Blade pitch angle	deg
ε	Deflection	m^2/s^3
Φ	Global flow coefficient	$-$
Ψ	Global load coefficient	$-$
ϕ	Local flow coefficient	$-$

ψ	Local load coefficient	$-$
Γ	Circulation	m^2/s
γ	Blade stagger angle	deg
ω	Angular velocity	$1/s$
ω_s	Specific speed	$-$
χ	Hub to shroud ratio	$-$

Subscripts and Superscripts

1	Upstream rotor section
2	Downstream rotor section
3	Downstream stator section
d	Design value
$full$	Full Model
m	Meridional direction or average vector
o	Static (total)
θ	Tangential component
r	Radial direction
red	Reduced Model
s	Shroud
x	Axial component
$\bar{}$	Mean value
$\hat{}$	Estimated value
$\tilde{}$	Approximated value

Dedicated to Alessandro, David, Giovanni, Gino and Lorenzo

Introduction

In the last years, fans and blowers community, like many others, is probably witnessing the most important push in rethinking all manufacture activities since the last decades. This is mainly caused by two factors: first is what scholars are identifying like the fourth industrial revolution and second is the change in regulation that established minimum efficiency grade for Energy related Products (ErP).

With "Fourth Industrial Revolution" scholar refers to current trend of strong customization of products, automation and data exchange in manufacturing technologies. Some of them identify this reality whit the term "Industry4.0" (*i4.0*). Even if it is hard to find a univocal and exhaustive definition of such a multidisciplinary and horizontal phenomenon, it is by now evident that the *i4.0* is pushing the engineers towards a new approach to the industrial activity. Main players that will definitively drag this perspective into reality will be:

1. Machine learning, metamodeling and virtual prototyping, for faster design and prototyping

2. Multi-objective optimization techniques, for both extensive and intensive exploration of the entire design space

3. Big Data, open data, Internet of Things (IoT), for centralization and storage of information

4. Augmented Reality and 3D printing to reduce cost of research and development of new products

From the other side on 1 January 2013, EU Commission Regulation No. 327/2011 came into effect within the European Union, mandating minimum Fan and Motor Efficiency Grades (FMEG's). For applicable fans the 2013 minimum FMEG's have resulted in approximately 33 % of those fans sold before 1 January 2013 now being illegal within Europe. On 1 January 2015, the Regulation 327 minimum FMEG's was increased again. In the USA, on February 2013, the federal government published a framework document in the Federal Register, outlining the approach to fan efficiency regulation within the USA. The framework reflected a desire to be consistent with many elements of the European approach in Regulation 327. With both Europe and the USA now regulating or declaring intent to do so, it is likely that Asian countries will introduce regulations setting minimum fan or fan and motor efficiencies. Currently, Malaysia, Korea, and Taiwan have considered adopting fan efficiency requirements based on the Air Movement and Control Association (AMCA) Standard 205 Energy Efficiency Classification for Fans, as a mandatory requirement for government and private-sector projects. Further, within the European Union minimum FMEG's most likely will continue to increase, and the same regulation pattern followed by a stepped increase in minimum fan or fan and motor efficiency will play out in both the USA and Asia.

In this moment *i4.0* represents the only way to withstand this reform in regulation that is radically changing the fans and blower community. In fact, for fan industry, some of *i4.0* players, like meta-model based optimization, big data analytic and 3D printing are, effectively, mature tools that can practically increase productivity, quality and flexibility

within the manufacturing industry. Paradigm of *i4.0* will, in practice, create an environment that is strictly connected to the market and customer requirements. This objective can be thus achieved changing the way design in fan technology is perceived and switch from a "derivative" design of components, using old parts saving on costs related to development of new products, to a more peculiar custom design of fan components. This means switch from an optimization mainly focused on manufacturability and time to market, to optimization of products that includes performance at reasonable costs. If from one side, in this scenario, exploiting potentiality of *i4.0* plays a fundamental role in improving products quality in fans manufacturers, from the other, switching from the old design concept to another has its cost, that, in this case, can be relevant. This because accessing the potentiality of *i4.0* means learning a typically different knowledge from the turbomachinery background, that includes statistics, mathematics, computer science and various engineering disciplines.

Together, the new-born *i4.0* and the quick change in regulations, are giving birth to a new specialized figure for fan design and optimization. Acquisition of this kind of figure or knowledge from companies will be crucial in respect to the possibility to keep a strong position on the market or, in absence of other perspectives, give the way to different realities.

During the past few years, the axial fans community dedicated great attention to the role that *i4.0* can have in the optimization of a design process or product performances. In fact, nowadays, the design procedure relies on optimization techniques through the use of massive simulation processes; computation-intensive design problems are becoming increasingly common in manufacturing industries and can still represent an excessive computational burden for a rapid and reliable design process. To address such a challenge, approximation or metamodeling techniques are often used providing an accurate solution with a comparable degree of accuracy. Metamodeling techniques, that have been developed from many different disciplines including statistics, mathematics, computer science, and various engineering disciplines, have been found to be a valuable tool to support a wide scope of activities in modern engineering design, especially design optimization.

Objective of the present thesis

The main objective of this work is the implementation of elements of classical fan rotor blade design and performance analysis into the new design frameworks inspired by elements of the *i4.0*. In fact, very little effort in the last years was devoted to interweaving metamodels and optimization techniques with old design or performances analysis procedures. It is, then, of fundamental importance to analyse how those players are acting, separately and together, to change the paradigm of fans and blowers industrial reality.

A classic fan rotor design approach is a process composed by several steps which refer to different disciplines. In fact, a classic design involves elements from aerospace design and from classical turbomachinery for what concerns the blade design and performance analysis, elements of modern Computational Fluid Dynamics (CFD) for what concerns detailed flow analysis (losses, unsteady behaviour, noise etc.) and elements from manufacture and experiments for what concerns the laboratory tests. Usually, some phase requires iterations to match the design specifications. Each of these steps has its criticism and limitations, making the entire design a challenging and multidisciplinary task.

The *i4.0* is altering this complicated but straightforward classic approach, changing the global structure of the design and providing modern tools for each local design step. In other terms, if from one side, elements of computer science and operation research, such as Multi-Objective Optimization Problem or Heuristic Algorithms, are making the entire

design a far apart more complicated iterative process, on the other, it is *i4.0* itself that is providing the instruments and tools to alleviate this burden. In particular, metamodeling, optimization theories and 3D printing can facilitate the design process and alleviate the computational and manufacturing costs.

Concerning the metamodels, replace computation-intensive functions with approximated models will facilitate the use of advanced and nested optimization methods, such as those based on Evolutionary Algorithms. Furthermore, metamodels can have a significant impact in the design. In fact, the simplified design and analysis techniques that have been developed in the past, often relies on cumulative experience as a result of engineers designing fans for a specific application over decades; the empirical rules and correlations, which have been the cornerstone of both design and analysis, have proven their limitations and difficult applicability to several target design conditions. The development of metamodels based on the massive use of simulation processes can deeply improve the reliability of classical design and analysis tools, making them valuable instruments.

The optimization techniques and Surrogate-based optimization have proven to be effective and reliable tool to quickly find local and global optima; for all these reasons, a great attention should be put on the implementation of design and analysis classical tools in this new design framework.

This is the background in which this thesis take place, sum of more than 3 years collaboration with the turbomachinery group in Sapienza University of Rome.

The present document is divided into three main chapters and one appendix. The first provides a brief review of the classical design approach historically adopted by fan designers, the physics and the correlations that govern the process, their limitation and potentiality. The chapter also provide a quick description of two software for the performance analysis of axial fans that have been developed during the last years by the research group.

Second chapter describes the entire process of metamodeling; the sampling problem, the model creation and, then, the model validation. The focus of this chapter is on the metamodels and on the statistics for model validation that have been extensively used in the papers in appendix.

The third chapter focus on the optimization problem and, in particular, on the multi-objective optimization. After a brief survey of the optimization algorithm that can be used in multi-objective optimization problems, the focus is put on the genetics algorithms and on the surrogate-based optimization. Particular emphasis is put on the surrogate-based optimization which adopts evolutionary algorithm, having been successfully applied to an important variety of difficult problems. The different approaches that a designer can adopt are extensively described, putting great attention on their limitations and advantages.

The appendix reproduce some of the papers published during the three years of the doctoral project. These papers are based on the work contained in the chapters of this thesis and represent a progression of methods that can be adopted in optimization design. Paper 1 and paper 2 are based on the codes developed in the framework presented in Chapter 2. Paper 3 is a study of the potentiality of Surrogate Models implementation in classical performance analysis tools and is, clearly, an application of the concepts presented in Chapter 3 to the tools presented in Chapter 2. Paper 4 focus on a surrogate-based multi-objective design optimization of truly reversible profile family for axial fans, based on evolutionary algorithms; this work is based on Chapter 2 and Chapter 3 and study the impact of different optimization frameworks on the optimization problem.

All the developed and implemented codes, the blade designer, AxLab, the codes for metamodeling and for the optimization are written in Python language, at exception of the actuator disk which is implemented in OpenFOAM finite volume solver written in C++.

Chapter 1

Classical approach for design and analysis of axial fans

Any intelligent fool can make things bigger, more complex, and more violent.
It takes a touch of genius — and a lot of courage to move in the opposite direction.

Ernst F. Schumacher

1.1   Introduction

Industrial fan designers, working within individual fan companies, have classically adopted and empirically developed elements of aerospace design processes. The resulting methods reflect the cumulative empirical experience of engineers designing fans for a specific application over decades. The resulting design processes represent a form of local optimum, facilitating the design of industrial fans for a specific application. However, the engineers using nowadays those design processes, were not involved in their original development. They know these processes work, but they do not know why. Decades of tacit knowledge are embedded in the empirical design process and to simply set that aside in favour of new computational design methods would result in that tacit knowledge being lost. It is in this framework that this chapter fits, trying to apply well-known design processes and correlations from the aerospace design know-how to the axial fan design scenario, in the more clear and consistent manner as possible.

The aim of this chapter is to present the classical design approaches historically adopted by fan designers, the physic and the correlations that govern the process, their limitations and potentiality. A classical design approach can be schematized (see Figure 1.1) in four main steps: (i) the Design Space definition, (ii) the Stage Design, (iii) the CFD verification and finally the Test. In particular, this chapter focus on the second step, the Stage Design loop, giving a brief survey on the more common design relationships reported in literature and presenting a quasi-3D blade design approach based on hybrid approach developed by the turbomachinery group at Sapienza. Furthermore, two in-house numerical tools for the direct analysis are presented.

The Design Space is defined by the required duty point, in terms of the volume flow rate and the energy transfer (Q, gH), together with the geometric and cinematic constraints imposed by the application; in so doing, the dimensionless global duty parameters (the flow coefficient and the work coefficient) and the well-known dimensionless specific speed and specific diameter, given by [8] and [9] are defined. Taken together, these parameters and constraints facilitate definition of the fan Design Space, Table 1.1 and identify the design point on a Balje Chart, Figure 1.2.

The flow within any single blade row may vary considerably from hub to casing, thus it may seem optimistic to expect global dimensionless group to be able to deal with this complex internal flow. The flow can be modeled at meridional stream surfaces and the
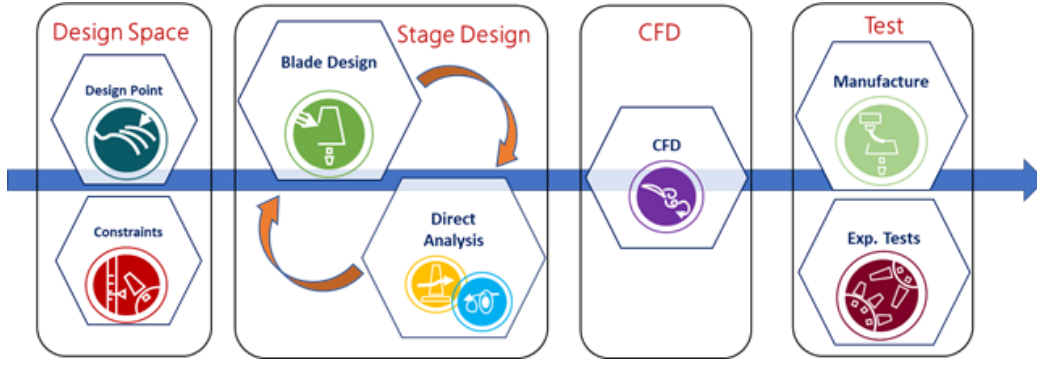
FIGURE 1.1: Flow chart of a classical design approach.

Design point objectives	Formula
Shroud diameter	D_s
Angular velocity	ω
Global flow coeff.	$\Phi_d = Q/(\omega D_s^3)$
Global work coeff.	$\Psi_d = gH/(\omega D_s)^2$
Specific speed	$\omega_s = \Phi_d^{1/2}/\Psi_d^{3/4}$
Specific diameter	$d_s = \Psi_d^{1/4}/\Psi_d^{1/2}$

TABLE 1.1: Global design parameters.

global flow and work coefficient introduced in Table 1.1 can be redefined as follows:

$$\phi_d(r) = \frac{c_m(r)}{U(r)} \qquad \psi_d(r) = \frac{gH}{U(r)^2}, \tag{1.1}$$

where $c_m(r)$ is the local meridional velocity and $U(r) = \omega r$ is the local bleed speed.

The Stage Design loop comprises two fundamental steps, the Blade Design (or Inverse Design) and the Direct Analysis. The designer iterates from one to the other until the resulting geometry converges on the duty point performance. The first is a classic inverse design problem, concerning the definition of the blade geometry and the characterization of the fan configuration. The second is a direct analysis of the geometry generated by the first. The fluid-flow through the blade-to-blade passage is predicted, and the resulting performance of the blade geometry established. Both steps are thoroughly described in specific sections (1.5 and 1.6). The entire Stage Design loop (design-analysis-design) is iterated until the design point is achieved within the geometric and cinematic constraints of the application. This loop can be seen as a sort of primitive optimization process which explores only a small portion of the entire design space, converging to a local optimum that is strongly influenced by the design choices that are usually based on empirical relations and methodologies.
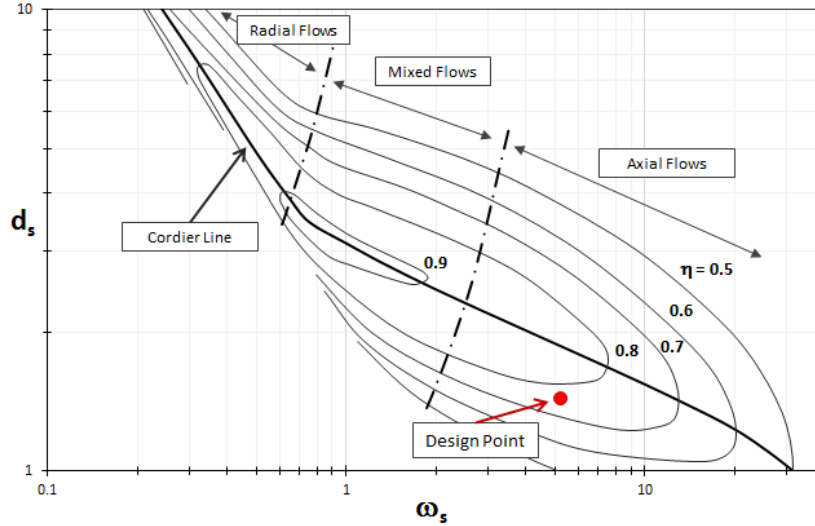
FIGURE 1.2: Example of a preliminary design location on a Balje Chart.

1.2 Basic equations

1.2.1 Coordinate system

Turbomachines consist of rotating and stationary blades arranged around a common axis, which means that they tend to have some cylindrical shape. It is therefore natural to use a cylindrical polar coordinate system aligned with the axis of rotation for their description, the design and analysis. In general, the flow in a turbomachine has components of velocity along all three axes (the axial x, the radial r and the tangential or circumferential θ); however, to simplify the analysis it is usually assumed that the flow does not vary in tangential direction. In this case, the flow moves through the machine on axis-symmetric stream surfaces. The component of velocity along an axis-symmetric stream surface is called the meridional velocity, $c_m = \sqrt{c_x^2 + c_r^2}$. The total flow velocity is made up of the meridional and tangential components and can be written as:

$$c = \sqrt{c_x^2 + c_r^2 + c_\theta^2} = \sqrt{c_m^2 + c_\theta^2} \tag{1.2}$$

The swirl, or tangential, angle is the angle between the flow direction and the meridional direction:

$$\alpha = tan^{-1}(c_\theta/c_m) \tag{1.3}$$

The analysis of the flow-field within the rotating blades of a turbomachine is performed in a frame of reference that is stationary relative to the blades. In this frame of reference, the flow appears as steady, whereas in absolute frame of reference it would be unsteady. This makes any calculations significantly easier, and therefore the use of relative velocities and relative flow quantities is fundamental to the study of turbomachinery. The relative velocity w is the vector subtraction of the local velocity of the blade U from the absolute velocity of the flow c. The blade has velocity only in the tangential direction, and therefore the components of the relative velocity can be written as:

$$w_\theta = c_\theta - U, \quad w_x = c_x, \quad w_r = c_r \tag{1.4}$$

The relative flow angle is the angle between the relative flow direction and the meridional direction:

$$\beta = tan^{-1}(w_\theta/c_m) \tag{1.5}$$

A typical stage of axial flow compressor is shown in Figure 1.3. The flow enters the stage at an angle α_1 with an absolute velocity c_1. By vector subtraction, the relative velocity entering the rotor will have a magnitude w_1 at a relative flow angle β_1. The rotor blades are designed to smoothly accept this relative flow and change its direction; at the outlet, the flow leaves the rotor with relative velocity w_2 at a relative flow angle β_2. By vector addition, the absolute velocity at rotor exit c_2 is found at flow angle α_2. This flow should smoothly enter the stator row, which it then leaves at a reduced velocity c_3 at an absolute angle α_3.
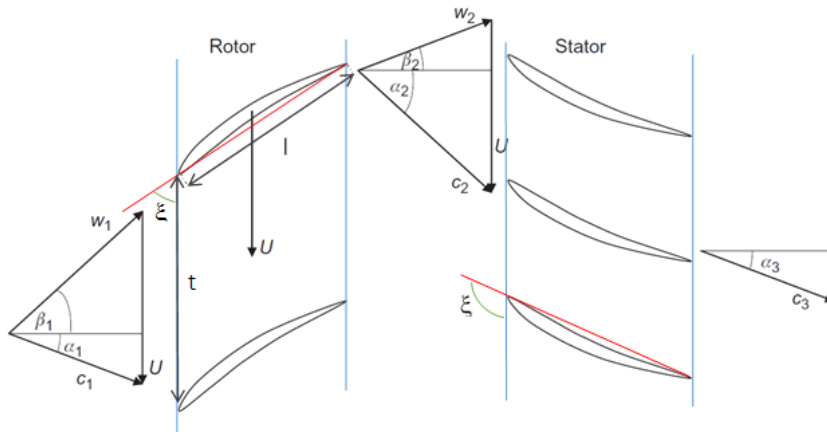
FIGURE 1.3: Geometry and aerodynamic parameter of a single stage axial fan; circumferential view.

1.2.2 The fundamental laws

In most turbomachines, the working fluid is guided in steady flow through an annular duct comprising a hub and casing. Fluid deviation in passing through the stator blade row is produced in Newtonian reaction to blade lift forces akin to those of an airfoil. In the same manner, the rotor blades also generate lift forces, which further modifies the swirl distribution, thus producing rotor torque and therefore a demand for shaft input power. In this manner, energy is transferred from the rotor to the fluid in the case of a fan, pump or compressor, resulting in an overall rise in specific enthalpy and an associated pressure rise. It is evident then that the design and performance analysis of a turbomachine must invoke principles and physic laws that govern the fluid flow through the rotor cascade.

The momentum equation

Newton's second law of motion is one of the most fundamental principles in mechanics. The momentum equation relates the sum of external forces acting on a fluid element to its acceleration, or to the rate of change of momentum in the direction of the resultant external force. Considering a system of mass m, the sum of all the body and surfaces forces acting on m along some arbitrary direction x is equal to the time rate of change of the total x-momentum of the system:

$$\sum F_x = \frac{d(mc_x)}{dt} \tag{1.6}$$

For a control volume where fluid enters steadily at a uniform velocity c_{x1} and leaves steadily with a uniform velocity c_{x2}, then:

$$\sum F_x = \dot{m}(c_{x2} - c_{x1}), \tag{1.7}$$

that is the one-dimensional form of the steady flow momentum equation.

Moment of momentum

In dynamics, useful information can be obtained by employing Newton's second law in the form where it applies to the moments of forces. This form is of central importance in the analysis of the energy transfer process in turbomachines. For a system of mass m, the vector sum of the moments of all external forces acting on the system about some arbitrary axis A-A is equal to the time rate of change of angular momentum of the system about that axis, as follows:

$$\tau_A = m \frac{d(rc_\theta)}{dt}, \tag{1.8}$$

where r is the distance of the mass center from the axis of rotation measured along the normal to the axis and c_θ is the velocity component mutually perpendicular to both the axis and radius vector r. For a control volume the law of moment of momentum can be obtained; Figure 1.4 shows the control volume enclosing the rotor of a generalized turbomachines. Swirling fluid enters the control volume at radius r_1 with tangential velocity $c_{\theta 1}$ and leaves at radius r_2 with tangential velocity $c_{\theta 2}$. For one-dimensional steady flow, we have:

$$\tau_A = \dot{m}(r_2 c_{\theta 2} - r_1 c_{\theta 1}), \tag{1.9}$$

which states that the sum of the moments of the external forces acting on fluid temporarily occupying the control volume is equal to the net time rate of efflux of angular momentum from the control volume.
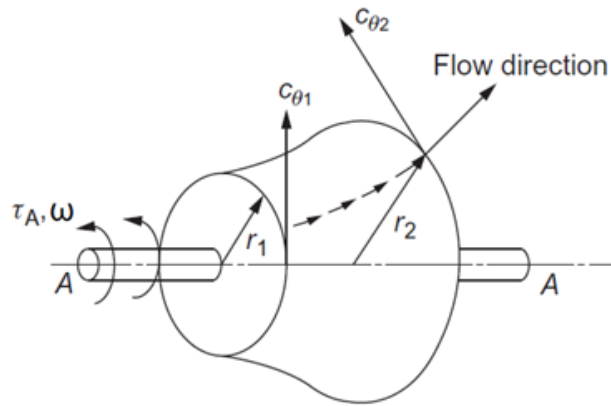
FIGURE 1.4: Control volume of a generalized turbomachines.

The Euler work equation

For a pump or a compressor rotor running at angular velocity ω, the rate at which the rotor does work on the fluid is:

$$\dot{L}_e = \tau_A \omega = \dot{m}(U_2 c_{\theta 2} - U_1 c_{\theta 1}), \qquad (1.10)$$

Thus, the work done on the fluid per unit mass or specific work is:

$$L_e = \frac{\dot{L}_e}{\dot{m}} = \frac{\tau_a \omega}{\dot{m}} = U_2 c_{\theta 2} - U_1 c_{\theta 1} > 0 \qquad (1.11)$$

We can apply the First Law of Thermodynamics to the same control volume defined in Figure 1.4 and obtain the steady flow energy equation $\dot{Q} - \dot{L}_e = \dot{m}(h_{o2} - h_{o1})$ that, for any adiabatic turbomachine gives:

$$L_e = h_{o2} - h_{o1} = U_2 c_{\theta 2} - U_1 c_{\theta 1}, \qquad (1.12)$$

where $h_o = h + 0.5c^2$ is the stagnation enthalpy. This equation is referred as *Euler's pump or compressor equation* and represents the general form of the Euler work equation. By considering the assumptions used in its derivation, this equation can be seen to be valid for adiabatic flow for any streamline through the blade rows of a turbomachine. It is strictly valid only for steady flow but it can also be applied to time-averaged unsteady flow provided the averaging is done over a long enough time period. For incompressible fluids, *i.e.* liquids or low Mach number gases, we may follow the same analysis through, using the incompressible flow energy equation to obtain the corresponding form of the Euler pump equation, namely:

$$L_e = (p_{o2} - p_{o1})/\rho = U_2 c_{\theta 2} - U_1 c_{\theta 1}, \qquad (1.13)$$

where $p_o = p + 0.5\rho c^2$ is the stagnation pressure.

1.3   Meridional flow analysis

Complete 3D flow can be reproduced by the juxtaposition of a number of two dimensional flows, reducing the simulation of a fan rotor behavior in the integral solution of a series of 2D cascade simulations across the blade span. This is not an unreasonable assumption for axial turbomachines of high hub tip ratio. However, when the hub to shroud ratio become smaller than 4/5 [9], and under particular work conditions, radial reassessment inside the blade vane becomes appreciable. As a consequence, the redistribution of mass flow (with respect to radius) affects the outlet velocity profile affecting, in turn, all cinematic properties of the fluid. The temporary imbalance between the strong centrifugal forces exerted on the fluid and radial pressures restoring equilibrium is responsible for these radial flows. This radial motion will continue until sufficient fluid is transported to change the pressure distribution to that necessary for equilibrium. The so-called *radial equilibrium method* is an analysis based upon the assumption that any radial flow that may occur is completed within a blade row; it means that some distance downstream of the blade row the radial velocity will approach zero.

Figure 1.5 illustrates the nature of this assumption; Radial Equilibrium Approach (REA) simplifies the real path of a meridional streamline represented by the red dotted line with the blue solid line. Figure also illustrates how velocity triangles change to account the radial reassessment inside the blade vane. The flow is assumed axisymmetric so

that the effect of the discrete blades is not transmitted to the flow. By adopting cylindrical polar coordinates (x, r, θ) where the x-axis is the rotation one of the turbomachines, quantities in the section 2 in figure are calculated by well-known radial equilibrium for incompressible flow:

$$\frac{1}{\rho}\frac{dp_o}{dr} = c_x \frac{dc_x}{dr} + \frac{c_\theta}{r}\frac{d(rc_\theta)}{dr} \tag{1.14}$$
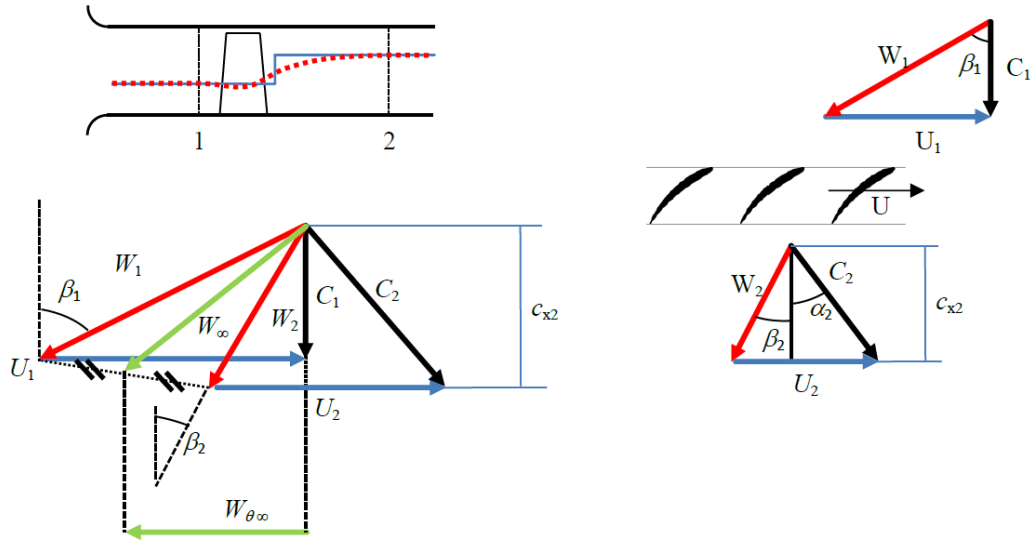
FIGURE 1.5: Inlet and outlet velocity triangles sketch in case of fluid radial reassessment.

1.4 Blade geometry and design parameters

The design and performance prediction of axial flow compressors and turbines has been based, in the main, upon measurements of the flow-through two-dimensional cascades of blades. A cascade blade profile can be conceived as a curved camber line upon which a profile thickness distribution is symmetrically superimposed. Great part of the algorithm used in both the direct and inverse problems are historically based upon considerations made on $2D$ cascades. Since very early days in turbomachines models based on $2D$ cascade calculation have proven to be reliable instruments to deal with design and performance analysis, consisting in a simple framework useful to simplify the complex $3D$ fluid behaviour inside blades vanes. In Figure 1.6 two blades of a compressor cascade are shown together with the notation needed to describe the geometry. Geometric parameters that characterize the cascade blade are:

- stagger angle, γ; angle between the chord line and the rotation axis direction

- solidity, $\sigma = l/t$; the chord-space ratio

- blade inlet angle, β_1'; angle of the tangent to the camber line at the leading edge

- blade outlet angle, β_2'; angle of the tangent to the camber line at the trealing edge

- camber angle, $\theta = \beta_1' - \beta_2'$; the change in angle of the camber line between the leading and trailing edges
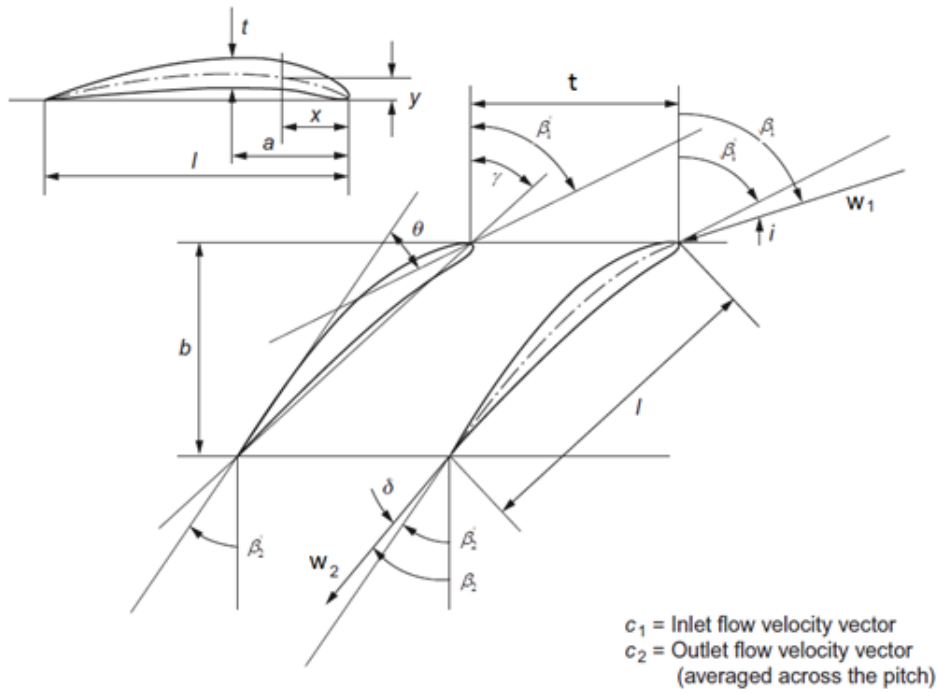
FIGURE 1.6: Compressor cascade and blade notation.

The change in angle of the flow is called deflection, $\varepsilon = \beta_1 - \beta_2$, and in general this will be different to the camber angle due to flow incidence at the leading edge and deviation at the trailing edge. Incidence is the difference between the inlet flow angle and the blade inlet angle, $i = \beta_1 - \beta_1'$. The deviation is the difference between the exit flow angle and the blade exit angle, $\delta = \beta_2 - \beta_2'$. For circular arc camber lines, stagger and camber angle are geometrically correlated, $\gamma = \beta_1' - \theta/2 = (\beta_1' - \beta_2')/2$. Figure 1.7 shows the geometrical correlations for a circular arc camber lines.

The Angle of Attack (*AoA*) is defined as follows:

$$AoA = \beta_m - \gamma, \tag{1.15}$$

where the vector mean flow angle β_m may be expressed in terms of the inlet and outlet flow angles, β_1 and β_m, through:

$$tan\beta_m = \frac{1}{2}(tan\beta_1 + tan\beta_2) \tag{1.16}$$

1.4.1   Analysis of cascade forces

For the design and analysis of a ducted axial fan with cylindrical hub, it is quite reasonable to assume that the stream surfaces at entry to the annulus remain cylindrical as they progress through the machine, especially if: (i) tip gap is moderately low in respect to the overall rotor diameter, (ii) the rotor is low loaded and (ii) blade design is close to free vortex containing so the radial flow redistribution across blade span. In this situation a selected section of the rotor blade can be studied two-dimensionally using cascade models as depicted in Figure 1.8. Let us consider flow through the control volume *abcd* surrounding one section of the rotor blade. Lines *ab* and *dc* were selected to coincide with same streamlines through adjacent passages, while *ad* and *bc* sides were just selected parallel
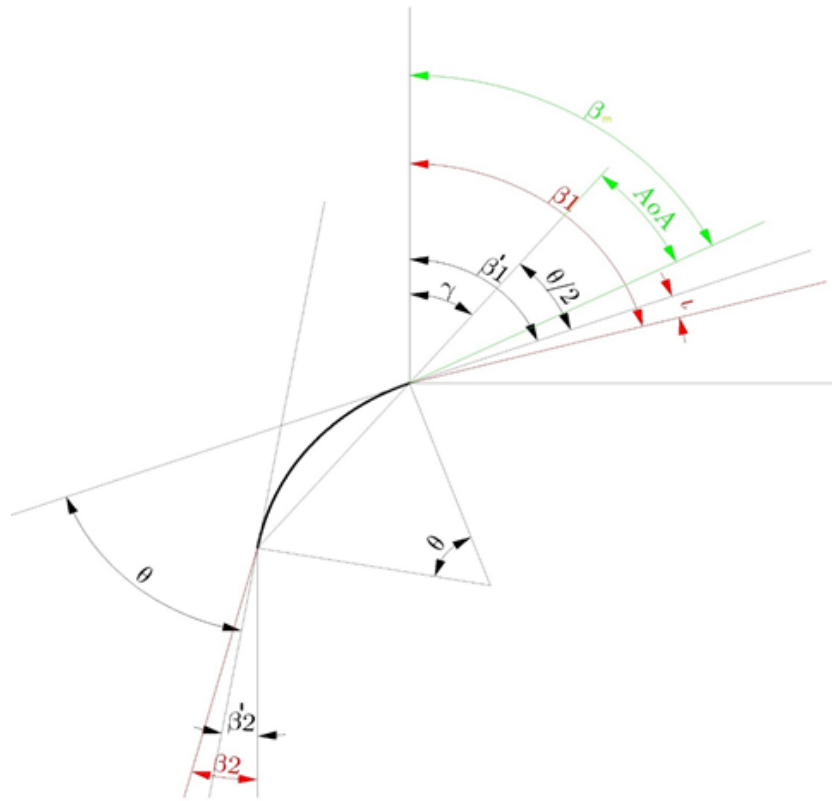
FIGURE 1.7: Angles definition for circular arc camber lines.

to the reference frame velocity U equal in length to the blade pitch t. In this model we are considering that each streamline inside the control volume behaves in the same way of *ab* or *dc* streamlines, so thermal, kinematic and dynamic properties just depends on axial coordinates (x) and not from azimuthal position ($r\theta$) (axisymmetric hypothesis). Velocity diagrams reported in Figure 1.8 reproduce kinematic properties of the flow at the entrance of control volume (*ad* segment) and exit (*bc* segment), respectively indicated with 1 and 2 subscripts. Inlet and outlet segments (*ad* and *bc*) are arbitrarily taken respectively far upstream and far downstream the cascade in order to be far from secondary effects generated by blades such as the wake region downstream cascade or inlet distortion upstream cascade blades. Considering that there is no radial reassessment of the fluid U velocity remains the same across the blade vane. Axial velocity remains constant across the blade vane, assuming that flow density is constant and that cross-sectional area of control volume is kept constant along streamlines and the blade thickness is negligible.

Lift and drag forces

In order to derive equations that express the dynamic behaviour inside the blade vane it is important to define two indicator of profile aerodynamic loading in a form identical for the one found for isolated airfoils:

$$C_L = \frac{L}{\frac{1}{2}\rho w_m^2 l} \qquad C_D = \frac{D}{\frac{1}{2}\rho w_m^2 l}, \tag{1.17}$$
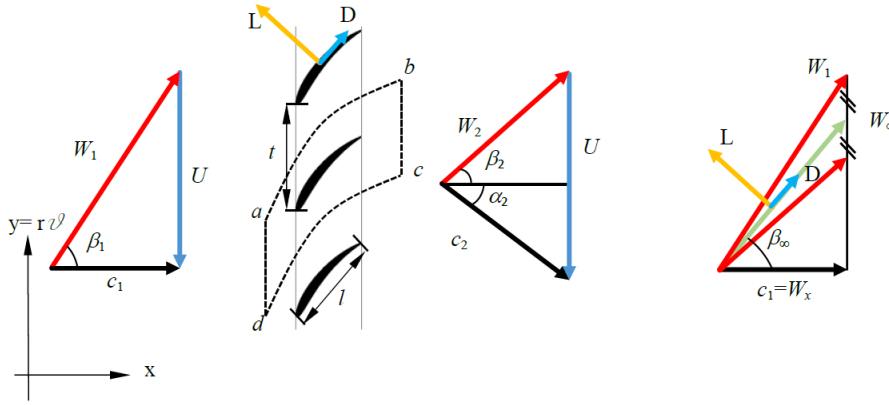
FIGURE 1.8: Cascade geometry, velocity and force diagrams for a fan rotor.

which are respectively the lift coefficient and the drag coefficient. Here L and D forces represent the forces exerted form the airfoil on the fluid for unit of length in the z direction so perpendicular to the x-y plane. In order to write a force balance Figure 1.9 reports, in
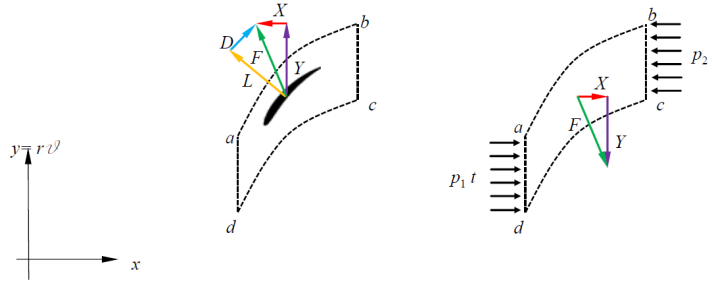
FIGURE 1.9: Aerodynamic forces acting upon a single blade of a cascade (left), mutual and pressure forces acting on the control volume abcd (right).

the left side, aerodynamic forces action on the single airfoil of a 2D cascade, while on the right side, forces action on selected control volume. The vectorial sum F of lift and drag forces acting on the airfoil is then projected on x and y axis to obtain X and Y forces. A balance of forces on the x axis acting on the control volume can be written as:

$$X + p_1 t \cdot 1 - p_1 t \cdot 1 = 0 \quad \Rightarrow \quad X = (p_2 - p_1)t \tag{1.18}$$

Forces acting on ab and cd surfaces, for the axisymmetric hypothesis, are equal and opposite and may thus be ignored. Referring to the total pressure in the relative frame, $p_o = p + \frac{1}{2}\rho W^2$, we have:

$$
\begin{aligned}
X &= \frac{1}{2}\rho(w_1^2 - w_2^2)t - (p_{o,1} - p_{o,2})t \\
&= \frac{1}{2}\rho w_x^2 t(\tan^2\beta_2 - \tan^2\beta_1) - \Delta p_o t \\
&= \rho w_x^2 t \tan\beta_m(\tan\beta_1 - \tan\beta_2) - \Delta p_o t
\end{aligned}
\tag{1.19}
$$

where $\Delta p_o = (p_{o,1} - p_{o,2})$ represents the total pressure losses across the blade passage. $p_{o,2}$ in reality it is strongly dependent on position upon bc segment due to the wake presence at the cascade outlet. On the other hand far downstream the trailing edge of the airfoil wake diffuses along the blade passage t and the flow becomes uniform and axisymmetric again, still according with previous hypothesis.

A similar discussion can be reproduced to obtain force on y axis using momentum conservation law:

$$-Y = \rho w_x^2 t (\tan\beta_2 - \tan\beta_1), \tag{1.20}$$

obtaining for X projection

$$X = Y\tan\beta_m - \Delta p_o t \tag{1.21}$$

Using Figure 1.8 it is possible to write:

$$X = L\sin\beta_m - D\cos\beta_m \tag{1.22}$$
$$Y = D\sin\beta_m - L\cos\beta_m \tag{1.23}$$

By deriving D from the latter expression, and by substituting it into X equation, it is possible to derive the lift vectorial expression:

$$L = X\sin\beta_m + Y\cos\beta_m \tag{1.24}$$

By using Equation 1.21 (remembering that $w_x = w_m\cos\beta_m$) it is possible to derive the lift formulation:

$$L = (Y\tan\beta_m - \Delta p_o t)\sin\beta_m + Y\cos\beta_m = \frac{Y}{\cos\beta_m} - \Delta p_o t \sin\beta_m$$
$$= \frac{\rho w_x^2 t(\tan\beta_1 - \tan\beta_2)}{\cos\beta_m} - \Delta p_o t \sin\beta_m = \rho w_x^2 t(\tan\beta_1 - \tan\beta_2)\cos\beta_m - \Delta p_o t \sin\beta_m \tag{1.25}$$

With the same logic, it is possible to derive the drag vectorial expression:

$$D = Y\sin\beta_m - X\cos\beta_m = \Delta p_o t \cos\beta_m \tag{1.26}$$

Using Equations 1.25 and 1.26, it is possible to express drag and lift coefficients as:

$$C_D = \frac{\Delta p_o t \cos\beta_m}{\frac{1}{2}\rho w_m^2 l} \quad C_L = 2\frac{t}{l}(\tan\beta_1 - \tan\beta_2)\cos\beta_m - C_D\tan\beta_m \tag{1.27}$$

Last equation represents a pivotal equation linking cascade loading parameters(lift and drag coefficients) to cinematic parameters such as inlet and outlet angles, fluid deflection and cascade geometry through solidity. This open the discussion on two different sides: design and analysis procedures. During design practice designer's task is to select a suitable blade shape and cascade geometry to achieve the required flow deflection from the inlet angle β_1 to outlet angle β_2 whit the minimum loss of energy. During this process the selection of geometrical parameters, that determine the overall dimensions and cost of the machine, is a trade-off to cascade load that determine losses and so machine efficiency. In the case of axial fans, that generally present a blade spacing quite wide, e.g. $t/l \gg 1$, a guide to preliminary profile selection is provided by the published C_L and C_D, data for isolated airfoils such as that given by [10] or [11]. This reveals that a lift coefficient of value $C_L = 1.2$ would be close to the maximum achievable for many airfoils. For a fan application a more conservative design value of say $C_L = 0.8 \div 1.0$ would be desirable to increase the allowable stall margin [8]. Equation 1.27 is also useful during analysis

process. When knowing blade shape and cascade geometry, it is possible to estimate C_L and C_D coefficients or to read from published data and then estimate deflection from the known inlet angle β_1 to the unknown outlet angle β_2.

Circulation

It has been shown that the effect of an airfoils cascade upon a uniform stream can be represented far upstream and downstream by a continuous distribution of vortices equally spaced of intensity Γ [8], Figure 1.10. The circulation Γ, is defined as the contour integral of velocity around a closed curve. The fluid deflection of a uniform stream, that is the main aim of a turbomachine cascade, is accomplished by the vorticity and hence by the circulation developed by the blades. The array produces a change in relative tangential velocity w'_θ that can be expressed as:

$$w'_{\pm\theta} = \mp \frac{\Gamma}{2t} \tag{1.28}$$
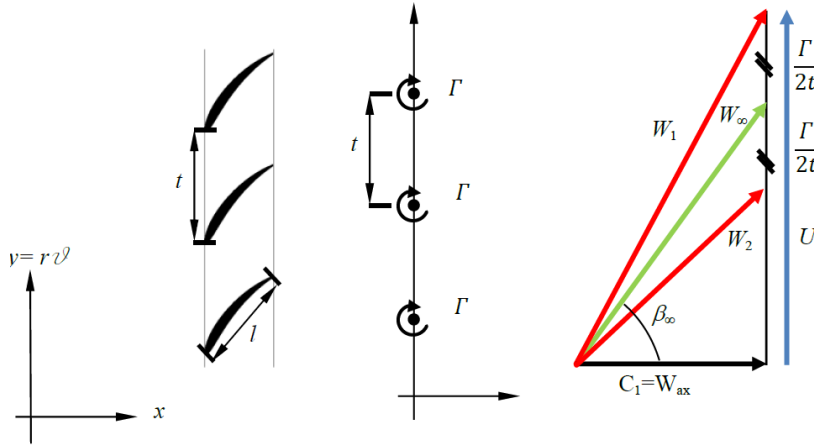
FIGURE 1.10: Turbomachinery cascade and the equivalent infinite vortex array. On the right side are reported velocity triangles for a diffusive cascade.

Figure 1.10 shows how the circulation is related with the change of the velocity triangles. Since the mean and the outlet relative velocity can be expressed as:

$$w_m = \sqrt{w_{\theta,m}^2 + c_{x,m}^2}, \qquad w_2 = \sqrt{w_{\theta,2}^2 + c_{x,2}^2} \tag{1.29}$$

Introducing Equation 1.28 in the last expressions, we finally obtain:

$$
\begin{aligned}
w_m &= \sqrt{(U + w'_{\theta,m})^2 + c_x^2} = \sqrt{\left(U - \frac{\Gamma}{2t}\right)^2 + c_{x,m}^2} \\
w_m &= \sqrt{(U - 2|w'_{\theta,2}|)^2 + c_x^2} = \sqrt{\left(U - \frac{\Gamma}{t}\right)^2 + c_{x,2}^2}
\end{aligned}
\tag{1.30}
$$

The Kutta-Joukowski theorem [9] relates the lift generated by an airfoil to the circulation Γ, the density ρ and the relative velocity between the airfoil and the fluid at infinity:

$$L = \Gamma \rho w_m \tag{1.31}$$

Combining Equations 1.17 and 1.31 it is possible to express the circulation as:

$$\Gamma = 0.5 w_m C_l l \tag{1.32}$$

In conclusion, the circulation Γ links the aerodynamic characterization of the blade profile and the operating cinematic condition of the blade itself. This connection has been applied for the development of both design and analysis methods and will be discussed in the following sections.

1.4.2 Cascade performance

Within fans and compressors, the flow is moving from a low static pressure at inlet toward a higher static pressure at exit. The fundamental difficulty is getting the flow to negotiate this pressure rise without generating high loss or separating. The designer must choose an appropriate level of blade loading, such that the flow can achieve the required pressure rise, while not over-designing the machine, such that there are too many blades. This section describes the key phenomena present in compressor cascade that determine their design and performance.

Losses and blade loading

The efficient performance of a blade is limited by the growth and separation of the blade surface boundary layers. Lieblein [12] showed that in the region of minimum loss, the wake thickness and consequently the loss in total pressure are primarily related to the diffusion in velocity on the suction surface of the blade. The fall in velocity on the suction surface is high and much greater than the overall change, as shown in Figure 1.11. Lieblein defined a term to quantify this diffusion on the suction surface, which he called the *local diffusion factor*:

$$DF_{loc} = \frac{c_{max,s} - c_2}{c_{max,s}} \tag{1.33}$$

The local diffusion factor is relatively hard to determine. More used is *diffusion factor* (DF) based on a surface velocity distribution similar to those actually measured on the NACA 65 series and the C4 series (British). This parameter requires knowledge of only the inlet and exit velocities from the blade and the pitch-chord ratio and is very useful for preliminary design purposes:

$$DF = \left(1 - \frac{c_2}{c_1}\right) + \left(\frac{c_{\theta 1} - c_{\theta 2}}{2c_1}\right)\frac{1}{\sigma} \tag{1.34}$$

The first term on the right-hand side, $1 - c_2/c_1$, represents the mean deceleration of the flow. The second term, $(c_{\theta 1} - c_{\theta 2})/2c_1$, represents the flow turning. The pith-chord ratio, $1/\sigma$, determines how well the flow is guided by the blades. A low value implies lower pressure gradients across the blade passages required to turn the flow and, hence, less diffusion. The loss in a blade row increases rapidly as the flow starts to separate, which occurs when the diffusion factor exceeds about 0.6. A well-designed blade with moderate loading will operate with a $DF \simeq 0.45$.

Fluid deviation

The flow leaving a compressor blade does not follow the blade camber line at the trailing edge. This deviation arises partly because the flow is diffusing within the blade passages. This means that the streamlines are diverging and therefore the flow is not moving in a single direction. This effect is exacerbated by the spacing of the blades because the flow is
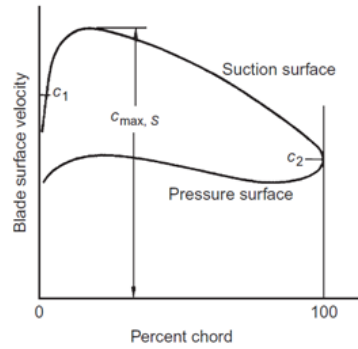
FIGURE 1.11: Typical velocity distribution on a compressor cascade
blade[9].

guided less by the blades when they are further apart. Howell [13] developed an empirical
relationship between the nominal deviation, δ, occurring at the nominal design incidence
angle, or in other words in the case of *shock free entrance* ($i = 0$ and $\beta' = \beta$) as follows:

$$\delta = m\theta \sqrt{\frac{t}{l}}, \tag{1.35}$$

where $m = 0.23 + \beta_2/500$. Deviation increases further as the incidence changes from the
nominal condition and any flow separation will cause a rapid increase in deviation.

1.5   Rotor blade design

In the field of turbomachinery, multiple fan design methods and concepts can be iden-
tified, and, often, important design choices are made based on empirical correlations or
on the designer's experience. Even though such design choices appear to be numerous
and developed for the particular class of flow machines under consideration, the design
process itself can be laid out in simple steps:

- Definition of the required duty point, geometric and cinematic constraints

- Definition of the radial load distribution

- Definition of the blade geometry using a cascade approach

This section concerns the second and third step, being the first treated in Sec. 1.1. The
blade geometry definition can be based on experimental data on 2D stationary cascade
or on hybrid methodologies based on the coupling between the aerodynamic response
characterization of a blade profile and the chosen vortex distribution. A brief survey
on the empirical method is given in Sec. 1.5.2, while Sec. 1.5.3 presents a developed
quasi-3D blade design methodology. Figure 1.12 schematizes the design process and how
the design choices, the meridional flow analysis and the geometry definition are linked.
Design choices are highlighted in blue, design process elements are highlighted in yellow
and the process output is highlighted in green.
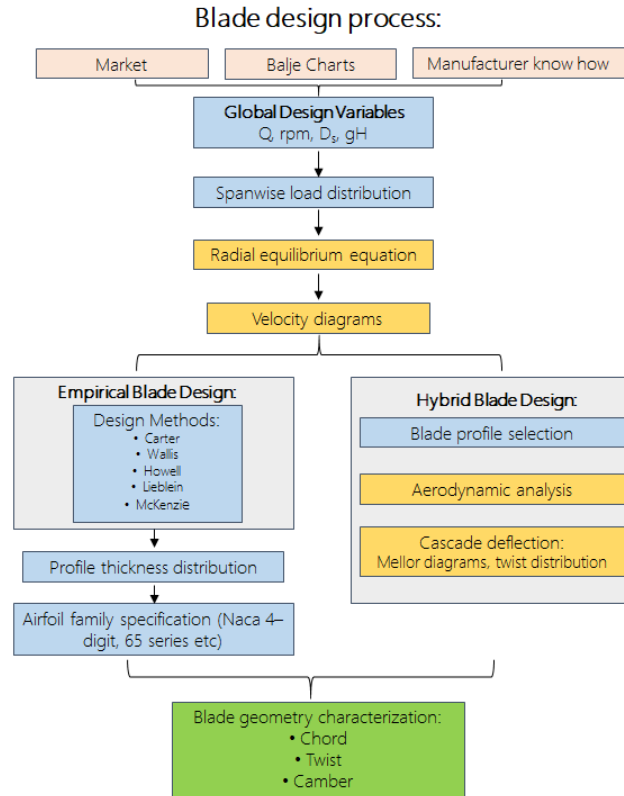
FIGURE 1.12: Blade design process, from global design variable to blade
geometry design.

1.5.1 Vortex selection

As a consequence of assumed incompressible radial equilibrium (Equations 1.14), the radial axial velocity is univocally fixed by the definition of the radial load distribution; this is dealt by setting the swirl velocity $c_{\theta,2}$, as one of the most important parameter for design. Historically the most common solution is to adopt the *Free Vortex* flow (FV), entailing a constant $\phi(r)$ distribution [14]. The simplicity of the flow under FV conditions is, superficially, very attractive to the designer and many axial turbomachines have been designed to conform to this flow. Characteristics of this flow are the large fluid deflection near the inner wall and the spanwise constant design blade circulation. A further serious disadvantage is the large amount of rotor twist from root to tip, which adds to the difficulty of blade manufacture [9]. Nowadays, rotors of axial flow turbomachines are often of controlled vortex design [14]. This means that in contrast to the classic FV design concept, the prescribed circulation and thus, the Euler work, as well as the isentropic total pressure rise increases along the dominant part of the blade in a prescribed manner. As discussed in [15] and [16], controlled vortex design offers the following potential benefits:

- It guarantees a better utilization of blade sections at higher radii, *i.e.* it increases their contribution to the rotor performance [17]

- It gives a means to reduction of hub losses by unloading the blade root

- It offers a means for improving the static efficiency by reducing the hub diameter, and thus moderating the outlet loss

- It serves as a conceptual basis for obtainment of easy to manufacture fan blade geometry, even with spanwise constant stagger angle (avoid highly twisted blade [18])

These considerations led to the formulation of many other types of vortex design. The *Forced Vortex* is the inverse of the FV and varies directly with r. Different types of vortex are located in between these opposite solutions and are obtained with combination of the Free and Forced Vortex distribution and feature intermediate characteristics. At this point, the possible choices for a designer are:

Free Vortex
$$c_{\theta 2} = b/r \qquad (1.36)$$

Exponential Vortex
$$c_{\theta 2} = a + b/r \qquad (1.37)$$

Mixed Forced Vortex
$$c_{\theta 2} = ar + b/r \qquad (1.38)$$

Mixed Unforced Vortex
$$c_{\theta 2} = ar^{0.5} + b/r \qquad (1.39)$$

Forced Vortex
$$c_{\theta 2} = ar \qquad (1.40)$$

Power Law
$$\frac{c_{\theta 2}}{c_{\theta 2,t}} = \frac{r}{r_t} \left[\frac{1 - (\chi \frac{r_t}{r})^m}{1 - \chi^m} \right] \qquad (1.41)$$

In these equations a and b are constants and t represents the tip section of the blade, the exponent m can be chosen by the designer and $\chi = r_{hub}/r_{tip}$. *Power Law*, described by Equations 1.41 was developed by Lewis [8] to overcome the characteristic of free vortex at the hub where free vortex design results in unrealizable hub loadings for low hub/tip ratio propellers and bad downstream flow at the hub where swirl velocities are high. As a remedy for this, Lewis postulated a near-free-vortex design whit swirl velocities and thus blade loadings, which taper rapidly to zero in the hub region. The swirl velocity distributions of the listed vortex are shown in Figure 1.13. The designer can select all
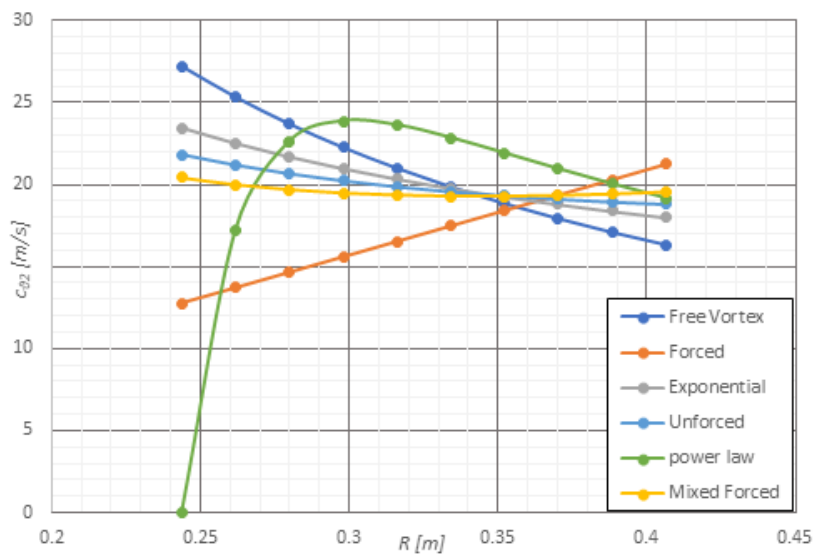
FIGURE 1.13: Example of radial swirl distributions for different vortex.

vortex shown in the equations starting from the following general definition:

$$c_{\theta 2} = gar^m + \frac{b(1-g)}{r},$$ (1.42)

where a and b are still constants and the coefficient $g \in [0,1]$ allows allows to manage the weight of free component or forced one into the vortex distribution. The coefficients a and b are defined by introducing Equations 1.42 in the Euler Work Equations 1.13 and performing a mass average. Integrals can be approximate using first order Newton-Cotes formulae.

$$L_e = \frac{\Delta p}{\rho} = \frac{1}{Q} \int_A c_{x,2}(r) L_e(r) dA = \frac{2\pi\omega}{Q} \int_r c_{x,2}(r) c_{\theta,2}(r) r^2 dr$$ (1.43)

Once that the $c_{\theta,2}$ is defined, the unknown in the radial equilibrium Equations 1.14 is the axial velocity $c_{x,2}$. Taking in account the different radii, the system of non-linear equation can be solved by numerical methods. Figure 1.14 highlights how different vortex affect the velocity and the Euler Work radial distribution. The axial velocity is constant along the span in the FV case, while in all other cases, it increases between hub and tip section, with an almost linear trend for all of them except for the power law. The last cited presents a logarithmic trend which asymptotically tends to a typical FV trend. This means that the more external area of the blade will have to facilitate the passage of most part of fluid, subsequently, $c_{x,2}$ takes its asymptotic trend with higher values if compared with FV case.
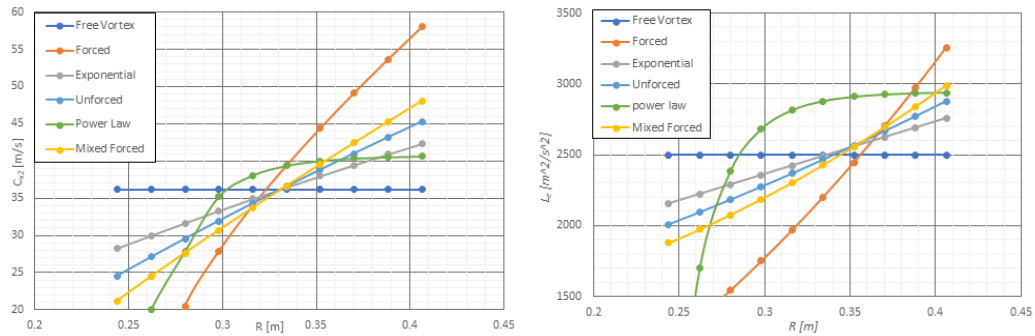
FIGURE 1.14: Example of radial distributions for different vortex of axial absolute velocity and Euler work.

1.5.2 Empirical blade design

Blade design is a non-closed problem being the geometric correlation presented in Section 1.4 not sufficient to univocally define the unknown parameters (camber, pitch and solidity). Traditional methods, based on experimental data on $2D$ stationary cascade, adopts empirical relations to close the blade design problems. This subsection gives a brief survey on the more common relationships reported in literature, trying to present the blade design logic in a straightforward manner. Historically, the design approach is to assume zero incidence ($\beta_1 = \beta_1'$), which ensures a smooth and continuous surface pressure distribution on the blade [9]. All the design approaches assume that the radial load distribution and the cinematic components $c_{x,2}, w_1, w_2$ are defined.

$C_{l,opt}$ **Carter-Wallis**

The first step of this method is based on McKenzie's empirical rule which relates the stagger γ with the mean flow angle β_m, determining a theoretical stagger angle for maximum efficiency [9]:

$$tan\gamma = tan\beta_m - 0.213 \tag{1.44}$$

Wallis proposed an optimal lift coefficient [19] $C_{l,opt} = 1.35(cos\beta_m/cos\beta_2)^2$ that can be introduced in Carter's relationship [20] between lift coefficient C_l and solidity σ [19]:

$$\frac{2cos^2\beta_2}{\sigma cos\beta_m}(tan\beta_1 - tan\beta_2) = 1.35 \tag{1.45}$$

Solidity is defined by combining the previous relationships:

$$\sigma = \frac{2cos\beta_m}{C_l}\frac{1}{c_x}(w_{\theta 1} - w\theta 2) \tag{1.46}$$

In order to determine the camber angle θ and close the problem, designer can opt for:

- circular camber line; θ is geometrically defined (see Sec 1.4) $\beta_1' = \gamma + \theta/2$

- generic camber line; θ is defined by using the Howell equation 1.35 to obtain β_2' and hence, θ

Howell-circular arc camber line

This method is applicable exclusively to circular camber line blades; by using McKenzie's empirical rule (Equation 1.44); the camber, for a circular arc, is univocally defined by $\theta = 2\beta_1' - \gamma$. The Howell equation 1.35 is used to derive the solidity:

$$\sqrt{\frac{t}{l}} = \frac{\beta_2 - \beta_2'}{\left(0.23 + \frac{\beta_2}{500}\right)\theta} \tag{1.47}$$

Lieblein diffusion factor

In this method, solidity is defined by setting the DF spanwise distribution and by inverting Equation 1.34:

$$\sigma = \left(\frac{w_{\theta,1} - w_{\theta,2}}{2w_1}\right)\frac{1}{DF - 1 - w_2/w_1} \tag{1.48}$$

A low DF value implies lower pressure gradients across the blade passages required to turn the flow and, hence, less diffusion. Lieblein showed that the loss in a blade row increases rapidly as the flow starts to separate, which occurs when the diffusion factor exceeds about 0.6 [12]. Once again, the camber angle can be set by opting for a circular-arc or generic camber line, with auxiliary equation from McKenie or Howell.

1.5.3   Hybrid blade design

The Hybrid Design Methodology (HDM) is derived from a method originally developed in the 1950's and reported by Mellor [21]. This method is significant as it is based upon results from a series of low-speed NACA-65 cascade studies. The NACA-65 profile has found widespread application in industrial fans as it has proven to be an effective profile for a wide range of industrial applications. The method developed by Mellor involved plotting inlet and outlet flow angles for blade section for a given camber and space-chord

ratio. Stagger angles were then varied over a range of angles of attack. The proposed methodology is a two-dimensional design where the complexity of three-dimensional flow through the blade-to-blade passage is partially modelled using a quasi-3D approximation, obtained by combining the flow conditions on the meridional plane and the circumferential plane. The flow is treated as an axisymmetric or circumferentially averaged 'meridional flow'. The blade is radially divided into sections from hub to casing with each cylindrical meridional stream surface intersecting the blade row to form a circumferential array of blade profiles known as cascade. The three-dimensional flow-field is, therefore, modelled by a series of such plane two-dimensional cascades, one for each of the cylindrical meridional surface spaced between hub and casing; in other words, the flow is treated as a series of superimposed 'cascade' flows.

The HDM matches the aerodynamic performance of the selected blade profile with the selected vortex and, therefore, load distribution along the blade span. In so doing, it defines the blade pitch and twist radial distributions. Thi methodology allows the designer, by changing the airfoil section or the vortex distribution, to modify the aerodynamic load along the blade span, for the same duty point and constraints.

The developed HDM composes a process, Figure 1.15. Design choices are highlighted in blue, design process elements are highlighted in yellow and the process output is highlighted in green. Once a design duty point is selected, the designer chooses the design load distribution along the blade span (free vortex, forced vortex, exponential vortex just to mention a few) and the blade profile. The solution of the radial equilibrium equation defines the radial flow coefficient distribution. Referring to the quasi-3D approximation previously described, this part concerns the meridional flow analysis. A feature of the HDM is the feedback loop regarding the losses (red loop in Figure 1.15). The design load coefficient $\psi_d(r)$, Equation 1.1, refers to the real work and, hence, to the actual design objective. Classically design methods are based on empirical or theoretical fluid deflection models and, therefore, refer to the ideal work (*i.e.* the Euler work). In order for the HDM to account for aerodynamic losses, it is mandatory to add a feedback losses loop that adjust the design load distribution to a target $\psi_t(r)$. The implemented losses model acts to reduce the work coefficient [7]; namely the convergence of the loop will lead to $\psi_t(r) > \psi_d(r)$. In so doing the losses loop prevents the design of an under-loaded blade incapable of reaching the target design point.

The choice of the profile selection is necessary to get the aerodynamic performance analysis, in terms of C_l and C_d against the *AoA*. The Kutta-Joukowski theorem and Equation 1.32 link the aerodynamic characterization of each two-dimensional blade section and the meridional flow distribution. The last step required for the creation of the Mellor Charts, concerns the evaluation of the radial distribution of fluid deflection the selected two-dimensional blade profile can ensure. This is dealt with the cascade approach that allows the solution of the circumferential plane using Equation 1.30. Once the design point and the load distribution are defined, the outlet relative velocity is a function only of the solidity $\sigma(r)$ and the *AoA* (which defines the lift coefficient). This enables the creation of a Mellor Charts (Figure 1.16, blue line) for each two-dimensional profile:

$$\beta_2 = f(AoA) \tag{1.49}$$

The last step in the HDM is a comparison between the fluid deflection induced by the blade section over a range of *AoA* and the target fluid deflection required by the selected load distribution. In the example presented in Figure 1.16, the target fluid deflection $\beta_{2,target}$ (red symbol) is compared with the profile deflection capability (blue line); the output is the AoA_{target} (green check). A smaller value of β_2 means a larger deflection
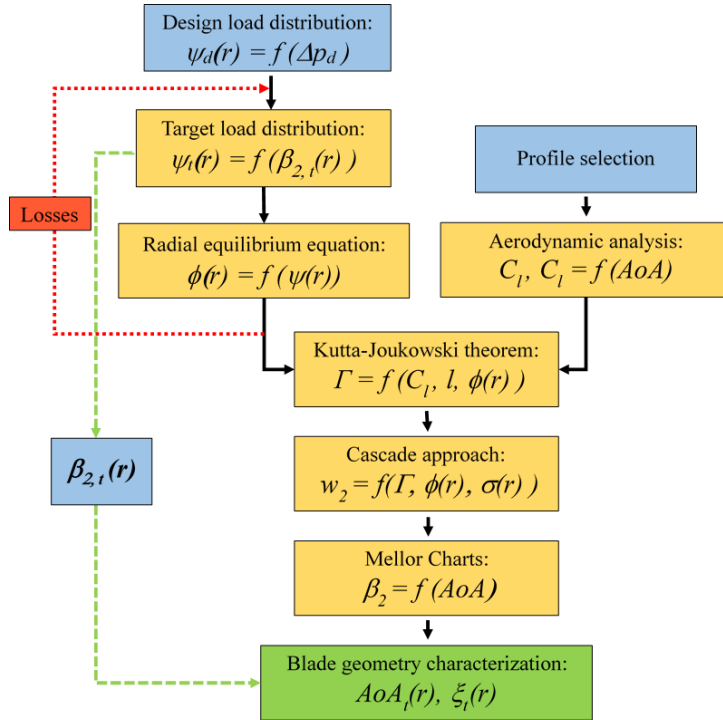
FIGURE 1.15: Hybrid Design methodology.
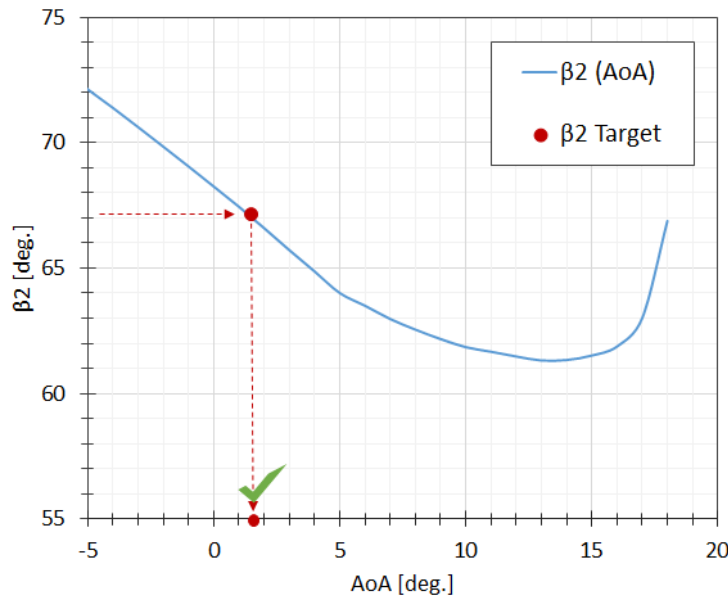
FIGURE 1.16: Example of a Mellor Chart.

imposed on the fluid, with the minimum β_2 value corresponding to the maximum lift coefficient the blade can provide. The objective of the design process is to ensure that the blade operates within its stable angle-of-attack range, where $AoA < AoA|_{\beta_{2,min}}$. By definition, the radial distribution of the AoA_{target} automatically defines the pitch radial distribution. The blade geometry characterization consequently becomes explicit, as does the rotor configuration. Consequently, by merging the design load information with the aerodynamic blade capabilities within the design method, the HDM provides a designer

with feedback on the feasibility of achieving the desired duty point with the chosen blade profile and load distribution.

1.6   Performance analysis of axial fan

1.6.1   Introduction to the virtual test rig package

Once blade geometry and rotor configuration are defined, performance of the design may be directly verified using different analysis tools. A virtual test rig consists of a set of tools for fan analysis developed in order to reduce as much as possible computational cost but preserving a comparable level of accuracy in performance prediction whit CFD. This section provides a brief description of two analysis tools developed in collaboration with the turbomachinery group in Sapienza University of Rome. The first is AxLab, a Python software for performance analysis of ducted axial fans based on quasi-3D blade element axisymmetric principle. This software represents the best $3D$ CFD alternative when the principal designer's goal is to optimize performance of a given fan without taking into account system effects. Model provided is an extreme simplification of reality but demonstrated great potentiality. The second analysis tool is based on a three-dimensional synthetic rotor simulation based in an Actuator Disk (AD) model, capable to simulate different kind of fan configuration that reflects the international standards today used for fan tests like ISO 5801 or AMCA, giving the possibility to the user to customize test rigs like in a proper fan lab, or to study the effects of a fan directly mounted in the final system configuration.

1.6.2   AxLab software

AxLab software is a python program for performance analysis of ducted axial fans. This software is based on a blade element axisymmetric principle whereby the rotor blade is divided into a number of streamlines. For each of these streamlines relations for velocities pressure are derived from incompressible conservation laws for mass, tangential momentum and energy. In particular the complexity of $3D$ flow inside the rotor of an axial fan is partially reproduced using a quasi-3D approximation, obtained by the juxtaposition of the flow conditions on the meridional plane and the circumferential plane. The algorithm described below reports models for the solution of flow conditions both in circumferential and meridional plane.

Compared to streamline curvature or though flow methods, although this model produces results less accurate, it is able to produce dependable results with small computing costs requiring solution of a simplified radial equilibrium equation at only one axial station, synthetizing flow behaviour inside the blade vane by means of different aerodynamic models. Even though time saved on a single simulation or a single characteristic curve is negligible, it becomes relevant if multiple configurations must be tested and this can be crucial during design of new blades or optimization of existing geometries.

AxLab process for performance calculation of one single operating point can be resumed in four main steps shown in Figure 1.17: (i) at first the problem is set by specification of blade geometry and calculating inlet velocity diagrams, then (ii) calculation on circumferential plane are performed obtaining values for β_2 for each section of the blade that will be used for (iii) calculation on meridional plane. Points (ii) and (iii) rely on considerations and equations presented in Sections 1.3 and 1.4. Figure 1.17 reports an iterative loop that must be run when using the deviation model implemented in the code, named LanD and Gamma, that estimate β_2 value by means of functions of itself ($\beta_2 = f(\beta_2)$). In this case, points (ii) and (iii) are repeated in loop until convergence on

outlet angle β_2 is reached with a tolerance decided by the user. Starting condition for this loop are evaluated at the end of point (i). When convergence is reached (iv) outlet variables and fan performance are evaluated. Phases (i) and (iv) are extensively described by Lewis [8], while the iterative procedure between points (ii) and (iii) is described [7].
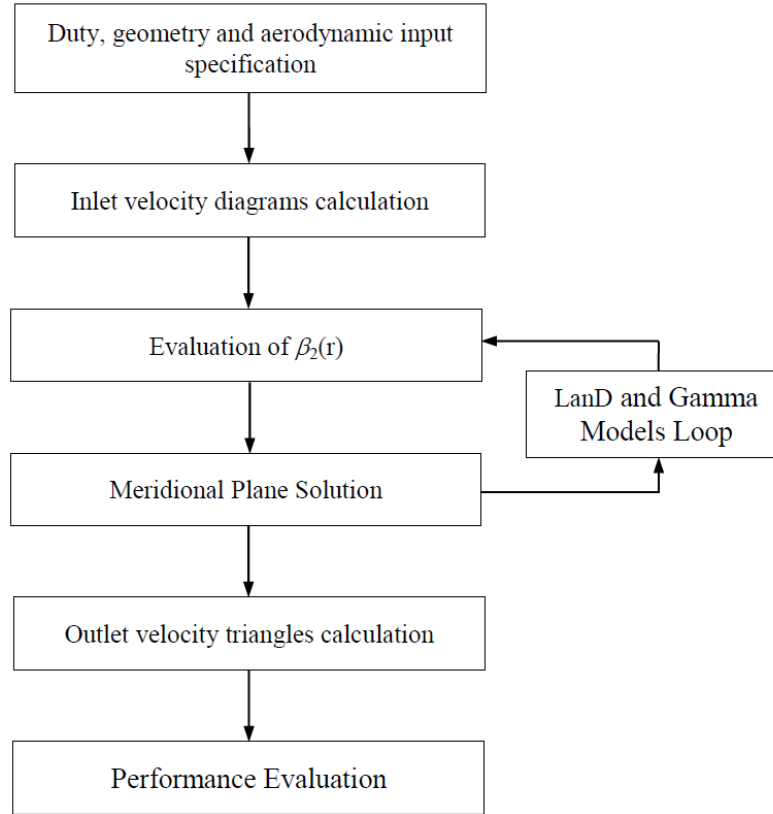
FIGURE 1.17: AxLab analysis sequence chart.

It is evident that evaluation of outlet angle of a given cascade geometry represents the core concept at the base of performance analysis of fans and off design performance evaluation. In this framework, estimation of outlet angle β_2 from a cascade of known geometry consists the first step for performance estimation. In fact, all machine main features, such as total pressure rise, absorbed power, absorbed torque and total efficiency, depend on this estimate. The implemented models for β_2 calculation, can be classified into two groups, depending on the theoretical principles from which they were generated: 2D-Single-Blade (2DSB) and Empirical models. Empirical models are a set of rules and relations evolved from available experimental two-dimensional cascade data. Correlations are based on variation of performance parameters (outlet angle β_2, deviation angle and cascade losses) with maximum profile thickness, cascade solidity and inlet flow conditions. Correlations were obtained from experiments restricted in the region of minimum losses on two families of blade section: C4 circular-arc camberline and NACA 65-(A10)10 series. A series of correction enables the user to take into account deviation for different profiles though only by mean of different thickness distribution (τ/l), different camber and camberline shape ($g(\theta)$). In this case so estimation for outlet angle β_2 will result in:

$$\beta_2 = \beta_2(\sigma, \tau/l, \theta, g(\theta), \beta_1) \tag{1.50}$$

2DSB models uses all blade section geometric properties. In this case a real bidimensional flow simulation is performed in order to calculate aerodynamic parameters of a single airfoil of the cascade, in particular C_L and C_D coefficients in function of the blade angle of attack. Estimation for outlet angle β_2 will result in:

$$\beta_2 = \beta_2(\sigma, C_L, C_D, \beta_m, \beta_1) \qquad (1.51)$$

It must be stressed out that new deviation models can be easily implemented in the code; this flexibility is the most important feature of AxLab, making this tool perfect for numerical design optimization and application for metamodel correlations.

1.6.3 Actuator disk solver

Prediction of fan operational characteristics such as power consumption, efficiency, total pressure rise and noise production assumed during the past years a pivotal role for fan industry. In fact, these characteristics are traditionally used to optimize the product design, reduce manufacture costs and reduce costs and time related to test and certifications of products. In recent years, the objective of fan optimization has, in most cases, been re-focused on the optimization of the fan-system coupling in a view to solve for the dynamics of such coupling (either mechanically or aerodynamically). This has been true when ventilating systems are equipped with components such as bended inlets, spinner cones, gravity dampers, that could be responsible for influencing the fan aerodynamic response. In all these cases, when using CFD, accounting for a real fan geometry inside the domain would be extremely expensive from a computational point of view and too slow for industrial purposes. When the objective under investigation is the whole ventilation system, it is necessary to account for the single components by means of "reduced-order" methodologies.

Recent push is therefore oriented in the development of a methodology for substituting time consuming CFD investigations of operational characteristics of axial fan for industrial ventilation by "synthetics" models. This kind of models can reproduce main operational characteristics of fans, allowing designers to explore a wide range of design space and solve optimization problems. Actuator Disc (AD) model simplify the fan as a discontinuity in pressure within a three-dimensional duct system by adding body forces inside the momentum equation. The simplifying assumption used in the actuator disc modelling technique result in the blade-to-blade flow field not being modelled, reducing computational costs. Reduction in computational cost can be used to simulate the environment in which the fan is operating testing complex systems and the behaviour of the fan inside them. The possibility to have prediction for a large amount of different geometries in short time supports the development of new performance correlations and design procedures, that are the key point to place on the market innovative, more effective and more efficient products.

Commonly "AD analysis" or "AD approach" refers to the meridian plane analysis of a turbomachine using cascade theory that, as described in Section 1.6.2, enables to overcome gross and unnecessary approximation accepted in the radial equilibrium solution approach, considering the progressive development of axial velocity profile through blade row. Originally developed by Betz on his well-known work for wind turbine theory, was then imported for compressor analysis by Horlock [22]. Since its development, history of the use of actuator disk model has a recurrent trend: (i) reduce computational time of another computational method, or simplify calculation in order to take into account system effects. For example, Gannon et al. [23] incorporated, in their streamline throughflow method code, a step change in the form of a prescribed tangential velocity distribution,

and they were able to model the meridional streamline position to within 0.3% of the an-alytical solution of Dixon [9]. Thiart et al. [24] defined an AD method that was used to investigate the effect of distorted inlet conditions on the performance of a large diameter axial flow fan by incorporating it into a CFD code. This was based on the work by Per-icleous et al. [25] who simulated an agitator in a chemical reactor, also using CFD. An axial flow fan AD model has subsequently been used extensively by Meyer et al. [26] and Bredell [24] to investigate various aspects of the performance of air cooled heat exchanger systems.

The AD model synthetizes the effect of the fan by momentum exchange between the blades and the fluid. This can be estimated by adding a source term fi into momentum equation:

$$f_i = \frac{1}{2} w_m^2 \sigma F_i \frac{1}{\Delta z}, \qquad (1.52)$$

where w_m is the average velocity vector, σ the local solidity, Δz the axial thickness of the actuator disk, $i = x, y, z$ and F_i the i-component of the aerodynamic coefficient. To compute this term, it is necessary to model the blade as a series of radial sections and derive, for each blade section, the polar curves of the profile. The solver computes w_m and AoA at runtime according to the local flow and calculate F_i from these polar curves (that are given as input). As the blade is modeled in a discrete number of sections, from hub to shroud, F_i are estimated at intermediate radii by linear interpolation of C_l and C_d. The AD is not able to reproduce all the tip-leakage flow effect, being modelled neither the blade passage nor the tip gap. However, the losses due to the presence of the tip gap are estimated making use of the model presented by Vavra [27], affecting the flow field especially in the near-tip region and leading, in certain configuration, to flow recircula-tion at the tip. Regarding the AD developed in the turbomachinery group in Sapienza, the incompressible Navier-Stokes equations were solved with OpenFOAM 2.4.x, a finite volume solver written in C++ [28]. Several advances in traditional actuator disk model can be introduced like introduction of Coriolis force, blade cross flow, delay stall and in the end the use of different turbulent closure models.

Chapter 2

Metamodeling

E ancora che la natura cominci dalla ragione e termini nella sperienza,
a noi bisogna seguitare il contrario, cioè cominciando dalla sperienza,
e con quella investigare la ragione.

Altough nature commences with reason and ends in experience,
it is necessary for us to do the opposite, that is to commence with experience,
and from this to proceed to investigate the reason.

Leonardo da Vinci

2.1 Introduction

Computation-intensive design problems are becoming increasingly common in manufacturing industries. The computation burden is often caused by expensive analysis and simulation processes in order to reach a comparable level of accuracy as physical testing data. To address such a challenge, approximation or metamodeling techniques are often used. Metamodeling techniques have been developed from many different disciplines including statistics, mathematics, computer science, and various engineering disciplines. The analytical model of an already established model, such as CFD or FEA, is often called metamodel, surrogate model (SM) or surface response and operations needed to create a metamodel are named metamodeling. Metamodels have been found to be a valuable tool to support a wide scope of activities in modern engineering design, especially design optimization.

As a matter of fact, the modern engineering design process often relies on numerical analysis codes to evaluate candidate design, a setup which formulates an optimization problem which involves a computationally expensive black-box function. Such problems are often solved using an algorithm in which a metamodel approximates the true objective function and provides predicted objective values at a lower computational cost.

Approximation of the model is the pivotal point that will determine how much the metamodel will be useful or not. The goal of approximation, in general, is to achieve a model that behaves exactly as the original model at a reasonable cost. Metamodel activity can be effectively splitted into three main activities: (i) sampling, (ii) metamodel choice and (iii) model validation. These steps are briefly illustrated in this chapter, in particular focusing on two metamodels approaches that have been widely used in the published works.

2.2 Design of experiments

Within the theory of optimization, an experiment is a series of test in which the input variables are changed according to a given rule in order to identify the reasons for the

changes in the output response [29]. Thus, Design of Experiments (DOE) is inherently a multi-objective optimization problem regarding the selection of the points that maximize the accuracy of the information obtained by experiments (whether numerical or physical). In addition, in the design applications, which are of primary interest in this work, we would like to construct a surrogate model that could be used to predict the performance of other designs. In this case, our primary goal is to choose the points for the experiments so as to maximize the predictive capability of the model. In other terms, the creation of a metamodel requires a number of training points; the way in which these training points are created and the location of these points affects the accuracy of the metamodel as well as the number of points required to create the metamodel.

Statistical experimental design, together with the basic ideas underlying DOE, was born in the 1920s from the work of Sir Ronald Aylmer Fisher [30]. Fisher was the statistician who created the foundations for modern statistical science. The second era for statistical experimental design began in 1951 with thework of Box and Wilson [31] who applied the idea to industrial experiments and developed the RSM. The work of Genichi Taguchi in the 1980s [32], despite having been very controversial, had a significant impact in making statistical experimental design popular and stressed the importance it can have in terms of quality improvement.

In order to perform a DOE it is necessary to define the problem, choose the variables (which are called factors by the experimental designer) and define the design space, or region of interest, which is the range of variability for each factor. Each factor can assume different values, or levels, according to its discretization within the design space. The DOE technique and the number of levels are to be selected according to the number of experiments which can be afforded. In experimental design, the objective function and the set of the experiments to be performed are called response variable and sample space respectively.

Classic sampling methods are based on Design of Experiments and tend to spread samples points around boundaries of the design space leaving few in the centre to reduce random error influence on fidelity of a dataset. Classic DOE include fractional [33] or fractional factorial, Central Composite Design (CCD) [33] or Box Behnken [33], alphabetical optimal [34, 35] and Plackett-Burman [33]. On the contrary from what happens in physical experiments, computer experiments involve mostly systematic errors and a good experimental design tends to fill the design space rather than to concentrate on the boundary as stated in Saks [36] and Simpson [37]. Furthermore for deterministic computer codes CCD and D-optimality designs, can be inefficient or even inappropriate. Koehler and Owen [38] described several Bayesian and frequentist "space filling" designs, including maximum entropy design [39], mean squared-error designs, minimax and maximin designs [40], Latin hypercube designs, orthogonal arrays, and scrambled nets. More diffused in literature are orthogonal arrays [41, 42], various Latin hypercube designs [43, 44, 45, 46, 47], Hammersley sequences [48, 49], and uniform designs [50]. A comparison of these sampling methods can be found in [51]. Concerning the sample size it is found in the reference that depends on the complexity of the problem that must be approximated. In general a higher number of points provide a more information but at higher cost. When the function is low order after reaching a certain sample size the accuracy is not affected by a larger sample size.

2.3 Metamodeling

A metamodels, surrogate models or response surface, is an approximation of a model (experiment or simulation) used to construct simpler and lower computational cost models [52]. It is built basing on the response of the models to a limited amount of intelligently chosen points to capture the relationship between the input and output variables. The physical model is treated as a black box and SMs understand the connection between input and output data with a bottom-up approach. Clearly, employing such models entails a loss in accuracy due to the lack of physics, replaced by a pure empirical and inductive relationship among available data.

The objective function, or response variable, *y* is an unknown vector function of the input variables $f(\mathbf{x})$. The response surface $\tilde{y}$ is an approximation of this function and is represented as:

$$\tilde{f}(\mathbf{x}) = f(\mathbf{x}) + \varepsilon(\mathbf{x}), \tag{2.1}$$

with $\varepsilon(\mathbf{x})$ the error between the original and modelled function. $\tilde{f}(\mathbf{x})$ is the regression function, behind which is concealed the techniue used: artificial neural network [53], least squares methods [54], Kriging [55], support vector machines [56], radial basis functions [57], [58] and rational functions are some of them.

Considering their empirical nature, all the SMs need to be trained through as many data as possible to calculate the internal weights among the factors. Every factor is linked to another following the architecture typical of the chosen SM. In general, the more data are available, the more the SMs are accurate in the prediction of the Physics. Unfortunately, this is not always true. Indeed, the ability of a SM in the prediction is often a combination of a good number of training samples and the fitting level of complexity of the model. In other words, when the chosen SM is very complex, a lot of training samples are required, otherwise it is not possible to calculate all the factor's weights. On the other hand, when the surrogate model is very simple, a too large number of training samples can yield to lack of accuracy, because there are not enough unknowns (weights) for all the inputs.

Training a good SM is often an iterative problem, where the first samples, derived from experimental data and simulations, are used to construct the first surrogate model which will be refined with additional samples.

2.3.1 Least squares method

Least squares method (LSM) is a standard approach in regression analysis and it is used to solve overdetermined systems. This method can be interpreted as a method for data fitting and was developed by Gauss around 1795 and published several years later [54]. It consists of adjusting the coefficients of a model function (the response surface) so that it best fits a data set (the results of a DOE run). A polynomial approximation is created by using a least squares fit approach [59] over a number of training points

The model function is a function $\tilde{f}(\mathbf{x}, \beta)$, where $\beta = [\beta_1, ..., \beta_p]^T$ is the vector of the *p* coefficients, or *regressors*, to be tuned, $\mathbf{x} = [x_1, ..., x_k]^T$ is the vector of the *k* input parameters and $\tilde{f}$ is a vector function of *p* elements that consist of powers and cross-products of power of $\mathbf{x}$ up to a certain degree $d \geq 1$.

Two important models are commonly used in LSM and include the first degree model ($d = 1$),

$$y = \beta_0 + \sum_{i=1}^{k} \beta_i x_i + \varepsilon \tag{2.2}$$

and the second-degree model ($d = 2$),

$$y = \beta_0 + \sum_{i=1}^{k} \beta_i x_i + \sum \sum_{i<j} \beta_{ij} x_i x_j + \sum_{i=1}^{k} \beta_{ii} x_i^2 + \varepsilon \qquad (2.3)$$

When modelling a quadratic response surface, the minimum number of regressors required to solve all the coefficients in the second order polynomial is $(k+1)(k+2)/2$, being k the number of factors; to fit quadratic response surfaces, at least the same number of points and three levels for each design factor are required.

The purpose of considering LSM is threefold:

- To establish a relationship, albeit approximate, between *y* and **x** that can be used to predict response values for given settings of control variables

- To determine, through hypothesis testing, significance of the factors whose levels are represented by **x**

- To determine the optimum settings of **x** that result in the maximum (or minimum) response over a certain region of interest

2.3.2 Artificial neural network

An *Artificial Neural Network* (ANN) is a mathematical tool employed in computer science, initially developed for pattern recognition and today largely employed mainly for: fitting, pattern recognition, clustering and prediction. Such systems learn to do tasks by considering examples, generally without task-specific programming.

An ANN is made up of elementary units, the *neurons*, which receive input, change their internal state according to that input and produce output depending on the input and an activation function. The neurons are linked together in order to singularly process an incoming information and exchange the processed information with other neurons. This network, formed by connecting the output of certain neurons to the input of other neurons, composes a directed and weighted graph, where the neurons are the nodes and the connection between the neurons are weighted directed edges. The weights and the activation functions can be modified by a process called training, which is governed by a training rule.

A single neuron is composed by three different functional operators. First, a scalar input X is multiplied by a scalar weight w and the resulting vector is summed to the scalar bias b to form the net input z. The final step is accomplished by the transfer or activation function $\sigma(z)$ that produces the neuron output a. The weight w and the input z represent the adjustable parameters of the neuron, producing a different response to the same input. The transfer function σ must be set in advance and determines the kind of the neuron; several possibilities are available, common options are linear function or tangential sigmoid, but according to the problem, one may use other sigmoid or inverse functions, as well as radial basis functions.

The idea below the ANN is that each neuron can be set so as to produce a certain individual transfer function; by coupling many neurons and let them communicate, sharing input and outputs, it is possible to obtain an overall model which can be trained in order to fit the problem.

In order to solve a regression problem, once selected the activation function and the overall architecture of the net, in terms of layer number and neuron on each layer, weights and bias for each connection between layers must be set. The process of tuning these parameters in order to fit the network to a certain dataset is known as "training".

A sample points is required to feed the net and train the parameters; generally the data are first preprocessed and classified, then the net is trained using a dedicated algorithm and, finally, the data are postprocessed. Usually, the sample is splitted into three sub-set: a "training dataset" containing the majority of the total samples, a "validation dataset" and a "test dataset". The aim of the training can be to minimize the mean squared error between the target t_{ik} and the response a_{ik} of the network. In order to do that, the training algorithm updates the biases and computes the response for the "training dataset". The "validation dataset" is used to evaluate the performances of the network; in fact, usually, the mean squared error reaches a minimum during the training and the final parameters of the network are those corresponding to the iteration in which that minimum occurred. The "test dataset" is used to further validate the network. The use of these three sets is needed to verify that a good response is available also for those points which are not directly involved in the training.

Different training algorithms can be used; the simplest is the gradient descent, which updates the parameters in the direction where the performance (*e.g.* the mean squared error) decreases faster. Several methods are available and provides different performances, according to the problem treated. The Levenberg-Marquardt algorithm is typically the first choice if the dataset is not too large, but the Bayesian Regularization can provide better accuracy for challenging problems. It is common to test many algorithms and then choose the best, since no *a priori* knowledge is often available, except for the experience of the analyst.

Multi-Layer Perceptron

When dealing with regression and function approximation, there are some categories of ANN which are known to be more suitable, as the *Feedforward Neural Network* (FNN). In this network, the information moves in only one direction, forward, from the input nodes, through the hidden nodes (if any) and to the output nodes; in other terms, there are no cycles or loops in the network.

An important class of FNN is the *Multi-Layer Perceptron* (MLP), which consists of three or more layers (an input and an output layer with at least one or more hidden layers); each layer takes information from upstream, elaborates it and sends it downstream, without interaction between the neurons of the same level. Figure 2.1 reports a sketch of a MLP with a single layer of k hidden neurons, working on i training samples, with j independent variables and returning m predicted dependent variables. In this scheme, multiple inputs (X_{ij}) are multiplied by weights (w_{jk}), and the resulting vector is then added to a bias vector (b_{1k}) to obtain the net input (z_{ik}). The neurons of the hidden layers are the inputs of the output layer; this final step is accomplished by the transfer or activation function ($\lambda(z_{ik})$) that produces the neuron's output (a_{ik}). Multi-layer networks use a va-
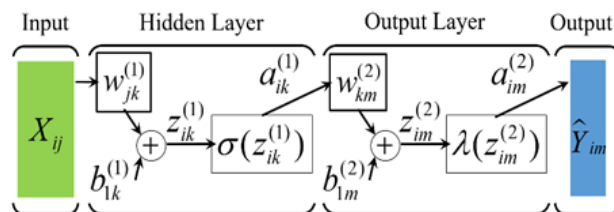
FIGURE 2.1: An example of MLP neural network.

riety of learning techniques, the most popular being back-propagation. Here, the output values are compared with the correct answer to compute the value of some predefined

error-function. By various techniques, the error is then fed back through the network. Using this information, the algorithm adjusts the weights of each connection in order to reduce the value of the error function by some small amount. After repeating this process for a sufficiently large number of training cycles, the network will usually converge to some state where the error of the calculations is small. In this case, one would say that the network has learned a certain target function. To adjust weights properly, one applies a general method for non-linear optimization that is called gradient descent. For this, the network calculates the derivative of the error function with respect to the network weights, and changes the weights such that the error decreases (thus going downhill on the surface of the error function). For this reason, back-propagation can only be applied on networks with differentiable activation functions. MLPs are useful in research for their ability to solve problems stochastically, which often allows approximate solutions for extremely complex problems like fitness approximation.

2.4   Model validation

Metamodels, especially global metamodels, are to be validated before being used as a "surrogate" of the computation-intensive processes. Model validation has been a challenging task, and it shares common challenges with the verification and validation of other computational models [60], [61]. There are different methodologies used nowadays for model validation: Meckesheimer et al. [49], [62] studied the cross-validation method and p-fold cross validation, Mitchell and Morris [63] described a variation of p-fold cross validation is the leave-k-out approach. Until now there are plenty of applications these models, but anyway, in literature there is still confusion above which is the best, if there is one, and what method should be used in relation with different methodologies of meta-modeling.

This section presents two methodologies for model fitness validation and statistical significance of the used factors that have been extensively used in all the works attached.

2.4.1   Model fitting test results

In practice, no model can fit perfectly the measured values because of measurements errors or relationships between factors response that cannot be described by the surrogate model, resulting in residual values at the design point. The quality of the model is assessed by the coefficients of determination R^2, *adjusted R^2*, *partial R^2* and *predicted R^2*. These coefficients are based on the partition of the sums of squares deviations or errors, that is here briefly introduced. We will refer to a regression analysis with n number of test, k regressors and m number of unique test (excluded replicates).

Partition of sums of squares

The partition of sums of squares deviations or errors is a measure of dispersion (or variability) and is a concept that permeates much of inferential statistics and descriptive statistics. When scaled for the number of degrees of freedom, it estimates the variance, or spread of the observations about their mean value. Partitioning of the sum of squared deviations into various components allows the overall variability in a dataset to be ascribed to different types or sources of variability, with the relative importance of each being quantified by the size of each component of the overall sum of squares. The partition of sums of squares is defined as:

$$TSS = SSR + ESS \tag{2.4}$$

Total Sum of Square (TSS); is defined as the sum, over all observations, of the squared differences of each observation from the overall mean. In regression model, the TSS is the sum of the squares of the difference of the dependent variable y_i and its mean $\bar{y}$:

$$TSS = \sum_{i=1}^{n}(y_i - \bar{y})^2 \tag{2.5}$$

Sum of Squared Residual (SSR); also referred to sum of squared errors of prediction (SSE), is a measure of the discrepancy between the data y_i and an estimation model $\hat{y}_i$. A small SSR indicates a tight fit of the model to the data.

$$SSR = \sum_{i=1}^{n}(y_i - \hat{y}_i)^2 \tag{2.6}$$

In case more than one value of the response variable for at least one of the values of the set of predictor variables is available, it is possible to split the SSR in two components, the Lack-of-Fit Sum of Square (LFSS) and the Pure Error Sum of Square (PESS):

$$SSR = LFSS + PESS \tag{2.7}$$

LFSS is used in the numerator in an F-test of the null hypothesis (that will be introduced in the following section) that says that a proposed model fits well. It is used to assess whether the model is adequate to describe the functional relationship between the experimental factor and the response an it is associated with variation due to factors other than measurement error. The LFSS is the weighted sum of squares of the differences between each average $\bar{y}_j$ corresponding to the same $\mathbf{x_j}$ value and the corresponding fitted value $\hat{y}_{ij}$ [64]. If c is the number replicated tests and t is the number of the data in each replicated block,

$$LFSS = \sum_{j=1}^{c}\sum_{i=1}^{t}(\hat{y}_{ij} - \bar{y}_j)^2 \tag{2.8}$$

PESS is the sum of squares of the differences between each observed y_{ij} value and the average of all $\bar{y}_j$ values corresponding to the same $\mathbf{x_j}$ value,

$$PESS = \sum_{j=1}^{c}\sum_{i=1}^{t}(y_{ij} - \bar{y}_j)^2 \tag{2.9}$$

Explained Sum of Squares (ESS); alternatively known as the model sum of squares, is a quantity used in describing how well a model, often a regression model, represents the data being modelled. In particular, ESS measures how much variation there is in the modelled values and this is compared to the TSS, which measures how much variation there is in the observed data, and to the SSR, which measures the variation in the modelling errors.

$$ESS = \sum_{i=1}^{n}(\hat{y}_i - \bar{y})^2 \tag{2.10}$$

Coefficient of determination R^2

R^2 is a statistic that represents a pure correlation between measured and predicted values and is indicative of response variation explained by a model. It is in the context of statistical models whose main purpose is either the prediction of future outcomes or the testing of hypotheses, on the basis of other related information. In regression R^2 measures how the regression surface approximates the real data set and provides a measure of how well

observed outcomes are replicated by the model, based on the proportion of total variation of outcomes explained by the model:

$$R^2 = \frac{ESS}{TSS} = 1 - \frac{SSR}{TSS} \tag{2.11}$$

However, being R^2 monotone in the number of variables when dealing with ordinary least square, a meaningful comparison between two models can be led with the *Adjusted R^2*.

Adjusted R^2

Adjusted R^2 is a statistic that is used to compare the explanatory power of models and its value increases only when an added term improves the model more than by chance [65]. Its value will always be less or equal to R^2. Unlike R^2, the *Adj R^2* increases only when the increase in R^2 (due to the inclusion of a new explanatory variable) is more than one would expect to see by chance. The *Adj R^2* can have a peak while increasing the predictors, while the R^2 continues to increase. If a set of explanatory variables with a predetermined hierarchy of importance are introduced into a regression one at a time, with the *$AdjR^2$* computed each time, the level at which *Adj R^2* reaches a maximum would be the regression with the ideal combination of having the best fit without excess, *i.e.*, unnecessary terms.

$$AdjR^2 = 1 - (1 - R^2)(n-1)/(n-k) \tag{2.12}$$

Adj R^2 does not have the same interpretation as R^2; while R^2 is a measure of fit, *Adj R^2* is instead a comparative measure of suitability of alternative nested sets of explanators. As such, care must be taken in interpreting and reporting this statistic. *Adj R^2* is particularly useful in the feature selection stage of model building.

Partial R^2

It can be defined as the portion of variation that cannot be explained in a reduced model, but can be explained by the predictors specified in a fuller model. This coefficient is used to provide an insight into whether or not one or more additional predictors may be useful in a more fully specified regression model [66]. The calculation for the *partial R^2* is relatively straight forward after estimating two models, the *full* and the *reduced*, and generating the ANOVA tables for them (see next section).

$$PartR^2 = ESS_{red} - \frac{ESS_{full}}{ESS_{red}} \tag{2.13}$$

Predicted R^2

R^2 and *Adj R^2* are calculated using data that were themselves used for model development. A model predicted capability for new observations is assessed using *predicted R^2*. It is calculated by systematically removing each observation from the data set, estimating the regression equation and determining the model's capability in predicting the removed observation. The predictive residual sum of squares statistic is used to calculate the value of predicted *predicted R^2* [67].

$$PredR^2 = 1 - \frac{SSR_{pred}}{TSS} \tag{2.14}$$

2.4.2 Analysis of variance

As introduced in Section 2.3.1, one of the advantage of a LSM in regression analysis is the possibility to determine, through hypothesis testing, the significance of the factors considered in the regression function. The statistical significance of the terms of the models can be evaluated using the analysis of variance (ANOVA) [68], that is a collection of statistical model used to analyse the differences among group means and their associated procedures. The observed variance in a particular variable is partitioned into components attributable to different sources of variation.

ANOVA is a particular form of statistical hypothesis testing heavily used in the analysis of experimental data and its terminology is largely from the statistical design of experiments. There are no necessary assumptions for ANOVA in its full generality, but the *F-test* used for ANOVA hypothesis testing has assumptions and practical limitations which are of continuing interest. These concepts are of fundamental importance in ANOVA applications and are briefly recap here.

Null hypothesis; in inferential statistics, the null hypothesis is a general statement or default position that there is no relationship between two measured phenomena, or no association among groups. Rejecting the null hypothesis, concluding that there are grounds for believing that there is a relationship between two phenomena, is a central task in the modern practice of science. The null hypothesis (H_0) is generally assumed to be true until evidence indicates otherwise. In regression, the null hypothesis always pertains to the reduced model, while the alternative hypothesis (H_1) pertains to the full model.

Null distribution; in statistical hypothesis testing, the null distribution is the probability distribution of the test statistic when the null hypothesis is true [69]. In a *F-test*, the null distribution is an *F-distribution*.

F-distribution; in probability theory and statistics, the *F-distribution* is a continuous probability distribution that arises frequently as the null distribution of a test statistic, most notably in the analysis of variance, *e.g.*, *F-test* [70].

F-Test

An *F-test* is a statistical test in which the test statistic has an *F-distribution* under the null hypothesis. It is used when comparing models that have been fitted to a data set, in order to identify the model that best fits the population from which the data were sampled, or, in other words, to identify statistically significant terms of the model. Common examples of the use of *F-test* include the study of the following cases:

- The hypothesis that a proposed regression model fits the data well (Lack-of-fit Sum of Square)

- The hypothesis that a data set in a regression analysis follows the simpler of two proposed models that are nested within each other

- The hypothesis that a means of a given set of normally distributed populations, all having the same standard deviation, are equal. This *F-test* plays an important role in the analysis of variance

Most *F-tests* consider a decomposition of the variability in a collection of data in terms of sums of squares. The statistic in an *F-test* is the ratio of two scaled sums of square reflecting different source of variability. These sums of squares are constructed so that the statistic tends to be greater when the null hypothesis is not true. In order for the statistic to follow the *F-distribution* under the null hypothesis, the sums of square should be statistically independent and each should follow a scaled chi-squared distribution. The

latter condition is guaranteed if the data values are independent and normally distributed with a common variance.

F-test in regression problem; in regression, when considering the full and the reduced model, each one respectively having k_{full} and k_{red} parameters, the full model will always be able to fit the data at least as well as the model with fewer parameters. But one often wants to determine whether the full model gives a significantly better fit to the data. A typical approach to this problem is to use an *F-test* to decide whether or not to reject the null hypothesis (the reduced model) on favour of the larger model.

$$F = \left(\frac{SSR_{red} - SSR_{full}}{k_{full} - k_{red}} \right) \Big/ \left(\frac{SSR_{full}}{n - k_{full}} \right) \tag{2.15}$$

Under the null hypothesis, the full model does not provide a significantly better fit than the reduced model, so *F* will have an *F-distribution* with $(k_{full} - k_{red}, n - k_{full})$ degrees of freedom. The null hypothesis is rejected if the *F* calculated from the data is greater than the critical value of the *F-distribution* for some desired false-rejection probability (*e.g.* 0.05)

F-test for Lack-of-Fit; the ratio of mean square for LFSS and PESS follows *F-statistic*. Low value of false-rejection probability for LFFS means that the analysed model does not fit to the experimental data.

$$F = \frac{\frac{LFSS}{m-k}}{\frac{PESS}{n-m}} \tag{2.16}$$

If the model is correct, *F* has an *F-distribution*. If it is wrong, the quotient as a whole has a non-central *F-distribution*. One uses the *F-statistic* to test the null hypothesis that there is no lack of linear fit; since the non-central *F-distribution* is stochastically larger than the central *F-distribution*, one rejects the null hypothesis if the *F-statistic* is larger than the critical *F-value*. This critical value corresponds to the cumulative distribution function of the *F* distribution with *x* equal to the desired confidence level and degrees of freedom $d_1 = m - k$ and $d_2 = n - m$.

p-value

In statistical hypothesis testing, the *p-value* is defined as the probability for a given statistical model, under the null hypothesis H_0, of obtaining a result equal to or more extreme than what was observed [71]. The hypothesis H_0 is rejected if any of these probabilities is less than or equal to a small pre-defined level of significance. A result is said to be statistically significant if it allows us to reject the null hypothesis.

p-value in regression problem; one can obtain *p-value* from an *F-test* for each term of the model, which are a measure of the probability of obtaining data at least as extreme as the data from the model, assuming the null hypothesis is true, *i.e.*, in this case, a particular term does not provide an effect on the results from the model. Therefore, the lower *p-values* for analysed terms, the greater effect these terms have on the response predicted by the model. The *p-value* answer the question: "what's the probability that we had get an *F-statistic* as large as we did, if the null hypothesis were true?"

- If *p-value*< 0.05 we reject the null hypothesis and we favour the full model. In this case, the empiric evidence is contrary to the null hypothesis and the observed data have statistical significance

- If *p-value*> 0.05 we fail to reject the null hypothesis and we favour the reduced model

For the same number of degree of freedom, the higher the *F-value*, the lower the *p-value*.

For all Source of Variation (**SV**) of the model equation, values characteristic of a so-called ANOVA table are calculated individually and presented in Table 2.1. The statistical significance of each term in the model equation can be evaluated by applying the aforementioned statistic tests to the *Adjusted Sum of Square* (*Adj. SS*), which calculates, for a specific, the reduction in SSR resulting from the inclusion of the x_i term to the model:

$$Adj SS(x_i) = ESS(x_i|red) = SSR_{red} - SSR_{full}, \qquad (2.17)$$

where the notation $(x_i|red)$ indicates the inclusion of the x_i term in the reduced model, which includes all the other variables. *Adjusted mean squares* (*Adj MS*) are calculated by dividing *Adj. SS* by the number of Degrees of Freedom (*DF*) for the specific term. These statistics are of primary importance when comparing the full model with the reduced model obtained by omitting the variable in question. Variation in the data unexplained by the model is represented by the *Residual Error* (*RE*) for which *Adj SS* is calculated as the SSR and *Adj MS* value for the *RE* is calculated as explained above.

Ratios of the *Adj MS* for all terms of the model equation and *Adj MS* of the *RE* are calculated. Because the ratios of variances follow an *F-distribution* [72], a statistical *F-test* is employed to identify statistically significant terms of the model.

SV	DF	Adj SS	Adj MS	F-ratio	p-value
Explained	$k-1$	$ESS_{tot} = \sum_i^n (\hat{y}_i - \bar{y})^2$	$EMS_{tot} = ESS_{tot}/(k-1)$	EMS_{tot}/MSR_{tot}	p_{ESS}
x_1	1	$ESS(x_1|red) = SSR_{red} - SSR_{full}$	$EMS_{x_1|red} = ESS$	$EMS_{x_1|red}/MSR_{tot}$	p_{x_1}
...	...	...	...	...	...
x_k	1	$ESS(x_k|red) = SSR_{red} - SSR_{full}$	$EMS_{x_k|red} = ESS$	$EMS_{x_k|red}/MSR_{tot}$	p_{x_k}
Residual	$n-k$	$SSR_{tot} = \sum_i^n (y_i - \hat{y}_i)^2$	$MSR_{tot} = SSR_{tot}/(n-k)$		
Lack of Fit	$m-k$	$LFSS = \sum_j^c \sum_i^t (\hat{y}_{ij} - \bar{y}_j)^2$	$LFMS = LFSS/(m-k)$	LFMS/PEMS	p_{LFSS}
Pure error	$n-m$	$PESS = \sum_j^c \sum_i^t (y_{ij} - \bar{y}_j)^2$	$PEMS = PESS/(n-m)$		
Total	$n-1$	$TSS = \sum_i^n (y_i - \bar{y})^2$	$PEMS = PESS/(n-m)$		

TABLE 2.1: ANOVA table.

2.5 Role of metamodeling in design optimization

A metamodel is an analytical function, thus an optimization based on such a model is very fast and does not require additional experiments or simulations to be performed.

Optimization performed using the metamodel instead of the original model is called Surrogate-based optimization. Benefits were indicated from Haftka and co-authors [73], [74]: (i) optimization can be performed using or connecting different (and often expansive) simulation codes that the model will replace without any additional complications; (ii) generally MBDO uses algorithms that evaluate different elements. This process is extremely simple to be parallelized decreasing computational time; (iii) metamodel acts as a filter for numerical or experimental noise; (iv) metamodel cant be compared with a theoretical model but renders to users an enhanced awareness of design space; and (v) since all design space is analyzed it is easier to detect errors in simulations.

Simpson et al. [75] and Wang and co-author [76] gave a focused review on meta-models and Surrogate-based optimization describing in detail all parts that compose a MBDO process: (i) sampling, (ii) approximation models, (iii) metamodel strategies and (iv) applications.

In conclusion, the use of metamodels can be very advantageous, and can be applied even when little is known about the problem, although it must be kept in mind that if the design space exploration (made with the DOE or the RSM model adopted) is poor, and the response variable is particularly irregular, the result of the MBDO can be far from the truth because of the bad estimation of the model coefficients or the choice of an unsuitable model.

For all these considerations, the use of metamodels in optimization loops is recognized as a critical issue and will be extensively treated in the following chapter.

Chapter 3

Optimization

<div align="right">

Παῦροι γάρ τοι παῖδες ὁμοῖοι πατρὶ μέλονται,
οἱ πλέονες κακίους, παῦροι δέ τε πατρὸυ ἀρείους.

For rarely are sons similar to their fathers,
most are worse, and a few are better than their father.

Homer, The Odyssey

</div>

In mathematics, computer science and operations research, optimization, or mathematical programming, is the selection of a best element (with regard to some criterion) from some set of available alternatives.

In a qualitative way the optimization procedure consists in a series of operations allowing to change a configuration in order to attain a desired performance, bound to the respect of some kind of constraints. In engineering application the procedure is typically recursive, since some explicit models of the problem are missing and a straightforward formalisation is not available. The procedure is then configured as a loop, invoked several times, within which are present various "subsystem", each one with a specific function. The optimization properly said is a part of this loop and is a mathematical problem, whose formalisation will be given later. Translating an operative challenge into a mathematical model is a necessary step for the optimization and its results will be obviously greatly affected by the hypothesis and approximations embedded in them.

3.1 Mathematical formulation of the optimization problem

A general optimization problem can be represented in the as:

$$
\begin{aligned}
\text{Minimize} \quad & f_i(\mathbf{x}) \\
\text{Such that:} \quad & g_j(\mathbf{x}) = 0 & j = 1, m \\
& h_k(\mathbf{x}) \leq 0 & k = 1, l
\end{aligned}
$$

where:

- $\mathbf{x} = (x_1, ..., x_n)$ is the vector of the design variables

- $f_i(\mathbf{x}) : \Omega \subseteq R^n \longrightarrow R$ is the $i - th$ objective (or fitness) function

- $g_j(\mathbf{x})$ is the $j - th$ equality constraint function

- $h_k(\mathbf{x})$ is the $k - th$ inequality constraint function

If $i = 1$ the problem is single objective, otherwise is multi-objective. Note that looking for the minimum of f is not restrictive, hence each maximization problem can turn into a minimization one by inverting the objective.

3.2   Multi-objective optimization

Usually, an engineering optimal design is a Multi-Objective Optimization Problem (MOOP), in which several fitness functions are involved . However, these objective are often inter-related and different goals can be in tension with each other; compromise solutions have to be sought and the final selection between such compromises inevitably involves deciding on some form of weighting between the goals. However, before this stage is reached it is possible to study design problems from the perspective of Pareto fronts and dominating solutions.

A Pareto set of designs is one whose members are all optimal in some sense, but where the relative weighting between the competing goals is yet to be finally fixed [77]. In other words, a Pareto set of designs contains systems that are sufficiently optimized that, to improve the performance of any set member in any one goal function, its performance in at least one of the other functions must be made worse. Moreover, the designs in the set are said to be *non-dominated* in that no other set member exceeds a given design's performance in all goals.

More formally, a vector $\mathbf{v}$ is said to dominate a vector $\mathbf{u}$ if it gives one smaller value than $\mathbf{u}$ for at least one fitness function:

$$\forall i = 1,...,n \quad f_i(\mathbf{v}) \leq f_i(\mathbf{u}) \quad \text{and} \quad \exists j = 1,...,n \quad | \quad f_j(\mathbf{v}) < f_j(\mathbf{u}) \tag{3.1}$$

A vector $\mathbf{x} \in \Omega$ is a Pareto optimal solution if and only if there is no vector $\mathbf{y} \in \Omega$ for which $(f_1(\mathbf{y}),...,f_n(\mathbf{y}))$ dominates $(f_1(\mathbf{x}),...,f_n(\mathbf{x}))$. The set of Pareto optimal solutions forms a Pareto front. Figure 3.1 illustrates an example of a Pareto front P of the feasible design space Y for two objective functions f_1 and f_2 that must be minimized. The optimal solutions for the corresponding fitness function are denoted as f_1^* and f_2^*. In conclusion, the presence of multiple objectives in a problem, in the principle, gives rise to a set of Pareto-optimal solutions; in the absence of any further information, one of these solutions cannot be be said to be better than the other, thus demanding a user to find as many Pareto-optimal solutions as possible.
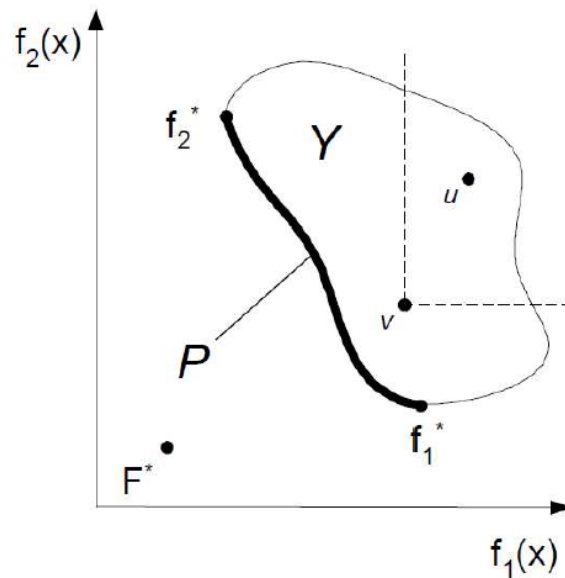
FIGURE 3.1: An example of Pareto front.

There are a number of technical difficulties associated with constructing Pareto sets and currently there appear to be two popular ways for this task:

- Choose a (possibly non-linear) **weighting function** to combine all the goals in the problem of interest into a single quantity and carries out a single objective optimization

- Construct the Pareto sets via the use of population based search schemes, or **evolutionary algorithm** (EA), in which a set of designs is worked on concurrently and evolved towards the final Pareto set in one process

The first approach has several limitations, being not clear what weighting function or constraint values to use and how to alter them so as to be able to reach all parts of the potential design space. In particular, the weighted single objective method will miss Pareto optimal points if the front is not convex.

The second approach is far more interesting because the designs are compared to each other and progressed if they are of high quality and if they are widely spaced apart from other competing designs. Moreover such schemes usually avoid the need for an explicit weighting function to combine the goals being studied. This approach is described in the following section having been extensively used in the works attached to this Thesis.

In general, all the EA are based upon the concept of *sorting* and *diversity preservation*, which are here introduced. In fact, in MOOP is important to have a selection criterion of the individuals among the Pareto front, being the main goal of the optimization problem not only to find a set of solutions as close as possible to the Pareto optimal front, but also to find a set of solutions as diverse as possible, to cover the entire front.

3.2.1 Sorting

When selecting individuals among a population, a *non-domination criterion* can be applied. In non-dominated sorting methods, the population is sorted according to an ascending level of non-domination. For the sake of clarity, here are described a naive and slow procedure of sorting a population into different non-domination levels, and a modern fast non-dominated sorting approach.

In a naive approach is possible to identify the first set of non-dominated solution, in a population of size N by comparing each solution with every other solution in the population to find if it is dominated. If M is the number of objectives, this requires $O(MN^2)$ comparison to find the first non-dominated front; this front receives a rank 1 and is temporarily discounted. The above procedure is repeated to find the second and higher non-dominated levels. The worst case is when there are N fronts and there exists inily one solution in each front, requiring an overall $O(MN^3)$ computations and $O(N)$ storage process.

The fast non-dominated sorting approach is based on the calculation of two entities: 1) domination count n_p, the number of solutions which dominate the solution p, and 2) S_p, a set of solutions that the solution p dominates. All solutions in the first non-dominated front will have their domination count as zero and, for each solution p with $n_p = 0$, we visit each member (q) of its set S_p to reduce its n_p by one. In doing so, if for any member q the domination count becomes zero, we put it in a separate list Q and these members belong to the second non-dominated front. This process continues until all fronts are identified. This approach requires $O(MN^2)$ comparison; in fact, for each solution p in the second or higher level of non-domination, n_p can be at most $N-1$, meaning that each solution p will be visited at most $N-1$ times before its n_p becomes zero. At this point, the solution is assigned a non-domination level and will never be visited again. Since there are at most $N-1$ such solutions, the overall complexity of the procedure is $O(MN^2)$, but the storage requirement has increased to $O(N^2)$.

3.2.2   Diversity preservation

Along the convergence to the Pareto-optimal set, it is also desired that an EA maintains a good spread of solutions in the obtained set of solutions. Traditional mechanism of ensuring diversity have relied mostly on the concept of *sharing*, which has been found to mantain sustainable diversity in a population with appropriate settings of its associated parameters. The main problem with sharing is that it requires the specification of a sharing parameter, σ_{share}, which sets the extent of sharing desired in a problem. Though there has been some work on dynamic sizing the sharing parameter [78] [79], a parameterless diversity-preservation is desirable because:

- The performance of the sharing function method in maintaining a spread of solutions depends largely on the chosen σ_{share} value

- The overall complexity of the sharing function approach is $O(N^2)$ because each solution must be compared with all the other solutions in the population

A new approach that replace the the sharing function approach with a *crowded-comparison* approach that eliminates both the above difficulties has been proposed by Deb [80]. This approach does not require any user-defined parameter for maintaining diversity among populations members which is now ensured by a density estimation based on a *crowding distance*, and by a *crowded-comparison operator*. In particular, the latter guides the selection process at the various stages of the algorithm toward a uniformly spread-out Pareto optimal front following the reported criterion:

- Between two solutions with differing non-domination ranks, the one with the lower (better) rank is preferred

- If both solutions belong to the same front, then the one that is located in a lesser crowded region is preferred

3.3   Optimization algorithm

A variety of optimization strategies are available in literature to solve MOOP. The choice depends upon various aspects, *in primis* the level of knowledge of the objective function and the fitness landscape. Figure 3.2 shows the three major class of optimization techniques researcher may use; finitely terminating methods (algorithms that terminate in a finite number of steps), iterative methods that converge to a solution (on some specified class of problems), or heuristics that may provide approximate solutions to some problems (although their iterates need not converge).

Iterative methods generate a sequence of improving approximate solutions, with the n_{th} approximation derived from the previous one. A termination criteria is implemented in the algorithm and it governs the convergence of the entire procedure. Iterative methods are used to solve problems of non-linear programming and can be classified according to whether they evaluate Hessian, gradients, or only the function values. Even if these methods are theoretically able to find the exact solution, they often require an excessively high computational effort and can fail to converge to the solution.

In this case heuristic (or stochastic) methods can be employed to provide a quicker, even if approximate, solution. This solution may not be the best of all the actual solutions to this problem, or it may simply approximate the exact solution. But it is still valuable because finding it does not require a prohibitively long time.

Among these methods, *evolutionary algorithm* (EA) often perform well approximating solutions to all types of problems because they ideally do not make any assumption
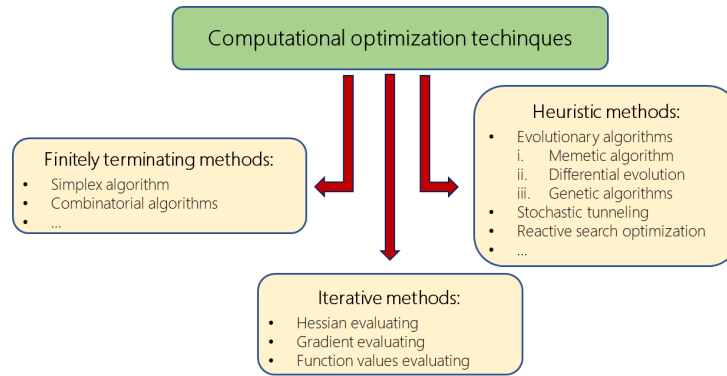
FIGURE 3.2: Different computational optimization techniques.

about the underlying fitness landscape. In addition, as described in the previous section, they are able to find a good spread of solutions in the obtained set of solutions. Over the past decade, a number of Multi-Objective Evoultionary Algorithm (MOEA) has been suggested [81], [82], [83], [84] and [85]. The primary reason for this is their ability to find multiple Pareto-optimal solutions in one single simulation run. Since EA works with a population of solutions, while moving toward the true Pareto-optimal region, it can be used to find multiple Pareto-optimal solutions in one single simulation run. A number of different EA were suggested to solve MOOP; among them, Genetic Algorithm (GA) and its variant Non-dominated Sorting Genetic Algorithm (NSGA) are the most popular and used. These methods have been used in the attached works and are here briefly described.

3.3.1 Genetic algorithm

Genetic algorithms (GA) are direct, parallel, heuristic methods for global search and optimization, which imitate the evolution process of the living beings. Unlike other methods, FAs treat a set of candidate solutions, forming a so called population, which is evolved many time following bio-inspired mechanism such as *selection*, *crossover* and *mutation*, until a convergence criterion is reached. GAs use the following terminology:

- *gene*: a representation of a scalar decision variable according to an encoding scheme (*e.g.* binary)

- *chromosome*: an encoding of a vector in the domain Γ consisting in a set of genes and individuating a possible solution, it is a synonym of individual

- *population*: a set of N chromosomes which will be evolved by the algorithm

- *generation*: each iteration of the algorithm involving the evolution of a population

- *selection*: the process of individuating n best candidates among a population, whose information will be transmitted to the next generation

- *crossover* or *recombination*: a process where couples of chromosomes (parents) are recombined to form a new ones (children) whose genes are the same of the parents but in a different order

- *mutation*: a random change of some genes of a chromosome, due to transcript error in nature, used to promote diversity in the population

A general scheme of a GA is shown in 3.3; In each generation, the fitness of every individual in the population is evaluated; the fitness is usually the value of the objective function in the optimization problem being solved. The more fit individuals are stochastically selected from the current population, and each individual's genome is modified (recombined and possibly randomly mutated) to form a new generation. The new generation of candidate solutions is then used in the next iteration of the algorithm. Commonly, the algorithm terminates when either a maximum number of generations has been produced, or a satisfactory fitness level has been reached for the population. It is evident that the processes of selection, crossover and mutation form the backbone of the entire algorithm and one can select among different methods to perform each of them.
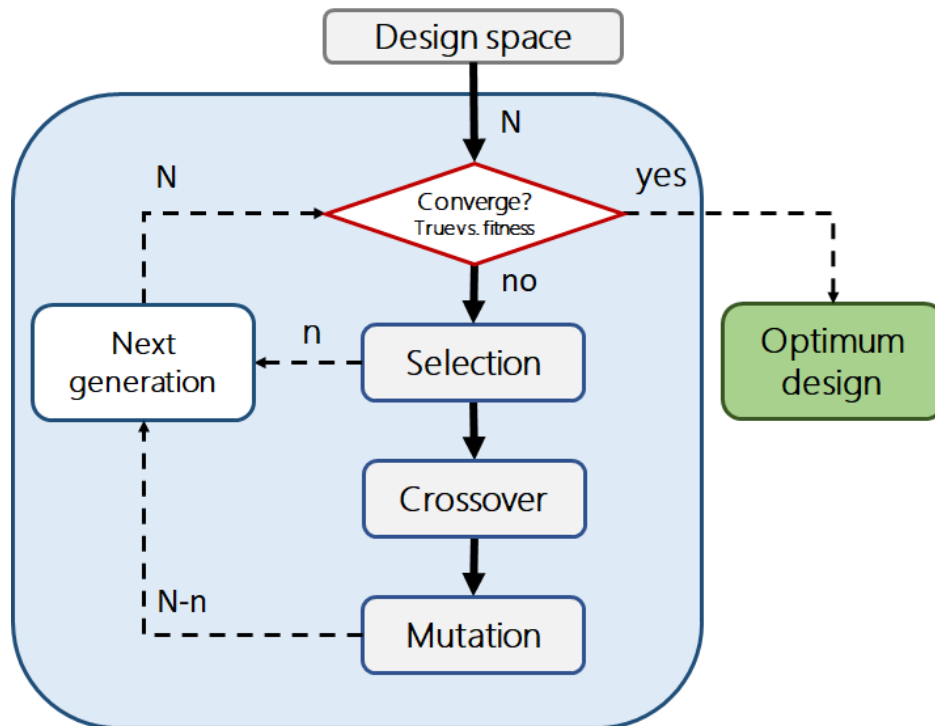
FIGURE 3.3: A general GA scheme.

Selection

Selection is a process in which individual genomes are chosen from a population for later breeding. In other terms, it allows to choose the most perspective n individuals, which will take part in the generation of next population or will be directly copied (elitism). Furthermore, selection gives an opportunity to $N - n$ individuals with comparatively bad value of fitness functions to take part in the creation of the next generation. This allows us to preserve the global character of the search process and not to allow a single individual to dominate the population, bringing to local extrema.

Selection algorithms are usually applied basing on both the non-dominated sorting and diversivety preservation methods presnted in section 3.2. Roulette wheel, tournament selection or the non-dominated sorting approach based on crowding distance proposed by Deb [80] are popular.

Retaining the best individuals in a generation unchanged in the next generation is called *elitism*. This approach ensures that the "good genes" are conserved and the solution proceeds monotonically towards a minimum. The rate of elite chromosomes preserved

in the generation can be set according to some indexes, but care must be taken to avoid excessive polarisation of the population by the fittest members, which can lead to local optimum.

Crossover

Crossover is a genetic operator used to vary the programming of a chromosome or chromosomes from one generation to the next. It involves more than one parent solution to produce a child solution and, in so doing, it allows the generation to propagate and evolve towards the optimum. There are different crossover techniques which differ on the recombination criterion. In a single-point crossover, a single point on both parents' organism string is selected; all data beyond that point in either organism string is swapped between the two parent organisms, resulting in the creation of two children. In scattered crossover, a random binary string of the same chromosome length is generated and then a gene from the first chromosome is chosen if the corresponding bit in the random string is one, or a gene from the second chromosome is chosen if the bit is zero. This method is valid only in case of non-linear constraints. In elitist methods the fraction of the new generation, other than elite children, produced by crossover can be selected.

Mutation

Mutation is a genetic operator used to maintain genetic diversity from one generation to the next. It is analogous to biological mutation and it alters one or more gene values in a chromosome from its initial state. In GA, mutation is used to avoid polarization in a population and guarantee a wide search of the design space. In fact, the solution may change entirely from the previous solution and GA can come to a better solution by using mutation. Mutation occurs during evolution according to a user-definable mutation probability that should be set low, otherwise the search will turn into a primitive random search. Mutation operators involve the generation, for each bit in the sequence, of a random variable that tells whether or not a particular bit will be modified. The selected bits can be modified following different rules (mutation types) as the bit string mutation or the flip bit, just to mention a few.

3.3.2 NSGA-II algorithm

NSGA-II by Deb [80] is an improved version of NSGA that address all its main criticism; the high computational complexity of non-dominated sorting, the lack of elitism and the need for specifying the sharing parameter σ_{share}.

NSGA-II uses the concept of a fast non-dominated sorting previously reported, together with an explicit diversity preserving mechanism based on crowded distance. The step-by-step procedure of the NSGA-II, reported in Figure 3.4 is simple and straightforward. First of all, an offspring population Q_t of size N is created starting from the parent population P_t using the usual binary selection, recombination and mutation operators. The two populations are combined together to form a R_t population of size $2N$, which is sorted according to non-domination. Since all previous and current populations members are included in R_t, elitism is ensure. The new population P_{t+1} is formed by picking individuals from different non-dominated fronts, in the order of their ranking, until N elements are chosen. Individuals picked from the last non-dominated front contributing to form the new population are chosen according to a niching strategy based on the the crowded-comparison operator, in order to select elements residing in the least crowded region of that front. In so doing, solutions compete each other also in terms of how dense they

are in the fitness space, thus diversity is explicitly considered when forming the offspring population.
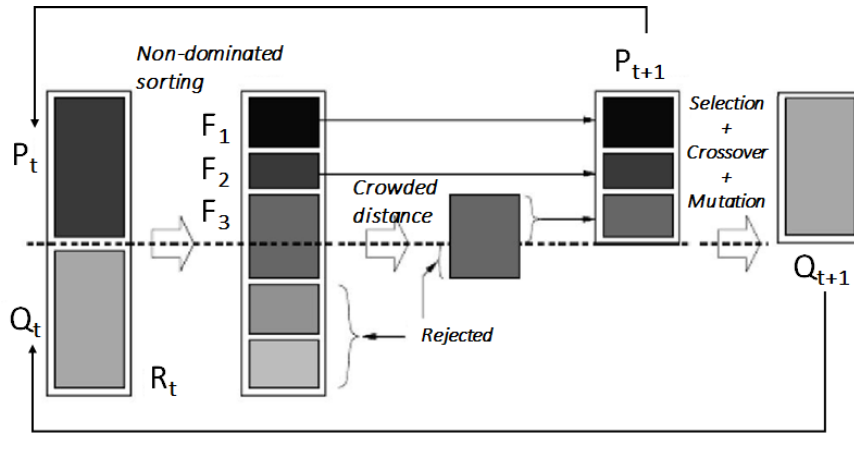
FIGURE 3.4: NSGA-II procedure.

3.4   Surrogate-based optimization

When dealing with optimization problems based on computer experiments, the simulation acts as the objective function since it assigns objective values to candidate designs. Such a black-box function precludes the use of optimizers which require an analytic function and, therefore requires specialized techniques. In addition, each simulation run can be computationally expansive and this severely restricts the number of simulation runs which can be performed. These optimization problems are ubiquitous in engineering and science, and Figure 3.5 shows their layout.
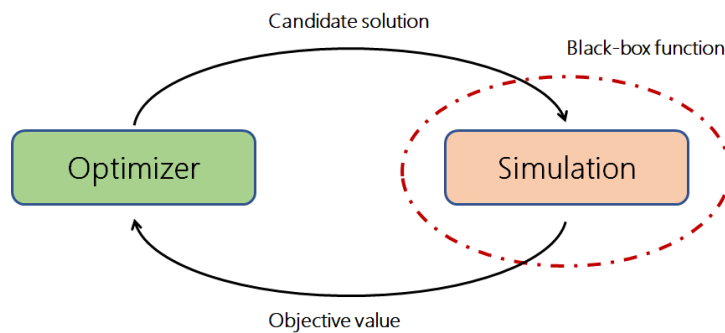
FIGURE 3.5: The layout of an expansive black-box optimization problem.

An established framework for handling such challenging optimization problems is that of *Surrogate-based optimization*, in which a metamodel approximates the true expansive black-box function and provides the optimizer with predicted objective values at a much lower computational cost [86], [87]. Surrogate-based optimization represents a class of optimization methodologies that make use of metamodeling techniques to quickly find the local or global optima. It provides us a novel optimization framework in which the conventional optimization algorithm, *e.g.* gradient-based or EA are used for sub-optimizations.

3.4.1 Framework of surrogate-based optimization

The basic strategy of using surrogate models in optimization is quite intuitive. The first step concerns the generation of an initial sample of vectors which are evaluated with the true expansive function and used to train a metamodel. Subsequently, the main optimization search is invoked. The generation of the sample vector deeply impact the overall search effectiveness as well as the metamodel accuracy and its predictive capability inside the design space.

A plethora of strategies have been proposed not only to validate the surrogate, but also to enhance its accuracy by adding a feedback loop in which the surrogate optimum design must be confirmed with calls to the true function and used to update the sampling. In so doing, it is possible to categorize the surrogate-based optimization into two groups:

I **Simple-level framework:** the optimization is entirely driven by the surrogate model

II **Bi-level framework:** the true function is used to evaluate the surrogate optimum designs

These approaches lead to different problems and limitations and are briefly analyzed in this section.

Simple-level framework

In this context all the solutions have been assessed in the SM and the achieved fitness is assumed to be comparable to that assessed by the real function. Since prediction with the SM is much more efficient than that by the expensive analysis code, the optimization efficiency can be greatly improved. In addition, SMs also serve as an interface between the analysis code and the optimizer, which make the establishment of an optimization procedure much easier. The comparison of the conventional and the surrogate-based simple-level optimization is sketched in Figure 3.6.
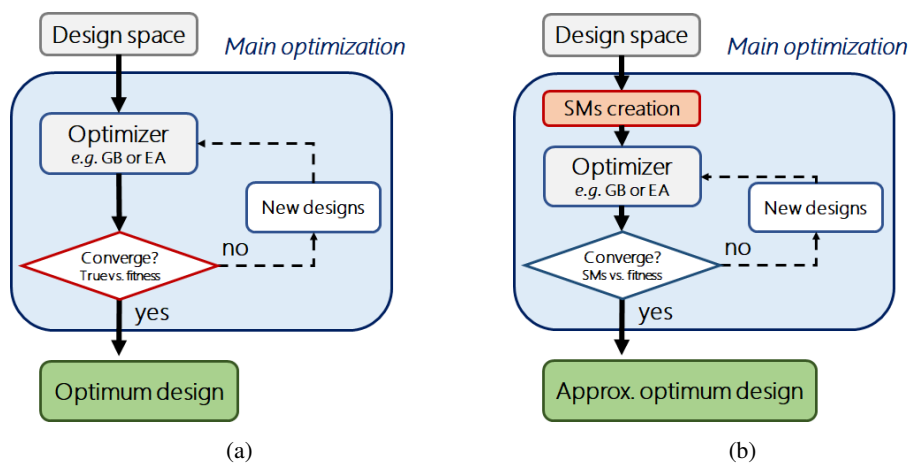
FIGURE 3.6: Comparison of conventional (a) and surrogate-based (b) simple-level optimization probelm.

This approach is commonly seen in literature ([88], [89] and [90] just to mention a few), because the use of a such a simple approach seems to be the most straightforward in using SM. However, it should be used carefully since its behaviour is highly dependent on the accuracy of the SM. In fact, when a SM is not properly selected, or it is constructed with a reduced-size training sample, or the sample is unevenly distributed, the constructed

model will usually be inaccurate. Therefore, if the optimization calculates the entire set of solutions exclusively with the SM, the entire approach will have more probabilities of converging to a false optimum, that, in a MOOP, is a Pareto front not corresponding to the true Pareto front in the real function.

Bi-level framework

It is evident the need to call the true functions (the expensive analysis codes) not only to validate the optimum solutions of the SM, but also to enhance the accuracy of the SM itself, by adding new sample points to the current sampled data set. To this scope, the entire process can be regarded as a bi-level optimization problem, as sketched in Figure 3.7; the main optimization concerns the creation and refining of the SMs and needs calls of the true functions. The sub-optimization uses the current SMs to determine the new sample sites by using any optimization algorithm such as gradient-based or EA.
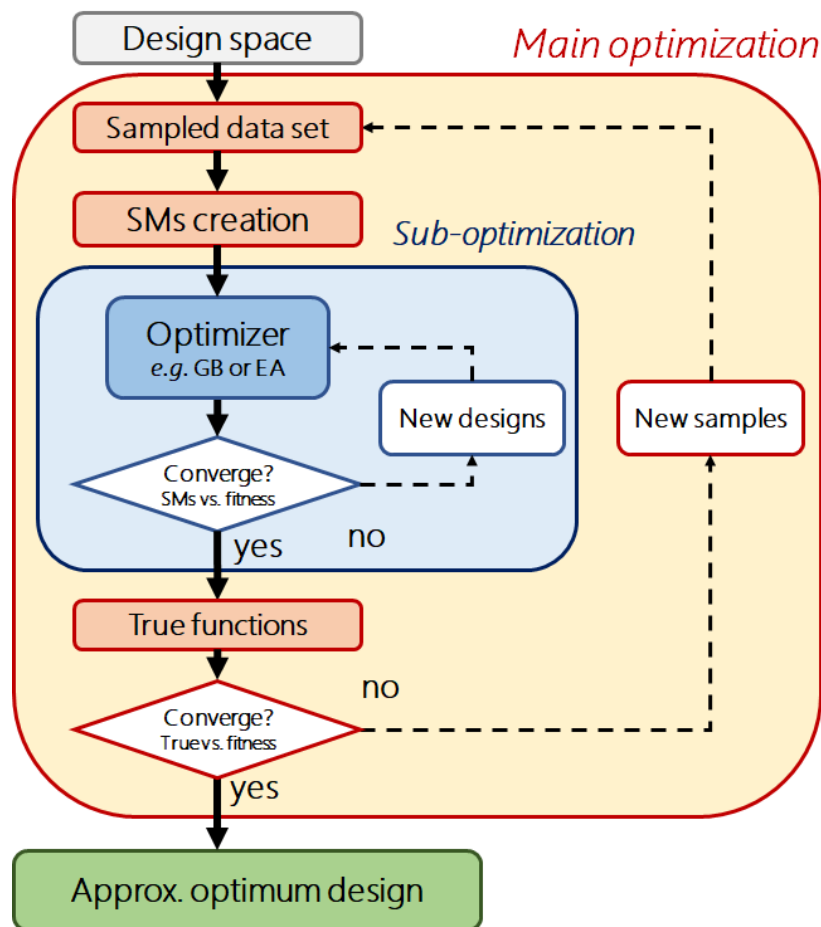
FIGURE 3.7: Flowchart of a bi-level surrogate-based optimization.

The selection of new points at which to call the true function, so-called infill points, represents the heart of the surrogate-based optimization process. Applying a series of infill points, based on some *infill criteria*, is also known as adaptive sampling (or updating), that is we are sampling the objective function in promising areas based on a constantly changing surrogate. It is therefore important to distinguish between the initial sampling step which is employed prior to the main optimization search, and the infill sampling step

which is performed during the search. Since the infill sampling vectors are iteratively generated based on an optimization search, the objective functions affect the sampling.

The success or failure of a surrogate-based optimization rests on the correct choice of model and infill criteria, or in other terms, in the balance between **exploration** and **exploitation**.

Elements of **exploration** in the infill criterion need the research of global optimum location. However, pure design space exploration can essentially be viewed as filling in the gaps between existing sample points. Pure exploration is of dubious merit in an optimization context [86] because time spent accurately modelling suboptimal regions is time wasted when all we require is the global optimum itself. Exploration based infill has its niche in design space visualization and comprehension where the object is to build an accurate approximation of the entire design landscape to help the designer visualize and understand the design environment they are working in or when the final SM is to be used in a realtime control system.

On the contrary, **exploitation**-based infill criteria are attractive methods for local optimization. However, exploiting the surrogate before the design space has been explored sufficiently, may lead to the global optimum lying undiscovered.

Thus, great caution must be taken in the choice of the infill criteria and a lot different methods have been proposed; Jones [91] proposed a classification of the infill criteria into two breeds:

- **One-stage approach:** the SM is not fixed when calculating the infill criterion, rather the infill criterion is used to calculate the SM. Goal Seeking and Conditional Lower Bound are often used

- **Two-stage approach:** the SM is fitted to the data and the infill criterion calculated based upon this model: Searching Surrogate Model (SSM), Expected Improvement and Statistical Lower Bound are the more common

The two-stage approach is far apart the most used. In particular, SSM is the more attractive because its simplicity and applicability for all the SMs; in this method, an optimizer such as EA is invoked to find the optimum, which in turn can be employed to refine the SMs. Such an approach has been found to be very efficient for local exploitation in the design space. This infill criterion highlights, once again, the importance that EAs have in MOOP and their capability to fulfil surrogated based approaches.

3.4.2 Surrogat-based multi-objective Evolutionary Algorithm

Multi-Objective Evolutionary Algorithms (MOEAs) have been succesfully applied to an important variety of difficult MOPs [92]. In fact, the main advantage of using such population-based techniques lies in their ability to locate solutions close to the global optimum. The number of calls of the fitness function to locate the good solutions is often too high, but can be reduced by adopting an hybrid approach (MOEAs and SM).

Traditionally, the number of proposals that make use of SMs in MOEAs have been classified according to the type of SM at hand [93], [94]. However, both works have shelved MOEA's point of view (*i.e.*, how the SM is incorporated into MOEA's evolutionary process). Jin [95] and Manríquez [52] proposed a classification based on the way EAs or MOEAs incorporate the SMs (how they are employed in the optimization loop). This kind of taxonomy is called *working style classification* and allows finding easily similar works placing greater emphasis on the methodology followed and not on the SM used. According to such a classification, the approaches are divided into *Direct Fitness Replacement* (DFR) methods and *Indirect Fitness Replacement* (IFR) methods [96].

Direct Fitness Replacement (DFR)

In DFR, the achieved fitness is evaluated with the SMs and is assumed to be comparable
to that assessed by the real function. Although the use of DFR seems to be the most
straightforward approach in using SMs, it should be use carefully since its behaviour
is highly dependent on the accuracy of the SMs and its predictive capability in different
points in the design space. Therefore, if the MOEA calculates the fitness of the population
exclusively with the SM, the entire approach is likely to converge to a false optimum or
a false Pareto front., vanishing the benefits of the simplification brought by the SM. For
this reason, in most cases the SM is used alternately with the original fitness function and
this alternation can be defined as the evolution control. Hence, DFR methods need to be
classified according to their evolution control.

- **No Evolution Control (NEC):** MOEAs calculate their solutions in the SMs ex-
  clusively and, therefore, the original fitness function is not used at all during the
  evolutionary process. The lack of feedback can lead to results far from real or mis-
  leading solutions.

- **Fixed Evolution Control (FEC):** only some generations or some individuals are
  evaluated in the surrogate model, while the remaining population is evaluated in
  the real function. This alternation allows the updating of the SM during the opti-
  mization, improving its accuracy since it is fed with points belonging to the search
  region. The model behaviour strongly depends on the switchback parameter.

- **Adaptive Evolution Control (AEC):** the frequency of control (number of solu-
  tions evaluated in the real function) is adjusted according to one criterion (*e.g.* the
  accuracy of the SM). This approach avoids any possible poor tuning setting of the
  FEC, however implies a complex optimization framework with nested loops.

Referring to the classification proposed in the previous section, NEC is a one-stage
approach that have provided good results only in problem with low dimensionality in both
decision and objective space. Having more challenging problem could produce inaccurate
SMs and, therefore, the MOEAs would produce unreliable solutions [52], [89].

FEC and AEC are two-stage approaches that have proven their efficacy in high di-
mensional problems; however, the first is strongly dependent on the switchback parame-
ters and requires many evaluations of the real objective function, while the second is not
extensively used because the difficulty in gathering information in order to identify the
signals for SM retraining.

Indirect Fitness Replacement (IFR)

In IFR, the original fitness function is used during the EA process, while one or more
components of the MOEA (typically the variation operators) are assessed in the SM. In
so doing, a number of solutions are produced, evaluated and compared using the SM.
After a stop condition, *n* best solutions are delivered to the parent approach and evaluated
with the real function. Using the approximated fitness indirectly is expected to keep the
optimization towards the true Pareto front and at the same time to reduce the risk of false
optimum convergence [97], [98].

Most of the existing works in this category use the MOEA in a direct coarse grain
search, while the SM intervenes in a local search, providing candidate solutions which are
then assessed in the real function. Therefore, the IFR approach uses the SM for exploita-
tion purpose, while the MOEA is employed for exploration.

The IFR method is clearly a two-stage approach and represents a viable option to re-
duce the number of function evaluations required to achieve good results of any MOEA

even if is the most computationally expansive method for surrogated-based multi-objective Evolutionary Algorithm.

3.4.3 Search driven sampling

The limitations of a simple level surrogate-based optimization have been shown to deeply affect the estimation of the Pareto front, but can be tackled by adopting a bi-level approach. However, both frameworks are based, at least for the first SMs creation, on classical DOE approaches, in which the metamodels are trained on a sample from a multivariate statistical distribution.

A recent method which differs significantly from the DOE approach, have been proposed by Tenne [99] in order to improve the optimization search. This method is an heuristic-based *Search-Driven Sampling* (SDS) in which a direct search optimizer is invoked for a short duration, and the vector it evaluated serve as the initial sample for the initial sampling and the metamodel training [100], [101].

The SDS approach focuses on the impact of the initial sample on the search effectiveness and not on the infill criteria that is performed during the search in a bi-level approach. The initial sample is generated by an EA which starts from a classic DOE sample. In so doing, the EA's operators drive the population to approach the optimum starting from an already "DOE-explored" objective landscape. It results in a augmented exploitation around local optima allowing, theoretically, the SMs to better predict the true-Pareto location.

The performance of the SDS strongly depends on the initial sample size. When the optimization budget or the relative sample size is large, SDS perform well since this enables a lengthier micro-EA search, which consequently provides good initial solutions to the main optimization search. DOE sampling methods perform better in small sample size, indicating that in such scenarios is important to distribute the small number of vectors effectively in the search space.

Chapter 4

Conclusions

This Thesis proposes methods for the implementation of elements from classical fan rotor blade design and performance analysis into the modern design optimization frameworks inspired by elements of the *i4.0*. Great attention has been put on the possibility of interweaving metamodels and optimization techniques, based on evolutionary algorithms, with old design and performance analysis procedures. All these different players have been presented and analyzed, highlighting the criticisms, the complexity and the benefits. In all the Thesis, the focus is on the links and connections that is possible to establish between these elements coming from many different disciplines.

The first Chapter presents elements of a possible classical design approach. A brief survey of the fundamental laws and the synthetic approaches that can be used for fluid flow analysis in an axial turbomachine, is given. Afterwards, the Chapter describes the possible methods for blade design; some of them come from literature and are based on well-known experimental correlations, others have been developed by the author and are based on the application of synthetic approaches for flow behaviour in cascade configuration. Experimental correlations or other aerodynamic characterizations of the blade profiles are adopted to close the design problem and add an element of criticism in the entire design approach.

The Chapter ends with a brief description of two developed in-house software for performance prediction of axial fans; AxLab (a Python code) and an Actuator disk approach (implemented in OpenFoam). These approaches are completely different and requires a very different computational time. AxLab is of two orders of magnitude faster than the Actuator Disk, but it cannot be useful when not only required the fan performances is required, but also the behaviour of the fan inside a more complex system. Even if the complexity of the physic reproduced by the two approaches is completely different (a throughflow quasi-3D code vs. a CFD code), their reliability in performance prediction is strongly dependent on the accuracy of the blade profile aerodynamic properties implemented in the codes.

In other terms, is not the synthetic approaches for fluid analysis and blade design that are unsuitable, but are the experimental correlations and the aerodynamic characterization, adopted to close the design problem, that introduce errors that strongly affect the final results. Paper 1 and Paper 2 show the benefits and limitations of adopting such classical approaches in both design and performance analysis of axial fan, highlighting the need of new correlations reproducing the axial fan work condition.

Metamodeling, presented in Chapter 2, represents a valuable tool to overcome this impasse. In fact, a metamodel, based on the massive use of a restricted number of accurate simulations, can be easily implemented in the design and analysis codes and it can successfully substitute the empirical correlations and other source of errors.

Paper 3 is the direct application of this strategy and demonstrates that the capability of a synthetic and simple code as AxLab in reproducing the flow conditions along a blade span and in predicting the fan performance, can be considerably improved with the use

of accurate metamodels for aerodynamic characterization of the blade profile. The paper shows how close is the AxLab-metamodel assisted flow prediction to a full 3D CFD simulation. The most important conclusion of this investigation, is that simple and quick-to-run codes, as AxLab, if correctly tuned by a metamodel approach, are reliable tools that can be used in multi-objective optimization processes.

Chapter 3 focuses in the optimization techniques, in particular on the Heuristic Algorithms and on the Surrogate-based optimization that have proven to be effective and reliable tool to quickly find local and global optima. Great emphasis is put on the risk of convergence to a false Pareto front when adopting a simple-level optimization framework or when making use of models or metamodels not properly tuned. Paper 4 is a preliminary search of which is the best optimization framework for solving the MOOP of truly reversible profile family for axial fans. Results show that, in this benchmark problem, an IFR approach has to be preferred to a NEC approach. A simple-level framework in which the MOEAs calculate the solutions only in the SMs has produced false Pareto-fronts in all the tested configurations, while the IFR approach has produced more reliable results, providing a good prediction capability during the iterations. The most interesting outcome of this work is that, in most cases, the IFR-based optimization is able to produce better results (individuals) than the true function-based optimization.

In conclusion, synthetic approaches, developed by the turbomachinery community in the past assisted my modern metamodels, can be successfully adopted in a modern Multi-objective Optimization Problem. In so doing, computational expansive design process can be replaced by faster optimizations able to explore the entire design space. However, caution is still required when selecting both the metamodels and the optimization framework in order to avoid false optima and unrealistic solutions.

Appendix

Papers

These papers are a selection of those produced during the PhD program and are reported in this Apendix because they represent the progression of methods that have been presented in the previous Chapters. These works make intensive use of the codes and software that have been developed starting from the concepts and the theoretical background described in this Thesis. are based on the work contained in the chapters of this thesis and represent a progression of methods that can be adopted in optimization design. Paper 1 and paper 2 are based on the codes developed in the framework presented in Chapter 2. Paper 3 is a study of the potentiality of Surrogate Models implementation in classical performance analysis tools and is, clearly, an application of the concepts presented in Chapter 3 to the tools presented in Chapter 2. Paper 4 focus on a surrogate-based multi-objective design optimization, based on evolutionary algorithms; this work is based on Chapter 2 and Chapter 3.

1. T. Bonanni, L. Cardillo, A. Corsini, G. Delibra, A. G. Sheard, and D. Volponi, "Derivative design of axial fan range: From academia to industry", V006T07A006–V006T07A006, 2016

2. T. Bonanni, A. Corsini, G. Delibra, D. Volponi, A. G. Sheard, and M. Bublitz, "Design of a single stage variable pitch axial fan", in *ASME Turbo Expo 2017: Turbomachinery Technical Conference and Exposition*, American Society of Mechanical Engineers, 2017, V001T09A011–V001T09A011

3. G. Angelini, T. Bonanni, A. Corsini, G. Delibra, L. Tieghi, and D. Volponi, "A metamodel for deviation in 2d cascade with variable stagger, solidity and reversible profiles", in *ASME Turbo Expo 2018: Turbomachinery Technical Conference and Exposition*, American Society of Mechanical Engineers, 2018

4. G. Angelini, T. Bonanni, A. Corsini, G. Delibra, L. Tieghi, and D. Volponi, "A preliminary investigation on surrogate-based optimization of truly reversible profile family for axial fans", *Currently under review on: Journal of Power and Energy*,

GT2016- 57469

DERIVATIVE DESIGN OF AXIAL FAN RANGE: FROM ACADEMIA TO INDUSTRY

Tommaso Bonanni[1], Lucio Cardillo[1], Alessandro Corsini[1], Giovanni Delibra[1], Anthony G. Sheard[2], David Volponi[1]

[1] Dipartimento di Ingegneria Meccanica e Aerospaziale
Sapienza University of Rome
Via Eudossiana, 18
I-00184 Rome, Italy

2 AGS Consulting, LLC
Box No. 79267
Atlanta
GA 30357
USA

ABSTRACT
The work presented in this paper concerns a useful method for axial fans preliminary design based on the "Derivative Design" concept. The emphasis is, on one side, on education and, on the other, on the practical help that such method can provide in the early preliminary design process.

A complete data set of an axial fan measured with ISO 5801 standards is the start point for the investigation and the prediction of the multiple possible performance that different fan configurations can provide, in terms of dimensionless duty coefficients. In particular, configurations with different number of blades, and hence of solidity, are studied. The typical options of derivative design are explored and relations for performance prediction are presented.

A detailed description of the derivative design methodology is followed by tests and validation. The tools employed are a fully three dimensional code, the Advanceded Actuator Disk Mode (AADM), and two other in-house codes, the Meanline Axisymmetric Calculation (MAC) and Axisymmetric Laboratory (AXLAB).

Results of the derivative design method are reported, showing a good accuracy against the AADM data. The MAC and AXLAB ensure still acceptable results when increasing the solidity of the machine. On the contrary, a decrease of solidity leads to higher relative errors in the prediction of the load coefficient.

In conclusion, an exploration of the possible fields of operation of a blade profile can be carried out by a correct prediction of the stage diffusion factor.

INTRODUCTION
The rapid increase of computational power and numerical techniques have totally changed, in the last sixty years, the designer's perspectives, providing ever more powerful and sophisticated tools. Furthermore, the tendency in some company to replace time and cost consuming experiments with simulations and empirical correlations, led, at times, designers to the development of individualistic performance correlations, or even design procedures. Traditionally, companies used the dimensional analysis for prototyping and determination of machine feasibility, resulting in a differentiated knowledge. In particular, confidentiality and intellectual properties issues have hid the design tools and correlations within engineering companies. In 1965, Smith [1] published a paper of great importance to a more universal approach to performance analysis. He showed that the dimensional analysis applied upon local dimensionless variable (namely the flow coefficient Φ and the load coefficient Ψ) can be the main framework for performance analysis of axial turbines. This work can be considered of primary importance in the standardization process of design procedure.

However, such an extraordinary know-how, could appear, at a first approach, fragmented and unrelated. It is in this framework that this paper took place; on one side, it is intended

to give an overview on the different correlations and kind of approach that a designer may employ.

The second issue of this work is related to a practical need of the industrial world, the identification of general turbomachinery products operating envelop (in terms of Φ and Ψ), which is a crucial task during the entire life of an existing range of machines. In fact it is common that in turbomachinery manufacturer companies, a product developed in the past, is then modified and re-adapted to similar tasks in order to meet customers' requests, with minimum development time and cost. Most manufacturers are in fact aware of the many difficulties and risks associated with new designs, encouraging "derivative design" [2]. If from one side derivative design can effectively have a positive impact on costs related to the design of a new product, from the other it adds restrictions to the degree of freedom available to the designer, generating families of "non-optimal" designs. Derivative design practice can include: i) impeller blade re-design, ii) scale the machine to a bigger or smaller size, iii) Impeller solidity modification acting on blade number, chord or height and iv) re-matching of ancillary components.

Even if design global and local design charts created by Balje [3], Smith[1], Casey [4] and Cordier [5] are in practice unused during preliminary design process, they still can be used to identify in a range of turbomachinery products the most suitable to modify for a selected duty point. This trend suggests the importance for every company to have detailed updated set of local and global design charts of their products, in order to have better performance estimation and produce a realistic prediction of market placement during derivative design process.

This "new" potentiality is crucial for manufactures that need to update their products in order to comply with standards in efficiency and, also, for academics giving the chance to students to explore different aspects and make practice with non-dimensional design charts.

NOMENCLATURE

Latin

C	Mean axial velocity	[m/s]
$c_{\theta,x}$	Absolute Tangential and axial Velocity	[m/s]
C_l	Lift coefficient	[-]
D	Fan diameter	[m]
l	Chord length	[m]
h	Blade height	[m]
p	Static pressure	[Pa]
Q	Volume flow rate	[m³/s]
t	Blade spacing; t=2πr/z	[m]
U	Rotation velocity	[m/s]
w	Relative velocity	[m/s]
z	Number of blades	[-]

Symbols

Δp_{tot}	Fan total pressure rise	[Pa]
Δh_{tot}	Total enthalpy rise	[J/kg]
β	Flow angle	[-]
γ	Stagger angle	[-]
Γ	Circulation	[m²/s]
δ	Tip Gap	[m]
ν	Hub to Tip ratio	[-]
ρ	Fluid Density	[kg/m³]
σ	Solidity; σ=1/t	[-]
Ψ	Load coefficient; $\psi = \Delta h_o / U^2$	[-]
Φ	Axial flow coefficient; $\phi = c_x / U$	[-]
ω	Angular velocity	[1/s]

Acronyms, subscripts and superscripts

1	Upstream rotor section
2	Downstream rotor section
AoA	Angle of attack
AXLAB	Axial Laboratory
DDM	Derivative Design Methodology
DF	Lieblein Diffusion factor
AADM	Advanced Actuator Disk Model
MAC	Meanline Axisymmetric Calculation
m	Mean line, midspan
tot	Total (enthalpy)
x	Axial direction
θ	Tangential direction

EDUCATIONAL ASPECT

The DDM, as thought at Sapienza University of Rome, is the result of previous experiences of the Turbomachinery Design Class. The course is offered to students of mechanical engineering during the last semester, second year, of the Master Degree and it is worth 9 ECTS (equivalent of 90 hours of lectures). The learning outcomes of this course are the presentation of flow phenomena in real turbomachinery configuration, CFD modeling and methods of turbomachinery design and performance correlation.

The DDM includes several different design and analysis tools for turbomachinery taught during the class; some, as MAC, have been developed in previous experience of the Turbomachinery Design Class, others, as the AADM, are provided as external tools, which, however, need the specific knowledge proper of the course. Proficiency in other open source software, completes the background knowledge needed for the DDM.

The DDM is used by the research group and by graduating students as a comparative tool of different design and analysis methodologies developed. Results achieved suggest the teaching staff to consider the DDM as year project of the Turbomachinery Design Class for the new semester, considering the completeness of the inherent topics to such a method.

DESCRIPTION OF THE TEST CASE

The considered axial fan is a rotor only, high-pressure single stage machine for ventilation and industrial process. The fan impeller has, in the original configuration, 9 blades, the shroud diameter is 686 mm. and the Hub-to-Shroud ratio is 0.45.

Table 1 summarizes the fan specification.

Shroud diameter	686 mm.	
Hub-to-Shroud ratio	0.45	
Minimum Tip Clearance	5 mm.	
Number of blades	9	
	Hub	*Tip*
Solidity	1.32	0.42
Chord	140 mm.	100 mm.

Table 1- *Fan Geometry*

The characteristic of the fan has been measured in a lab with ISO 5801 standards. Afterwards, these experimental data has been used to validate an in-house three dimensional code, the Advanced Actuator Disk Model (AADM) [6] developed in a similar vein to the Actuator Disk Model (ADM) proposed by Van der Spuy [7]. This approach synthetizes the effect of the fan by the momentum exchange between the blades and the fluid. This can be estimated by adding a source term f_i into momentum equation:

$$f_i = \frac{1}{2} W_\infty^2 \sigma F_i \frac{1}{\Delta z} \qquad (1)$$

where W_∞ is the average velocity vector, σ the local solidity, Δz the axial thickness of the actuator disk, i = x,y,z and F_i the i-component of the aerodynamic forces exchanged between blade and fluid. In order to compute this term it is necessary to model the blade as a series of sections, taken at different radii. For each section we derive the polar curve of the profile with XFoil [8] for low angles of attack and extended it with Viterna's methodology [9] up to -180<AoA<+180 deg. The solver computes W_∞ and AoA at runtime according to the local flow and calculate F_i from these and the polar curves (that are given as input) – as the blades is modelled here with 10 sections from hub to tip, F_i are estimated at intermediate radii by linear interpolation.

The incompressible Navier-Stokes equations were solved with OpenFOAM 2.4.x, a finite volume solver written in C++ [10].

The validation allowed to explore the behavior of the fan with two different configurations, respectively with 6 and 12 blades. The characteristic of the fan with 6, 9 and 12 blades are reported in

Figure 1 in terms of dimensionless axial flow coefficient Φ_m and load coefficient Ψ_m:

$$\Phi_m = \frac{C_x}{U_m} ; \quad (2) \qquad \Psi_m = \frac{\Delta h_{tot}}{U_m^2} ; \qquad (3)$$

$$C_x = \frac{Q}{\pi(r_{tip}^2 - r_{hub}^2)} ; \quad (4) \quad \Delta h_{tot} = \Delta p_{tot}/\rho \quad (5)$$

Where U_m is the rotation velocity at the mean radius, C_x is the mean axial velocity calculated with Eq. (4) and Δh_{tot} is the design total enthalpy rise that, for a low speed can be expressed in terms of total pressure rise (Eq.(5)).
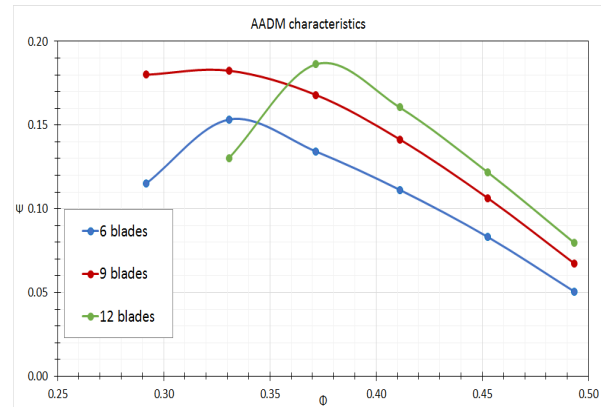
Figure 1- *Characteristics of the studied fan.*

DERIVATIVE DEISGN METHODOLOGY

The derivative design consists in the modification and adaptation of an already developed machine, in order to meet customers' requests, avoiding a new design.

The Derivative Design Methodology (DDM) presented in this paper consists of two main levels. The first one is a classic direct problem, in which we are asked to predict the fluid dynamic performances of an existing turbomachine of known blade and geometry. The subsequent step consists essentially in an inverse (or design) problem in which we are asked to estimate, for an existing fan, the change in terms that ensure a requested load coefficient for a given flow coefficient.

The inverse design methodology presents many educational features, providing a good summary of the basics of design; Horlock [11], Dixon [13], Lakshminarayana [14], Cumpsty [15], Lewis [16], R.A. Wallis [17], A.B. McKenzie [18], Sandrolini and Naldi [19].

Current design methodology is represented in Figure 2, where the flow chart schematizes the logic and highlights the connection between the global analysis of the flow and the aerodynamic response of the prescribed profile.

The first step for the designer is to define the global input parameters, such as the main dimensions of the fan, the number of blades, the blade profile and the definition of the operational range.

3   Copyright © 2016 by ASME

Then it is automatically defined a dimensionless parameters block in terms of flow coefficient (Φ_m) and solidity (σ).

The subsequent step is the aerodynamic performance analysis of the profile in terms of exit flow angle (β_2), angle of attack (AoA), lift coefficient (C_l) and circulation (Γ).

Afterwards, the meridian flow analysis, that involves the solution of the radial equilibrium equation, gives an update of axial velocity ($c_{x,2}$) after the rotor. This value implies a modification of β_2 and, hence, a new aerodynamic performance analysis. This loop is iterated until convergence of some parameter (i.e. the AoA).

As the loop is converged, it is possible to have the ideal performance prediction. However, the derivative design methodology is based on the meanline analysis that is essentially 2D, and so empirical and experimental correlation are required to take in considerations the high three dimensionality of the flow, and hence, the losses. In this way can be predicted the real performance of the fan in terms of Ψ_m and Diffusion Factor (DF).

The two axisymmetric codes used for testing the DDM follow the same procedure of Figure 2, except for the Meridian Flow Analysis. AXLAB resolves the Radial Equilibrium Equation and all the other equations along the blade span, while MAC resolves the equations only at the mean radius with an axial velocity equal to the mean velocity C_x.

The AADM is the third tool used in the DDM; it provides the entire characteristic curve of the fan in terms of Total Pressure rise for the configuration with 6, 9 and 12 blades.

The second part of the methodology, the inverse problem, needs the DF as input value. Plotting on a Φ - Ψ diagram the iso- $1/\sigma$ curves, we are finally able to predict the load coefficient ensured by the fan with a different solidity for a specific flow coefficient.

Even if not the best approach, the proposed methodology features positive aspects. First, this procedure links a number of correlations, formulas notions and concepts that could look like stand-alone but are strictly connected and related. Furthermore, it is perfect for instructive purpose because it is connected to the physic and aerodynamic of a turbomachinery component. For instance, referring to the Axisymmetric codes, the convergence is based on the blade aerodynamic performance, thus the need of a good aerodynamic analysis in terms of C_l and C_d.

DERIVATIVE DESIGN PROCEDURE

The model fan used for the calculation consists in in one rotor with zero swirl velocity ($c_{\theta,1}$) at the in inlet. Once selected the Global Design Input Parameters, the inlet velocity triangle is automatically defined. In fact, referring to equations (2) and (4), the inlet flow angle is:

$$\beta_1 = arctg\left(\frac{1}{\Phi}\right) \qquad (6)$$
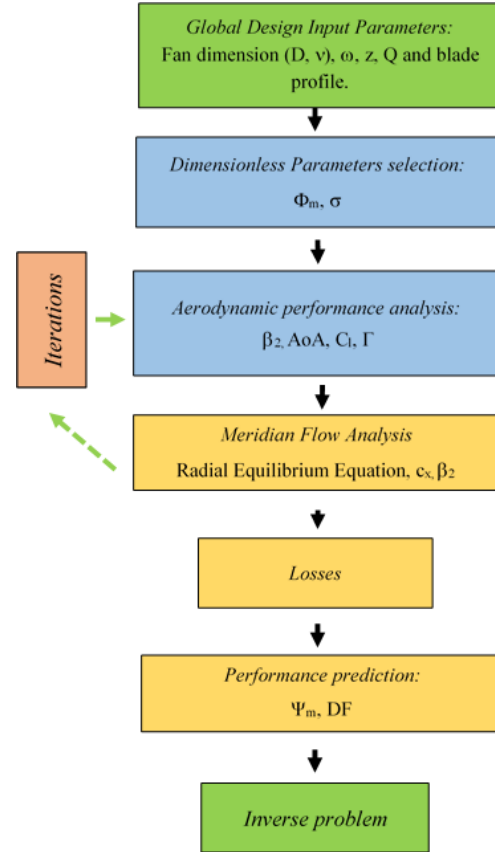
Figure 2 – *Derivative Design procedure.*

Figure 3 shows the velocity triangles in two annular section (before and after the rotor) in the particular case of a free vortex condition; the axial velocity (C_x) is constant not only along the span, but also before and after the rotor, resulting in inlet and outlet triangles with the same height. Figure 3 displays, also, the dimensionless velocity triangles.

Taking into account equations (2), (3), (4) and the "Euler pump equation"

$$\Delta h_{tot} = \Delta p_{tot}/\rho = U(c_{\vartheta,2} - c_{\vartheta,1}) \qquad (7)$$

with zero swirl inlet velocity, the outflow angle is:

$$\beta_2 = arctg\left(\frac{1-\Psi}{\Phi}\right) \qquad (8)$$

Clearly, the tangential velocity ($c_{\theta,2}$) represents the unknown of the direct problem.
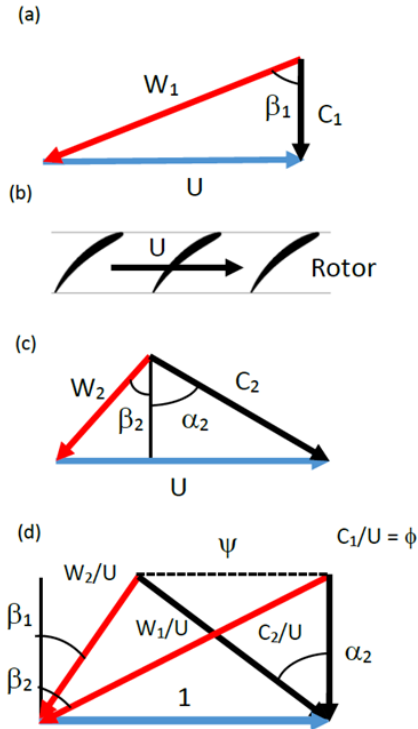
Figure 3 - *Fan model: inlet velocity triangle (a); rotor (b); outlet velocity triangle (c); dimensionless inlet and outlet triangles (d).*

Now that the input parameters are set, the method enters in the iterative procedure involving the aerodynamic performances of the profile. This part is based on the Kutta-Joukoski theorem that relates the lift generated by an airfoil to the speed of the airfoil through the fluid, the density of the fluid and the circulation. This theorem is of fundamental importance in the development of the theory of airfoils [13]. The theorem states that the lift force L is

$$L = \Gamma \rho w_m , \qquad (9)$$

where w_m is the relative velocity between the airfoil and the fluid at infinity and Γ is the circulation about the airfoil (defined as the line integral of the velocity). From the definition of lift coefficient C_l

$$C_l = \frac{L}{0.5 \rho l w_m^2} . \qquad (10)$$

Combining equations (9) and (10) it is possible to express the circulation as

$$\Gamma = 0.5 w_m C_l l \qquad (11)$$

It is known that C_l varies with the Angle of Attack, that, for a generic airfoil is defined as (see Figure 4)

$$AoA = \beta_m - \gamma , \qquad (12)$$

where γ is the Stagger angle (angle between the chord and the axial direction) and β_m is the vector mean angle, which may be expressed in terms of the inlet and outlet flow angles β_1 and β_2 through

$$\tan \beta_m = 0.5(\tan \beta_1 + \tan \beta_2) . \qquad (13)$$
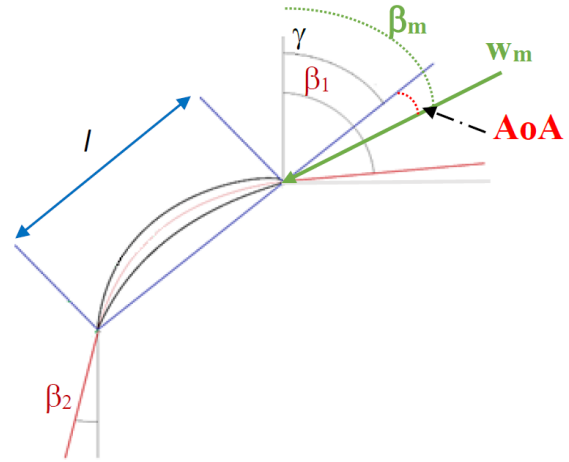
Figure 4 – *Blade geometrical parameterization*

The circulation Γ, as defined in Equation (11), represents the connection between the aerodynamic characterization of the blade profile and the operating conditions of the turbomachine in exam. The fluid deflection of a uniform stream, that is the main aim of a turbomachine cascade, is accomplished by the vorticity and hence the circulation developed by the blades. The array produces a change of relative tangential velocity w'_θ that can be expressed as [16]:

$$w'_{\pm,\vartheta} = \mp \frac{\Gamma}{2t} \qquad (14)$$

Figure 5 shows how the circulation is related to the change of the velocity triangles. Since the mean and the outlet relative velocity can be expressed as

$$w_m = \sqrt{w_{\vartheta,m}^2 + c_x^2}; \quad w_2 = \sqrt{w_{\vartheta,2}^2 + c_x^2} \qquad (15)$$

introducing Equation (14) in the last expressions result finally in:

$$w_m = \sqrt{(U + w'_\vartheta)^2 + c_x^2} = \sqrt{\left(U - \frac{\Gamma}{2t}\right)^2 + c_x^2}$$

$$w_2 = \sqrt{(U - 2|w'_\vartheta|)^2 + c_x^2} = \sqrt{\left(U - \frac{\Gamma}{t}\right)^2 + c_x^2} \qquad (16)$$

At the first step of the iteration, a first tentative value of β_m is set ($\beta_m = \beta_1 - 5°$), allowing to calculate a first estimate of AoA (Equation (12)). The aerodynamic analysis of the profile,

carried out with an external software, gives information on the lift coefficient as function of AoA. The match of these two information gives the current C_l value. Inverting Equation (13), the outflow angle β_2 is derived. Referring to Figure 3 the relative velocity vectors are:

$$w_{2,m} = \frac{c_x}{\cos \beta_{2,m}} \qquad (17)$$

It is now defined, from Equation (11) a first value for Γ.
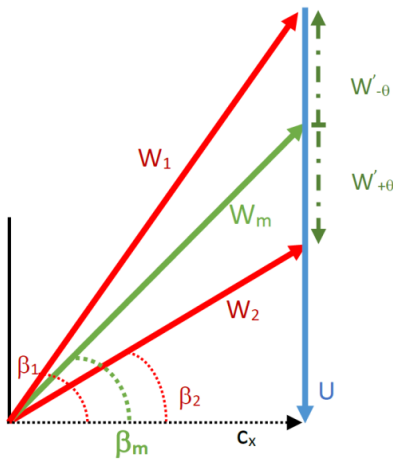
Figure 5 – *Velocity triangles for a compressor cascade*

Some iterations are now necessary for convergence. Figure 6 illustrates the logic of the subsequent iterations. A first value for Γ gives, using Equations (16) and (17), the relative velocity w_m and β_m. This angle updates the AoA, Equations (12) , and, consequently, the C_l value. Equation (11) returns the new value for the circulation Γ. The last step of the iterative procedure is the Meridian Flow Analysis. As mentioned earlier, MAC resolves the equations only at the mean radius, hence keeping the c_{x2} equal to C_x. On the other side, AXLAB takes into account the solution of the Radial Equilibrium Equations, and then a radial redistribution of the flow. This iterative procedure runs until a selected parameter (in our case the AoA) is converged. MAC converges after few iterations (less than 10, depending on the flow coefficient), while AXLAB needs more iterations.

The final output of the iterative procedure is the outlet flow angles β_2 and, then the unknown of the direct problem $c_{\theta,2}$:

$$c_{\vartheta,2} = U - c_{x,2} tg\, \beta_2 \qquad (18)$$

From Equations (3) and (7) it is possible, now, to calculate the ideal Euler work and the ideal load coefficient.
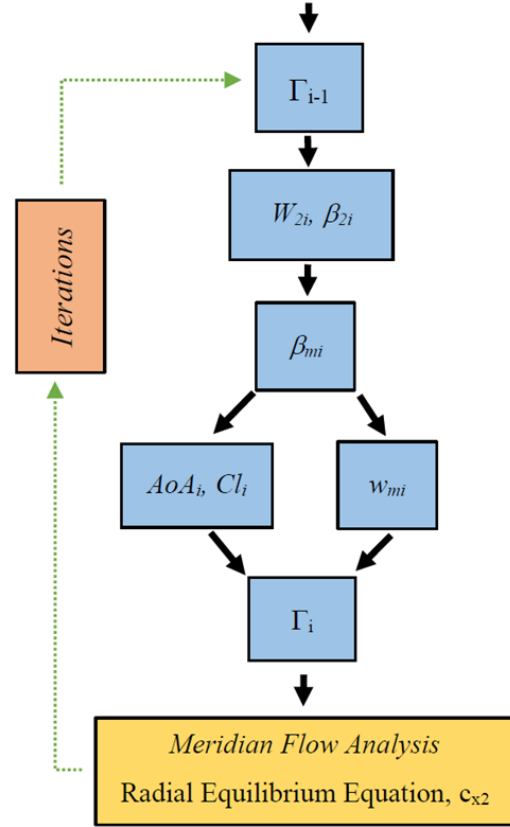
Figure 6 – *Iterative procedure*

The subsequent step of the Design Procedure consists in the losses estimate. Following the correlations proposed by Sandrolini [19], losses are divided in *profile* and *secondary losses*. The first refer to the losses due to the boundary layer growth and to the "reduction" θ/l of the annulus because of the displacement thickness:

$$Y_p = 2\left(\frac{\theta}{l}\right)\frac{2\sigma}{\cos \beta_2}\left(\frac{\cos \beta_1}{\cos \beta_2}\right)^2 \qquad (19)$$

The secondary losses are related to the tip gap and to the secondary flows:

$$Y_{s+\delta} = \left(0.16\frac{t}{h} + \frac{\delta}{h}\frac{1}{\cos \beta_2}\right)\frac{(\tan \beta_1 - \tan \beta_2)^2}{\cos \beta_m}\cos^2 \beta_1 \;,\; (20)$$

where h is the blade height and δ is the tip gap.

These losses act as a reduction of fan performances in terms of total pressure and load coefficient,

$$R_{tot} = \frac{\Delta P_{losses}}{\rho} = R_p + R_s = \left(Y_p + Y_{s+\delta}\right)\frac{w_1^2}{2} \qquad (21)$$

The AADM follows a complete different procedure; it is a three dimensional simulation that provides the Total Pressure raise of the fan.

The direct problem ends with the prediction of the Lieblein diffusion factor (DF) [20] and [21], even though this parameter was recently criticized because it is not supposed to predict blade stall in cases of highly tridimensional flow. For a fan stage with zero swirl at entry the reaction R is

$$R = 1 - \frac{\Psi}{2} \tag{22}$$

and generic expression of the DF for compressor stage of arbitrary reaction becomes [16]:

$$DF = 1 - \sqrt{\frac{\Phi^2 + (1 - \Psi)^2}{\Phi^2 + 1}} + \frac{1}{2}\left(\frac{t}{l}\right)\left(\frac{\Psi}{\sqrt{\Phi^2 + 1}}\right) \tag{23}$$

In conclusion, the direct problem returns the distribution of the load coefficient and the diffusion factor as a function only of Φ, Ψ and the pitch/chord ratio.

The inverse problem is based on Equation (23), which may be rearranged to provide a formulation for selection of the pitch/chord ratio to suit any specified duty,

$$\left(\frac{t}{l}\right) = \frac{2}{\Psi}\left[\sqrt{\Phi^2 + (1 - \Psi)^2} - (1 - DF)\sqrt{\Phi^2 + 1}\right] \tag{24}$$

More precisely, it is possible to plot on a $\Phi - \Psi$ diagram *iso-t/l* curves, for a certain DF. Once that the direct problem for a fan of prescribed input parameters (reported in

Table 1 for the current case) is completed, we ask if, while keeping constant Φ and DF, it is possible to estimate the pitch/chord ratio to fulfil a prescribed load coefficient or, vice versa, if we can estimate Ψ, while changing the solidity of the machine.

A positive answer to these questions, would allow the understanding of the response of a fan, in terms of a global parameters, to a geometrical change (for instance the number of blades), without having to recourse to new simulations or iterations.

RESULTS

The Derivative Design Methodology is tested on the reference fan (see

Table **1**). AADM, MAC and AXLAB have been run in order to reproduce the entire characteristic of the fan and, hence, to get the DF distribution. Using Equation (24), it is possible to obtain iso-t/l curves, one for each operating point of the characteristic (one for every tern Φ–Ψ–DF).

Figure 7 to Figure 12 report the results of the Derivative Methodology for two operating points: $\Phi=0.372$ and $\Phi=0.411$. These points are in the stable range of operation (see

Figure 1). The *t/l=1.7* curves, which refer to the reference 9 blades configuration, are drawn in red. The black crosses indicate the corresponding load coefficient.
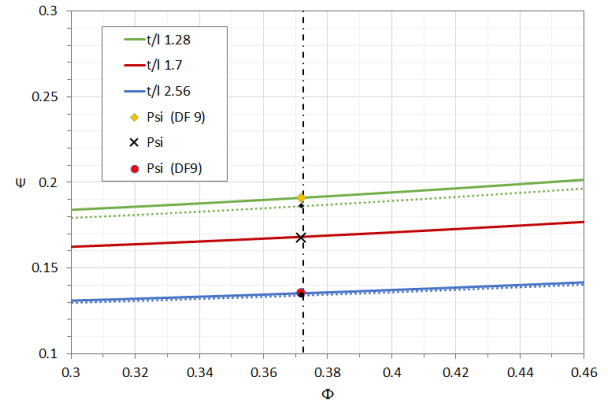
Figure 7 – *AADM, Φ=0.372; iso-t/l curves;*
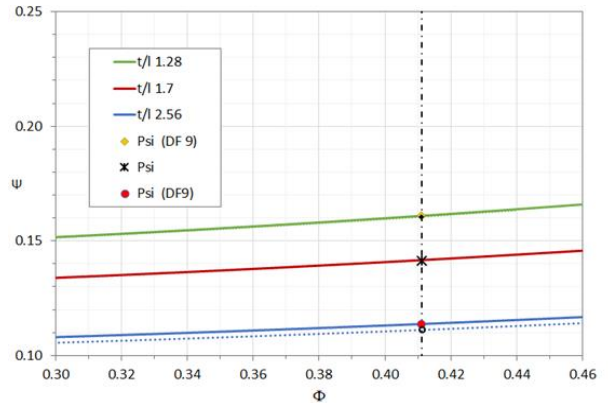
Figure 8 – *AADM, Φ=0.411; iso-t/l curves*

The obtained DF values are now used as entry values for the Equation (24); *iso-t/l* curves for configurations with 12 and 6 blades are drawn respectively in green and blue solid lines.

At this point, to have a proper comparison of the results, it has been necessary to run the AADM, MAC and AXLAB with 12 and 6 blades, resulting in new values of DF. The same *iso-t/l* curves can be drawn with these "correct" DF, giving the green and blue dotted curves.

Looking at the solid curves, for a given operating point (the black dashed lines), it is possible to have an estimation of the load coefficient Ψ. The yellow diamonds refer to the 12 blades configuration (green lines), while the purple circles refer to the 6 blades configuration (blue lines). These points are reported as "PSI (DF 9)", suggesting that Equation (24) has been calculated with a DF value obtained from the 9 blades configuration.

The black diamonds and circles report indicate the proper load coefficient as calculated with AADM, MAC and AXLAB with 12 and 6 blades.
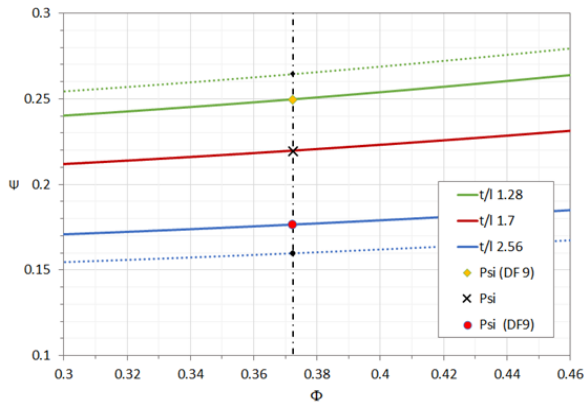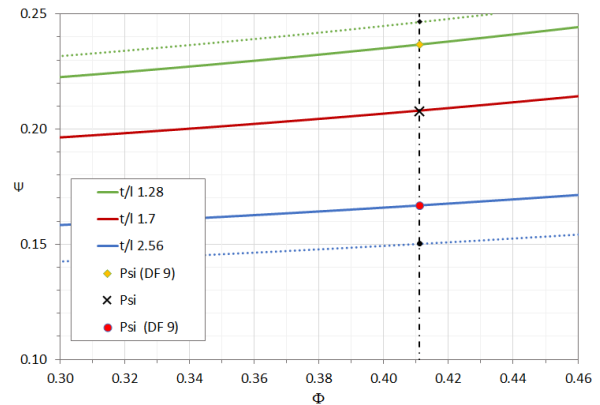
Figure 9 *–AXLAB, Φ= 0.372; iso-t/l curves;*

Figure 10 *– AXLAB, Φ=0.411; iso-t/l curves*

Figure 11 *– MAC, Φ=0.372; iso-t/l curves*
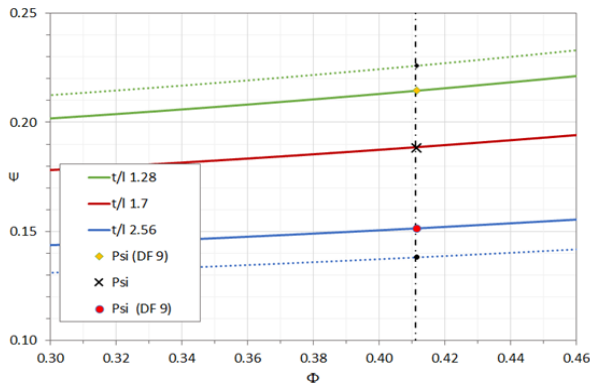
Figure 12 *– MAC, Φ=0.411; iso-t/l curves*

Looking at the results in terms of load coefficient prediction corresponds to an evaluation of the response of the machine in terms of a solidity change. Table 2 and Table 3 summarize the results for the configurations with 6 and 12 blades in terms of the relative error, defined as

$$error(\%) = \frac{\Psi - \Psi_{DF9}}{\Psi} \times 100 \ . \qquad (25)$$

Z=6	AADM		MAC		AXLAB	
Φ	0.372	0.411	0.372	0.411	0.372	0.411
Ψ	0.134	0.111	0.168	0.150	0.160	0.138
Ψ (DF9)	0.135	0.114	0.185	0.167	0.176	0.151
ERROR (%)	0.77%	2.21%	10.03%	11.03%	10.31%	9.49%

Table 2 *– Results of the 6 blades configurations.*
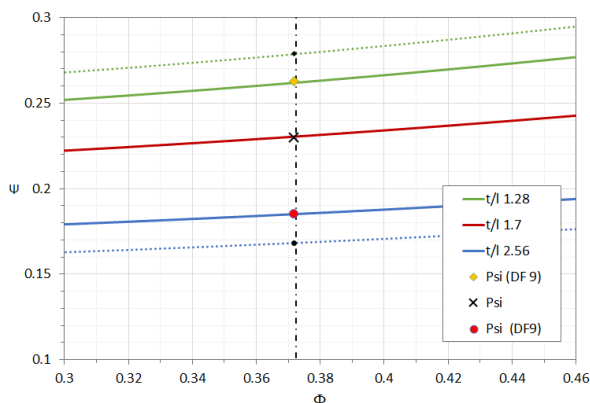
Z=12	AADM		MAC		AXLAB	
Φ	0.372	0.411	0.372	0.411	0.372	0.411
Ψ	0.186	0.161	0.279	0.247	0.265	0.226
Ψ (DF9)	0.191	0.161	0.263	0.237	0.250	0.214
ERROR (%)	2.50%	0.26%	-5.77%	-4.01%	-5.67%	-5.11%

Table 3 *– Results of the 12 blades configurations.*

The Derivative Design Methodology returns good results for the AADM. Passing from a configuration with 9 blades, to 6 and 12 blades, the DF changes slightly, resulting in a good estimation of the *iso-t/l* curves; the solid lines of Figure 7 and Figure 8 are very closed to the dotted lines.

The MAC and AXLAB have similar behaviour. For the 6 blades configuration, they overestimate the load coefficient (around 10%). The blue dotted lines are below the solid line, due to an overestimation of the DF value. On the contrary, passing to the 12 blades configuration, MAC and AXLAB report a circa 5% load coefficient underestimation. An increase

in solidity implies that the fan operates in a situation more similar to a turbomachine cascade; the blade passage is narrower, the fluid is more guided along the blade and the secondary flows are limited. It is helpful to remind that relations such as (14) come from a cascade approach. This means, obviously, that a meanline, and even an axisymmetric calculation, being not able to predict secondary flows, are more accurate with solid machine.

Figure 13 and Figure 14 show comparative graphs of the DDM for the three tools considered. Circles, diamonds and squares represent the load coefficient values computed with the DDM; solid, dotted and dashed line are the characteristic curves computed with the AADM, AXLAB and MAC.
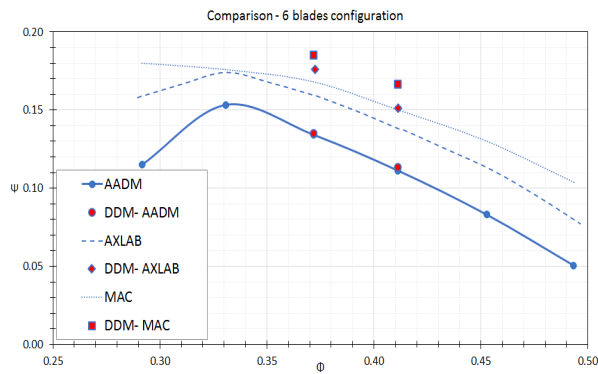
Figure 13 – *DDM comparative graph; 6 blades configuration*
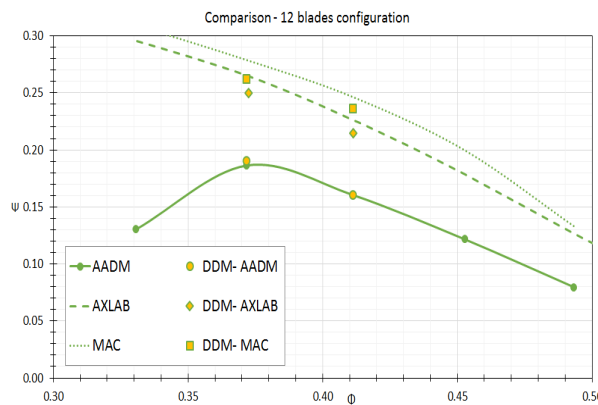
Figure 14 - *DDM comparative graph; 12 blades configuration*

These pictures highlight the relative error of the estimated load coefficient. The proximity of the DDM points computed from the AADM (purple and yellow circles) suggests the accuracy of the method itself; the higher relative error for DDM-AXLAB and DDM-MAC, is related to a not correct exstimation of the DF. Figure 15 shows the DF computed by the AADM and AXLAB for the exanimated flow coefficients

(the MAC have a similar behaviour to AXLAB and is not reported for sake of clarity). It is now evident that AXLAB is more sensitive to a change, in terms of solidity, of the fan configuration. In particular, the characteristic curves computed are more distant, one from the other, than the curves computed by the AADM; hence, the DF changes much more for AXLAB than for the AADM. This leads to the error in the estimation of the iso-t/l (solid against dashed line). The relative error is also plotted in Figure 16 and Figure 17.
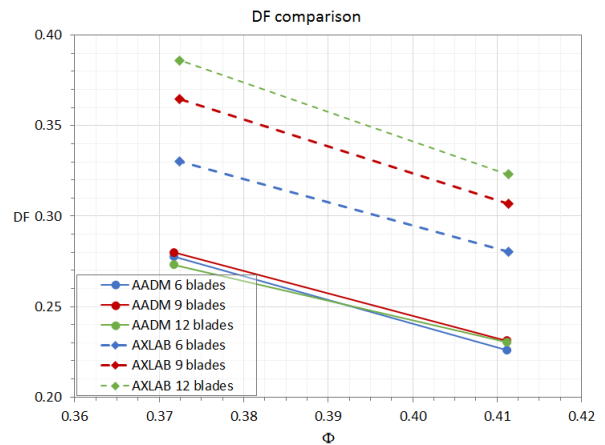
Figure 15 – *DF comparison for the 6, 9 and 12 blades configuration.*

Another interesting interpretation of the results derives still from Equations (24). We can predict the minimum pitch/chord necessary to fulfil a new duty point, still keeping the original DF. Table 4 and Table 5 report the result in terms of blade number z; not a change in aspect ratio neither of chord length has been taken in account. Obviously, the reported values for z must be rounded to an integer, leading to an error of one or two blades in the estimation.

Z=6	AADM		MAC		AXLAB	
Φ	0.372	0.411	0.372	0.411	0.372	0.411
Z	5.91	5.78	5.12	5.04	5.08	5.16

Table 4 – *Blade count results; 6 blades configuration.*

Z=12	AADM		MAC		AXLAB	
Φ	0.372	0.411	0.372	0.411	0.372	0.411
Z	11.30	11.91	14.03	13.24	13.84	13.63

Table 5– *Blade count results; 12 blades configuration.*
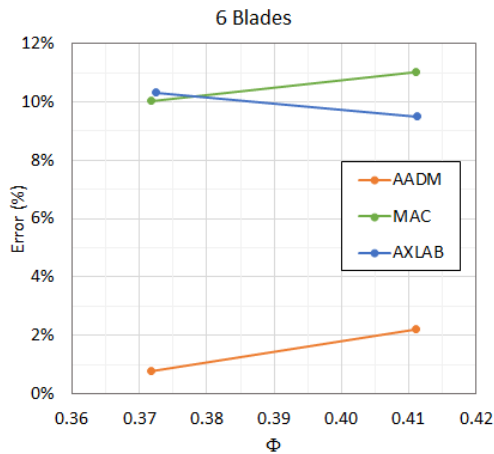
Figure 16 – *Relative error; 6 blades configuration*
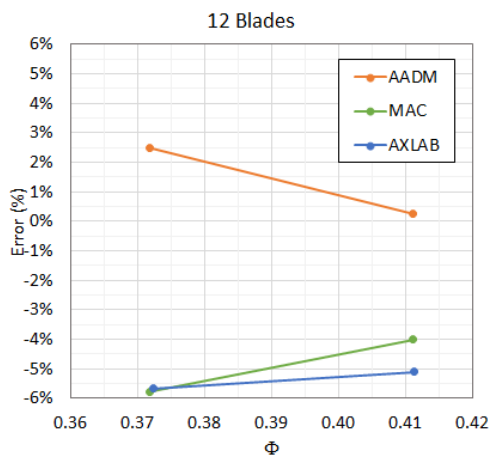
Figure 17 - *Relative error; 12 blades configuration*

CONCLUSIONS

The Derivative Design Methodology has been presented reporting a tool for design and solve a real industrial problem. The first part of the paper concerns an overview on the problem and on the procedure. Then follows a detailed description of the design methodology, in order to highlight the logic and to show the connection between the aerodynamic performances of the blade and the meridian flow analysis. Afterwards, results of the methodology, using input data of three conceptually different tools as the AADM, MAC and AXLAB, are reported. The DDM returns good results for the AADM, both in terms of load coefficient and number of blades prediction. The relative error is always lower than 2.5%, encouraging the use of this

methodology, which allows to save pointless time-consuming fluid dynamic simulations. The DDM with MAC and AXLAB have good results for the 12 blades configuration (relative error lower than 6 %), while a higher error (around 10%) is the output of the 6 blades configuration.

This paper is an opportunity to show, in an international technical conference, a design methodology taught at Sapienza University of Rome, providing a baseline for comparison with the work done in other university.

Results achieved suggested to consider this methodology as a helpful tool during future classes, showing how the basic turbomachine knowledge can overcome a real industrial problem.

REFERENCES

[1]. S. F. Smith, (1965), 'A simple correlation of turbine efficiency', *Proc. Seminar on Advanced Problems in Turbomachinery, Von Karman Institute.*

[2]. M. V. Casey, (1994), 'Computational methods for preliminary design and geometry definition in turbomachinery', *Turbomachinery Design Using CFD 22 p (SEE N95-14127 03-34). Vol. 1. 1994, Agard.*

[3]. O.E. Balje, (1981), 'Turbomachines', *John Wiley.*

[4]. M. V. Casey, (1987), 'A mean line prediction method for estimating the performance characteristics of an axial compressor stage', *International Conference on Turbomachinery-Efficiency Prediction and Improvement, Paper C 264/87.*

[5]. O. Cordier, (1953), *Brennstoff-Wiirme-Kraft, 5, 337.*

[6]. Corsini, A., Delibra, G., Minotti, S. and Rossin, S., (2015), 'Numerical assessment of fan-ducting coupling for gas turbine ventilation systems', *GT2015-42449.*

[7]. S. J. van der Spuy, T. W. von Backström and D. G. Kröger, (2011), 'Using Computational Fluid Dynamics to Simulate Multiple Axial Flow Fans in Air-Cooled Steam Condensers', *Paper No. POWER2011-55057, pp. 375-383.*

[8]. Drela, Mark, and H. Youngren. "X-Foil 6.96." Software December (2001).

[9]. Viterna, L .A., and Janetzke, D. C., "Theoretical and Experimental Power from Large Horizontal-Axis Wind Turbines," NASA TM-82944, Sept 1982.

[10]. Weller. H.G., Tabor, G., Jasak, H. & Fuerby, C. (1998), 'A Tensorial Approach to Continuum Mechanics usingObject-oriented Techinques1. Journal of Computational Physics, col. 12(6), pp. 620-631.

[11]. J. H. Horlock, (1958), 'Axial Flow Compressors', *London: Butterworths.*

[12]. H. Horlock, (1966), 'Axial Flow Turbines', *London, Butterworths*.

[13]. S.L. Dixon, C.A. Hall, (2010), 'Fluid Mechanics and Thermodynamics of Turbomachinery', *Butterworth-Heinemann, Oxford OX2 8DP*.

[14]. B. Laksmiranayana, (1996), 'Fluid Dynamics and Heat Transfer of turbomachinery', *John Wiley & Sons, New York*.

[15]. N. A. Cumpsty, (1989), 'Compressor Aerodynamics, Longman Scientific & Technical', *John Wiley & Sons, New York*.

[16]. R. I. Lewis, (1996), 'Turbomachinery performance Analysis', *Butterworth-Heinemann*.

[17]. R. A. Wallis, (1961), 'Axial Flow Fans, Design and Practice', *William Clowes and Sons, London*.

[18]. A. B. McKenzie, (1988), 'The selection of Fan Blade Geometry for Optimum Efficiency', *Proceedings of institution of mechanical engineering*.

[19]. S. Sandrolini, G. Naldi, (1996), 'Macchine', *Pitagora Editrice S.r.l. Bologna, Italy*.

[20]. S. Lieblein, F. C. Schwenk & R. L. Broderick, (1953), 'Diffusion Factor for Estimating Losses and Limiting Blade loadings in Axial-Flow-Compressor Blade Elements', *NACA Research Memorandum RM E53D01*.

[21]. W. H. Robbins, R. J. Jackson & S. Lieblein, (1955), 'Aerodynamic Design of Axial Flow Compressors VII – Blade-Element Flow in Annular Cascades', *NACA Research Memorandum RM E55G*

GT 2017-64517

DESIGN OF A SINGLE STAGE VARIABLE PITCH AXIAL FAN

Tommaso Bonanni, Alessandro Corsini,
Giovanni Delibra, David Volponi
Dept of Mechanical and Aerospace Engineering,
Sapienza University of Rome
Rome, Italy

Anthony G. Sheard
AGS Consulting LLC
Atlanta, GA, USA

Mark Bublitz
The New York Blower Company
Willowbrook, Illinois, USA

ABSTRACT

The European Union imposed minimum industrial fan efficiency levels in 2013 and then increased them in 2015. In the USA, the Department of Energy (DoE) is also developing regulations aimed at eliminating inefficient industrial fans from the market by 2023. A consequence of this regulatory activity is a need to apply design methods originally developed within the aerospace community to the design of high efficiency industrial fans.

In this paper, we present a process used to design, numerically verify and experimentally test a high-pressure single-stage axial fan. The goal was a fan design capable of working over a range of blade angles in combination with a single fixed cambered plate stator. We present the process used when selecting blade airfoil sections and the vortex distribution along the blade span. The selected methodology is based on a coupling between the aerodynamic response of each blade profile and the chosen vortex distribution, creating a direct link between the load distribution and the aerodynamic capability of the blade profile section. This link is used to develop radial distributions of blade twist and chord for the selected blade profiles that result in the required radial work distribution.

The design method has been enhanced through intermediate verifications using two different numerical methodologies. The methodologies are based on different approaches, in so doing providing confidence in the verification process. The final blade design has been analyzed using a three-dimensional computational fluid dynamic (CFD) code. Results of the CFD analysis indicate that performance of the final blade design is consistent with the design specifications.

The paper concludes with a comparison between predicted and experimentally measured performance. The need is clarified for balance between computational and empirical approaches. When used together the development effort results in a lower cost and higher efficiency design than would have been possible using either approach in isolation.

INTRODUCTION

Industrial fan designers have relied on empirical methods since the 1950's. In a market within which competitive advantage is driven by first-cost and lead-time, fan efficiency has not historically been a primary consideration. However, as governments become increasingly focused on cutting greenhouse gas emissions, they have developed regulations intended to eliminate the most inefficient industrial fans from the market. Minimum industrial fan efficiency levels became legally binding within the European Union in 2013, [1]. The USA Department of Energy (DoE) has continued a process of developing fan efficiency regulation through 2016 that is expected to become legally binding in 2017, [2]-[3].

Minimum current and forthcoming efficiency levels are now impacting industrial fan designers. Traditional empirical design methods reached their capability limit by the early 2000's and, since that time, they have been used to design industrial fans for new applications with similar, not improved fan efficiency. A compounding factor is the competitive industrial fan market place. Industrial fan designers are under pressure to design lower cost fans. A way to reduce cost is to reduce fan size whilst increasing blade-loading to achieve the same duty point. More highly loaded aerodynamic designs are typically less efficient than more lightly loaded designs. Consequently, industrial fan designers are caught between regulations mandating increased efficiency and a market demanding lower cost and, by implication, lower efficiency.

Although empirical design methods may have reached their capability limit, they have served the industrial fan community well for over five decades. The work of early pioneers was studied by Smith [4], who in 1965 reviewed two decades of linear cascade studies. Smith developed a universal approach to performance analysis based on the use of the local dimensionless variables flow coefficient Φ and load coefficient Ψ. This approach allowed a standardization of the

design process that was applied by Balje [5], Smith [4], Casey [6] and Cordier [7]. The resulting design charts constituted a starting point for turbomachinery designers and were also adopted by industrial fan designers, facilitating identification of the most appropriate fan configuration for a target duty point.

Standardization of the design process in the 1960's provided a theoretical sound starting point for turbomachinery designers. However, the actual design process reported in the existent literature was typically focused around the design of gas turbines, [8], [9], [10] and [11]. These design processes were classically derived from practical experience using compressor blade cascades. Although useful to the aerospace community, the resulting design processes were not directly applicable to the design of industrial fans. Industrial fans have significantly different operating requirements with respect to aerospace compressors. Hence, although the reported empirical design processes provide fan designers with useful insight into the challenges posed by the design process, they don't form a design process industrial fan designers can pick up and apply.

Industrial fan designers, working within individual fan companies, have classically adopted and empirically developed elements of aerospace design processes. The resulting methods reflect the cumulative empirical experience of engineers designing fans for a specific application over decades. The resulting design processes represent a form of local optimum, facilitating the design of industrial fans for a specific application. However, the engineers using nowadays those design processes, were not involved in their original development. They know these processes work, but they do not know why. Decades of tacit knowledge are embedded in the empirical design process and to simply set that aside in favor of new computational design methods would result in that tacit knowledge being lost. It is in this framework that this paper fits, trying to apply well-known design processes and correlations from the aerospace design know-how to the axial fan design scenario, in the more clear and consistent manner as possible.

In this paper, we present a design method that uses the results of traditional empirical design as a starting point. In so doing the new process is used within the context of traditional design processes. We present a process for design, numerically verifying and testing a high-pressure single stage axial fan. The design process starts by locating the desired design point on a Balje Chart. We then clarify the methodology used for blade and stator design, followed by the numerical verification of the resulting rotor and full-stage performance. Two numerical tools were used during the design process to verify that the new geometry was performing as intended; a quasi-three-dimensional axisymmetric code (AXLAB) and a three-dimensional synthetic rotor simulation based on an Actuator Disk model. These intermediate numerical verifications represent a critical part of the design process. They are quick-to-run and reliable tools, providing early feedback on the effectiveness of the chosen design strategy. Furthermore, in order to have a more detailed overview of the performance prediction and radial flow distribution through the blade-to-

blade passage, the rotor blade resulting from the design process has been analyzed by a full 3-D CFD simulation. A description of the experimental setup and the performance results concludes the work.

The paper concludes with a clarification of the need for balance between computational and empirical approaches. When used together, the combined design process produces lower cost and higher efficiency design than would have been possible using either approach in isolation.

DESCRIPTION ON THE FAN DESIGN SPACE

The reported research had a practical focus; to develop a high-pressure single stage axial fan for a specific duty point. Further, the design was required to work over a range of blade angles in combination with a single fixed cambered plate stator. Effectiveness of the design process was judged by the size of the resulting fans operating envelope. The operating envelope was defined as the operating range over which the fan was able to reach an efficiency of 60% or more. Fan diameter and speed were defined by the application; 813 mm diameter, tip clearance of 4 mm and rotational speed of 3600 rpm. The required duty point (Q, Δp), together with the geometric and cinematic constraints imposed by the application, defines the dimensionless global duty parameters (the flow coefficient and the work coefficient) and the well-known dimensionless specific speed and specific diameter, given by [8] and [12]. Taken together, these parameters and constraints facilitate definition of fan design space, Table 1.

Table 1. *Global design parameters*

Design point objectives	Formula	Value
Shroud diameter	D_s	0.813 m
Angular velocity	ω	376.99 rad/s
Global flow coeff.	$\Phi_d = Q/(\omega D_s^3)$	0.066 [-]
Global work coeff.	$\Psi_d = \frac{\Delta p_d}{\rho}/(\omega D_s)^2$	0.018 [-]
Specific speed	$\omega_s = \Phi^{1/2}/\Psi^{3/4}$	5.28 [-]
Specific diameter	$d_s = \Psi^{1/4}/\Phi^{1/2}$	1.42 [-]

Specific speed and specific diameter were used to plot the design point on a Balje Chart [5], Figure 1; the Cordier line, the line of best efficiency over the Balje Chart, is also reported. The design point falls between the 70% and 80% iso-efficiency contour. We may consider the characterization of the design point within the context of the flow coefficient Φ and load coefficient Ψ range empirically found to be optimal, Figure 2. This empirical approach enables the most appropriate type of industrial fan for a given design space. It has been presented by ESDU [13], providing industrial fan designers with a way to identify the type of fan most suitable for the application. In this

example, the design point falls within the axial fan design space.
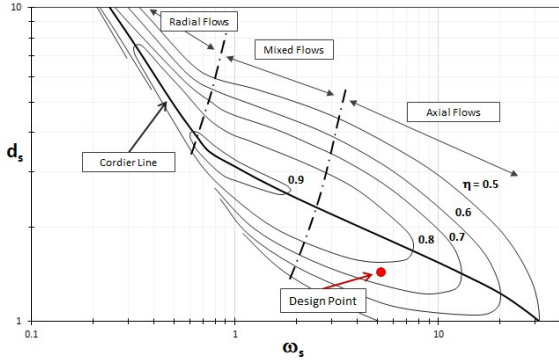
Figure 1 - *Balje Chart [5].*
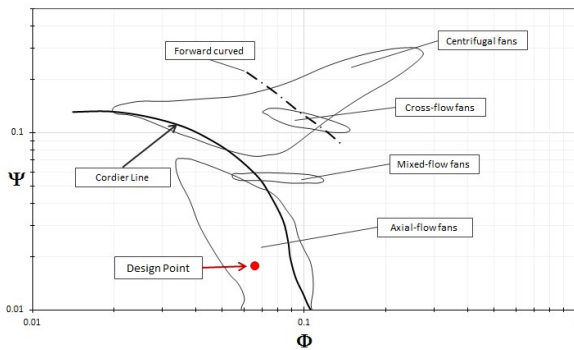
Figure 2 - *Optimum efficiency contours for various type of fan on Φ−Ψ plots [8].*

The blade-to-blade flow-field is characterized by leakage and secondary flow features. Although it is possible to model these flow-field features, it is not necessary to do so during the initial stages of the design process. During the initial stages, it is more appropriate to model the flow at meridional stream surfaces. The global flow coefficient and work coefficient, introduced in Table 1, can be redefined as follows:

$$\phi_d(r) = \frac{c_m(r)}{U(r)} \quad \text{design local flow coefficient}$$

$$\psi_d(r) = \frac{\Delta p_d / \rho}{U(r)^2} \quad \text{design local work coefficient} \tag{1}$$

where $c_m(r)$ is the local meridional velocity and $U(r)$ is the local blade speed. In this paper, we will refer to these coefficients at the mid-span radius r_{mid}, using the average meridional velocity and the mean blade speed.

STAGE DESIGN

The stage design comprises two fundamental steps. The designer iterates from one to the other until the resulting geometry converges on the duty point performance:

1. Inverse design
2. Direct analysis

The first is a classic inverse design problem, concerning the definition of the blade geometry and the characterization of the fan configuration. The second is a direct analysis of the geometry generated by the first. The fluid-flow through the blade-to-blade passage is predicted, and the resulting performance of the blade geometry established. Both steps are thoroughly described in specific sub-sections: *Hybrid Design Methodology* and *CFD-based direct problem*.

The inverse design concerns the aerodynamic design of the rotor blade, involving four design choices: the blade-profile selection, the vortex distribution along the blade span, the solidity and the twist distribution. Different blade design methods, developed using empirical rules from compressor cascade studies, are reported in literature. The design methodology reported in this paper, the *Hybrid Design Methodology*, is based on the coupling between the aerodynamic response of each blade profile, in terms of lift and drag coefficients (C_l and C_d), and the chosen vortex distribution.

The direct analysis problem uses computational methods that may be characterized as a 'virtual prototype' tools. The computational methods employed in this *CFD-based direct problem* are extensively described in a specific sub-section. Blade geometry previously generated by inverse design forms an input into the direct analysis element. The performance of the geometry is then predicted, as is the radial distribution of parameter at the blade trailing edge. These radial distributions then form an input into the stator design process. Hence, the direct analysis element both analyses performance of the previously generated blade geometry and facilitates stator design. In the application reported in this paper the stator design was constrained to a plate, rolled to a constant radius. The stator may therefore be conceptualized as cut from the surface of a cylinder. Although a significant constraint, inlet and exit angle could still be varied by varying stator chord. The radial distribution of stator chord is defined as:

$$l(r) = 2\tau \sin\left(\frac{\vartheta(r)}{2}\right), \tag{2}$$

where τ is the radius of curvature of the cambered plate and $\vartheta(r)$ is the camber radial distribution defined as:

$$\vartheta(r) = \alpha_2(r) - \alpha_3(r). \tag{3}$$

Rotor-only and stage performance are calculated using a progression of methods as the design develops. Initially an axisymmetric code is used, followed by an actuator disk code.

The entire stage design loop (design-analysis-design) is iterated until the design point is achieved within the geometric and cinematic constraints of the application. The aerodynamic parameters, used in the design-analysis-design loop, are defined in Figure 3 and the resulting fan geometry is summarized in Table 2.

The resulting design blade-to-blade velocities are low enough for the fluid to be treated as incompressible. The Reynolds number based on the chord and relative inlet velocity at the rotor tip is $1.2 \cdot 10^6$ at the design point. The relative rotor-stator distance from the rotor trailing edge to stator leading edge, measured at the hub, is half blade chord at the hub.

Table 2 - *Stage design geometry output.*

Stage Design data	Formula	Rotor	Stator
Hub to shroud ratio	$\chi = D_{hub} / D_{shroud}$	0.6	
Blade count	z [-]	12	11
Hub solidity	$\sigma_h = l_h / t_h$ [-]	0.97	1.13
Tip solidity	$\sigma_t = l_t / t_t$ [-]	0.56	0.66
Pitch hub	ξ_h [°]	26.3	103.6
Pitch tip	ξ_t [°]	11.8	105
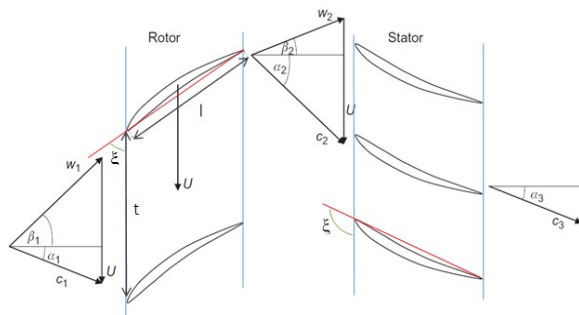
Figure 3 – *Geometry and aerodynamic parameters of a single stage axial flow fan; circumferential view.*

Hybrid Design Methodology for Inverse Problem

The *Hybrid Design Methodology* is derived from a method originally developed in the 1950's and reported by Mellor [14]. This method is significant as it is based upon results from a series of low-speed NACA-65 cascade studies. The NACA-65 profile has found widespread application in industrial fans as it has proven to be an effective profile for a wide range of industrial applications. The method developed by Mellor involved plotting inlet and outlet flow angles for blade section for a given camber and space-chord ratio. Stagger angles were then varied over a range of angles of attack.

The *Hybrid Design Methodology* presented in this paper is a two-dimensional design methodology. The complexity of three-dimensional flow through the blade-to-blade passage is partially modelled using a quasi-3D approximation, obtained by combining the flow conditions on the meridional plane and the circumferential plane. The flow is treated as an axisymmetric or circumferentially averaged 'meridional flow'. The blade is radially divided into sections from hub to casing with each cylindrical meridional stream surface intersecting the blade row to form a circumferential array of blade profiles known as cascade. The three-dimensional flow-field is, therefore, modelled by a series of such plane two-dimensional cascades, one for each of the cylindrical meridional surface spaced between hub and casing; in other words, the flow is treated as a series of superimposed 'cascade' flows.

The *Hybrid Design Methodology* matches the aerodynamic performance of the selected blade profile with the selected vortex and, therefore, load distribution along the blade span. In so doing, it defines the blade pitch and twist radial distributions. The *Hybrid Methodology* allows the designer, by changing the airfoil section or the vortex distribution, to modify the aerodynamic load along the blade span, for the same duty point and constraints.

The developed *Hybrid Design Methodology* composes a process, Figure 4. Design choices are highlighted in blue, design process elements are highlighted in yellow and the process output is highlighted in green. Once a design duty point is selected, the designer chooses the design load distribution along the blade span (free vortex, forced vortex, exponential vortex just to mention a few) and the blade profile. Consider the first design choice, the load distribution. The design presented in this paper utilizes a free vortex load distribution [15], entailing a constant $\psi_d\,(r)$ distribution. The free vortex load distribution results in a rotor exit velocity w_2 that has: i) a constant axial component $w_{2,m}$, ii) a tangential velocity component $w_{2,tg}$ that is inversely proportional to radius, iii) a radial velocity component $w_{2,r}$ that is zero.

The rotor exit velocity is defined as station 2 at the rotor blade trailing edge, Figure 3.

The choice of radial load distribution in turn defines the radial flow coefficient distribution as a consequence of assumed incompressible radial equilibrium [1]. Referring to the quasi-3D approximation previously described, this part concerns the meridional flow analysis. A feature of the *Hybrid Design Methodology* is the feedback loop regarding the losses (red loop in Figure 4). The design load coefficient $\psi_d\,(r)$, Equation 1, refers to the *real work* and, hence, to the actual design objective. Classically design methods are based on empirical or theoretical fluid deflection models and, therefore, refer to the *ideal work* (i.e. the Euler work). In order for the *Hybrid Design Methodology* to account for aerodynamic losses, it is mandatory to add a feedback losses loop that adjust the design load distribution to a *target $\psi_t\,(r)$*. The implemented losses model acts to reduce the work coefficient [17]; namely the

convergence of the loop will lead to $\psi_t(r) > \psi_d(r)$. In so doing the losses loop prevents the design of an under-loaded blade incapable of reaching the target design point.

The choice of the profile selection is necessary to get the aerodynamic performance analysis. The design presented in this paper utilizes a NACA-65 profile with a maximum thickness 12% of chord. The aerodynamic performance of the profile, in terms of C_l and C_d against the AoA, has been derived with XFoil [16], for each section taken at different radii.
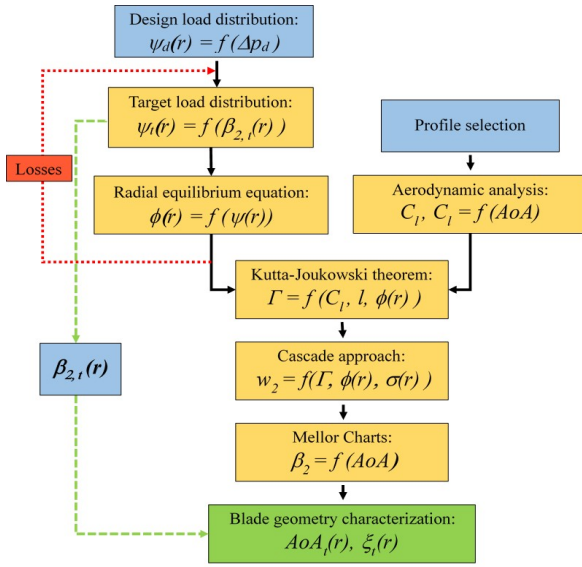
Figure 4 - *Hybrid design methodology.*

The aerodynamic characterization of each two-dimensional blade section and the meridional flow distribution are coupled using the Kutta-Joukowski theorem [12], which relates the lift generated by an airfoil to the circulation Γ (defined as the line integral of the velocity), the density ρ and the relative velocity between the airfoil and the fluid at infinity:

$$L = \Gamma \rho w_\infty(r) . \qquad (4)$$

This equation, combined with the definition of lift coefficient C_l

$$C_l = \frac{L}{0.5 \rho l w_\infty^2(r)} , \qquad (5)$$

leads to the formulation of the circulation Γ as function of the lift coefficient, the relative flow radial distribution and the chord length:

$$\Gamma(r) = 0.5 C_l w_\infty(r) l . \qquad (6)$$

The circulation Γ represents the link between the aerodynamic characterization of the blade profile and the operating condition of the blade itself.

The last step required for the creation of the Mellor Charts, concerns the evaluation of the radial distribution of fluid

deflection the selected two-dimensional blade profile can ensure. This is dealt with a cascade approach that allows the solution of the circumferential plane, resulting in [17]:

$$w_2(r) = \sqrt{\left(U - \frac{\Gamma(r)}{t} \right)^2 + c_m^2(r)} . \qquad (7)$$

Once the design point and the load distribution are defined, the outlet relative velocity is a function only of the solidity $\sigma(r)$ and the AoA (which defines the lift coefficient). This enables the creation of a Mellor Charts (Figure 5, blue line) for each two-dimensional profile:

$$\beta_2 = f(AoA) . \qquad (8)$$
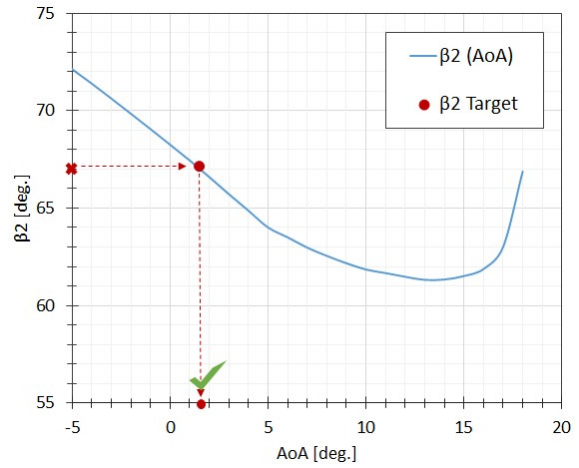
Figure 5 - *Mellor Chart.*

The last step in the *Hybrid Design Methodology* is a comparison between the fluid deflection induced by the blade section over a range of AoA and the target fluid deflection required by the selected load distribution. In the example presented in this paper, the target fluid deflection $\beta_{2\,target}$ (red symbol) is compared with the profile deflection capability (blue line); the output is the AoA_{target} (green check), Figure 5.

A smaller value of β_2 means a larger deflection imposed on the fluid, with the minimum β_2 value corresponding to the maximum lift coefficient the blade can provide. The objective of the design process is to ensure that the blade operates within its stable angle-of-attack range, where $AoA < AoA_{\beta2,min}$. By definition, the radial distribution of the AoA_{target} automatically defines the pitch distribution $\xi(r)$. The blade geometry characterization consequently becomes explicit, as does the rotor configuration.

Consequently, by merging the design load information with the aerodynamic blade capabilities within the design method, the *Hybrid Design Methodology* provides a designer with feedback on the feasibility of achieving the desired duty point with the chosen blade profile and load distribution.

CFD-based direct Analysis

Once blade geometry and rotor configuration are defined, performance of the design may be directly verified using computational fluid dynamics (CFD) tools. In addition, these tools are employed in order to get flow radial distribution after the rotor, required for the stator design. In the design method presented in this paper, two numerical tools have been used for the direct analysis:

1) A quasi-3D axisymmetric throughflow code (AXLAB), [17].
2) A 3-D synthetic rotor simulation based on the Actuator Disk inside Sapienza Virtual Test Rig [18].

AXLAB reproduces the complexity of 3D flow through the blade-to-blade passage using a quasi-3D approximation, obtained by the juxtaposition of the flow conditions on the meridional plane and the circumferential plane. This tool requires the solution of the radial equilibrium equation at only one axial station (after the rotor), synthetizing flow behavior inside the blade vane by means of different aerodynamic models. A losses model (the same described in the previous sub-section and extensively described in [17]) is implemented in the code. This model does not affect the fluid flow but affects only the total load coefficient.

The Actuator Disk model synthetizes the effect of the fan by momentum exchange between the blades and the fluid. This can be estimated by adding a source term f_i into momentum equation:

$$f_i = \frac{1}{2} w_\infty^2 \sigma F_i \frac{1}{\Delta z} \qquad (9)$$

where w_∞ is the average velocity vector, σ the local solidity, Δz the axial thickness of the actuator disk, $i=x,y,z$ and F_i the i-component of the aerodynamic coefficient. To compute this term, it is necessary to model the blade as a series of radial sections. For each blade section, we derived the polar curve of the profile using XFoil [16] and extended it with Viterna's methodology [19] up to -180<AoA<+180 degrees. The solver computes w_∞ and AoA at runtime according to the local flow and calculate F_i from these polar curves (that are given as input). As the blade is modeled in a discrete number of sections, from hub to shroud, F_i are estimated at intermediate radii by linear interpolation of C_l and C_d.

The Actuator Disk is not able to reproduce all the tip-leakage flow effect, being modelled neither the blade passage nor the tip gap. However, the losses due to the presence of the tip gap are estimated making use of the model presented by Vavra [20], affecting the flow field especially in the near-tip region and leading, in certain configuration, to flow recirculation at the tip.

Regarding the Actuator Disk, the incompressible Navier-Stokes equations were solved with OpenFOAM 2.4.x, a finite volume solver written in C++ [21].

Reynolds Averaged Navier-Stokes (RANS) closure relies on the high Reynolds implementation of the k–ε model by Launder. Computations were carried out in steady-state mode, using a Quadratic Upstream Interpolation for a Convective Kinetics (QUICK) discretization scheme for convective terms [22]; a Semi-Implicit Method for Pressure Linked Equations (SIMPLE) approach was selected for velocity-pressure coupling [23]. The linearized system of equations was solved using Generalized Algebraic Multi-Grid (GAMG) solver for pressure, and *smoothSolver* for all the other equations [24]. Convergence tolerance was set to 10^{-6} for pressure and 10^{-8} for the other quantities.

Simulations were run on a fully hexahedral mesh with 217k cells, on a domain that schematizes the fan inside a duct, mounted on a hub with a spinner cone. Because of the circumferential symmetry of the Actuator Disk approach, the simulated domain may be reduced to a portion of the entire system. Figure 6 shows the computational domain, the cell distribution and the Actuator Disk in red.

The two numerical tools both require less effort to set-up and run than a fully three-dimensional computational fluid dynamics (CFD) analysis. The AXLAB code requires the least effort, and is therefore used to verify initial performance of a new blade geometry. The Actuator Disk model requires more effort but provides a more accurate assessment of performance. It was consequently used later in the design process. The computing time required by the two tools is different; AXLAB is able to produce a duty point in few seconds, while the Actuator Disk requires around one hour.
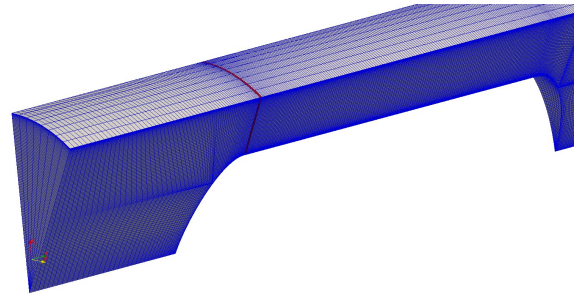
Figure 6 - *Actuator Disk computational domain and cell distribution.*

Even though the derivation and the effect of the losses are different, both the tools slightly overestimate the load coefficient. For this reason, the design process has stood to higher load coefficient values. However, both the axisymmetric code and the Actuator Disk tool correctly predict performance trends during the design process whilst changing global design parameter. This facilitated, for example, the evaluation of optimum blade number and the impact of blade angle. The two tools, therefore, made a useful contribution to the design process. These different methods may be regarded as representing a progression, with the second being progressively more accurate and computationally demanding than the first.

VIRTUAL PROTOTYPING AND CFD RESULTS

The final rotor design was then analyzed using a fully 3D CFD. The incompressible Navier-Stokes equations were solved with OpenFOAM 2.4.x in the rotating frame of references, adding centrifugal and Coriolis forces as source terms in the momentum equation.

RANS closure relies on the high Reynolds implementation of the k–ε model by Launder and then with the cubic k–ε model of Lien and Leschziner [25]. The latter was found in literature [26] to be able to tackle the shortcomings of linear models based on Boussinesq equation, by partially accounting for Reynolds stresses anisotropy in proximity of walls. This approach reasonably reproduces the features associated with turbomachinery flows, not usually captured by linear models. In particular, this model it suitable to accurately reproduce flow features in the near-tip region and in the casing treatment.

Computations were carried out in steady-state mode, using the same discretization scheme, solvers and convergence tolerance already described in the previous section. Simulations were run on a fully hexahedral mesh on a periodic blade-to-blade domain. The blade tip-to casing gap has been meshed with accuracy as well as the near-hub region of the blade. In total, the mesh comprises 4,100,000 hexahedral cells. The cell distribution at the junction between rotor and hub illustrates the mesh density, Figure 7. Mesh quality is summarized in Table 3. Boundary conditions imposed on the boundaries are defined in Figure 8 and summarized in Table 4.

Table 3 - *Rotor mesh quality and y+ values.*

	Minimum	*Maximum*	*Average*
Volume ratio	1	9	1.2
Aspect ratio	1	90	5
Skewness	0	0.65	0.1
Min. included angle	20	90	67
y+	0.3	2.9	1.7
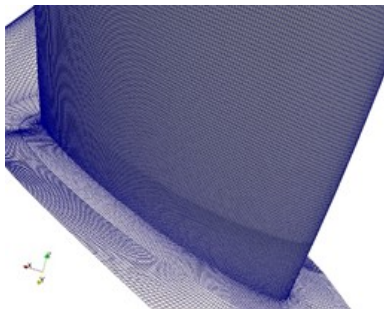
Figure 7 - *Cell distribution at the junction between rotor and hub.*
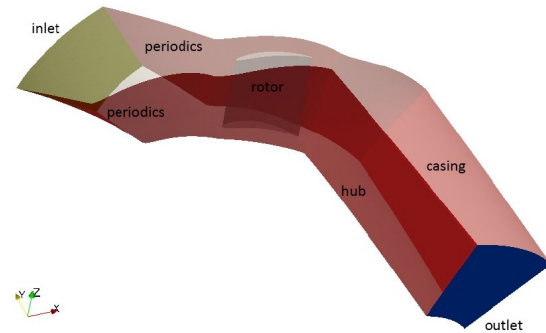
Figure 8 - *Computational domain and boundaries.*

Table 4 - *Boundary conditions.*

	Velocity	*k*	*ε*
Inlet	Q	TI=5%	ν_t/ν=100
Outlet	convective	convective	convective
Rotor blade	W=0.0	zero	zero gradient

Numerical simulations at two operating points were run with AXLAB, the Actuator Disk and the 3D CFD. The first simulation was conducted at the design point, the second at the design point flow rate less 17%. These two operating points were chosen as together they facilitate an assessment of the design point performance and design point stall margin.

As has previously been mentioned, the Actuator Disk model is a more accurate simulation of the flow-field physics than the AXLAB code. We therefore present flow and pressure coefficients plus total efficiency computed using the Actuator Disk and the 3D CFD, Table 5. At the design point, the Actuator Disk predicts a load coefficient of 0.122 in contrast to the 3D CFD that predicts 0.099 against the design target of 0.111. Both the simulation predicted a design point total efficiency above the 60% target.

Table 5 – *CFD results against the design specifications.*

	Actuator Disk		*3D CFD*		*Design*
ϕ_{mid}	0.270	0.328	0.270	0.328	0.328
ψ_{mid}	0.166	0.122	0.146	0.099	0.111
η_{tot}	65.5 %	70.3%	60.0%	65.1 %	>60 %

Analysis of the numerical simulations facilitates the evaluation of the extent to which the design flow has been achieved. To this end, the radial distributions of parameters both defined during the design process and computed are compared and plotted across the non-dimensional radius *r* [%]. As explained in the previous section, *design* values do not necessarily correspond to the *target* distributions. Consequently,

7

a velocity distribution comparison should be intended as a-posteriori analysis of the fluid deflection achieved by the different tools and not as the driving process of the design method itself.

The radial distributions of computed parameters are not directly comparable because of the limitations inherent in the AXLAB code and Actuator Disk model. We facilitate comparison of computed radial distributions of velocity, absolute and relative flow angles by studying each one-half blade-chord downstream of the blade trailing edge. In order to obtain a comparable analysis of the radial flow distribution computed by the three numerical tools, the results obtained with the 3D CFD have been circumferentially averaged.

Consider the radial distribution of the meridional component of relative outlet velocity $w_{2,m}$, Figure 9. The AXLAB code prediction (green line) is close to the design; the free vortex behavior is well modeled by AXLAB, that predicts an almost constant meridional velocity along the blade span, with a slight underestimation in the near-tip region and an overestimation near the hub. The Actuator Disk model (orange line) slightly enhances this trend; in the near tip region, the tip gap losses affect the flow field, which results decelerated. The 3D CFD (blue line) models the blade tip-to casing leakage flow and the secondary flow features that characterize the hub region. The resulting prediction of the meridional component is significantly different to the Actuator Disk model. There is a velocity deficit from 80 to 100% blade-span that may be attributed to impact of the blade tip-to-casing leakage vortex. In the central zone of the blade-span the meridional component is predicted to be higher than design.

Consider the radial distribution of the tangential and radial components of relative outlet velocity $w_{2,tg}$ and $w_{2,r}$, Figure 10. All the methods predict a similar trend of tangential component $w_{2,tg}$. As expected from the design logic, AXLAB underestimates further from the design $w_{2,tg}$, i.e. it overestimates the absolute tangential velocity. This greater estimated deflection leads to an overestimation of $\psi_t\,(r)$. The Actuator Disk distribution confirms the overestimation of the load coefficient (Table 5). The comparison also highlights the role of the losses models in the Actuator Disk, which predicts quite precisely the fluid deflection (compared to 3D CFD) but underestimates the losses due to three dimensional and geometric effects. In fact, even though the 3D CFD has a $w_{2,tg}$ lower than the design, the load coefficient is slightly lower than the design value, suggesting an important and complex role of the losses mechanism that are not completely modelled by the axisymmetric tools

Both the Actuator Disk and the 3D CFD highlight a negative radial motion $w_{2,r}$ from 0 to 85-90% of the span. In the near-tip region, the Actuator Disk estimates positive value of $w_{2,r}$ while it is almost null in the 3D CFD. This analysis suggests a contraction of the streamlines towards the central part of the span, explaining the meridional velocity profile of Figure 9.

Consider the radial distribution of absolute and relative outlet flow angles α_2 and β_2, Figure 11. The three tools predict similar trend in relative flow angle β_2. The differences that do exist are more apparent when studying the absolute flow angle α_2; this is due to the differences between predicted meridional outlet velocity that deeply affect the absolute flow angle (being the tangential component very similar).
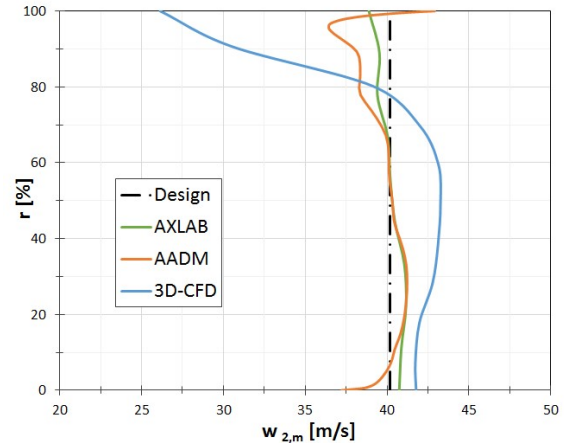
Figure 9 - *Relative outlet velocity; meridional component.*
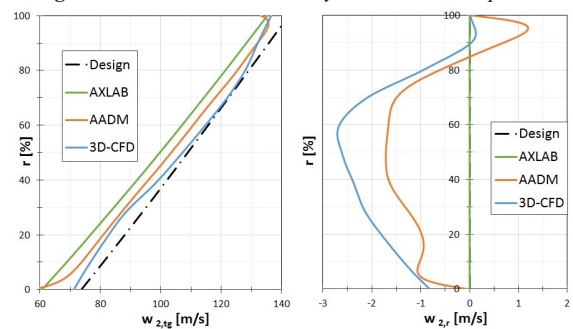
Figure 10 - *Relative outlet velocity; tangential and radial component.*
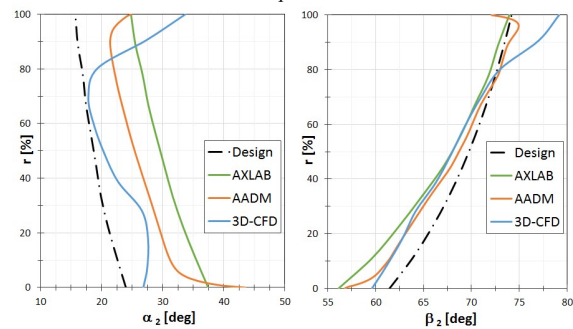
Figure 11 - *Absolute and relative outlet flow angle.*

A better explanation of the complexity of the flow field is given by Figure 12, that shows the blade-to-blade passage, the radial section where the velocity vectors have been probed and helicity density iso-surface. The helicity is the integrated scalar product of the velocity field and the vorticity field. The integrand of the helicity is the helicity density h [m/s^2] and is an indicator of the relation between turbulence and dynamic events happening in turbulence, giving a measure of the vorticity transported by the flow. The radial section shows the radial component $w_{2,r}$ with the purple line representing the zero-component iso-contour; the near-tip region is characterized by the presence of both positive and negative areas, justifying the almost null averaged value reported in Figure 10. The radial component analysis suggests the presence of the tip leakage vortex, confirmed by the helicity iso-surface These vortical structures are colored with the meridional component $w_{2,m}$; reverse flow (blue color) due to the tip vortex is present in the final part of the blade, while most of the vortex is convected with a meridional velocity lower than the mean value ($w_{2,m}$=41 m/s, light-blue). This explains the strong deceleration of the averaged meridional flux of Figure 9.

The disagreement between predicted parameters at the blade hub and tip is a consequence of neglecting wall boundary layer effects during the design process. Wall boundary layer results in blockage and leads to increased axial velocities at blade mid-height. Both the design approach and AXLAB are axisymmetric codes and they are not able to account for any radial or recirculating motion in the near-hub and near-tip region. The 3D CFD is able to reproduce all the vortical structures that evolve through the blade-to-blade passage, resulting in a more complex flow field not predicted by the Actuator Disk model.
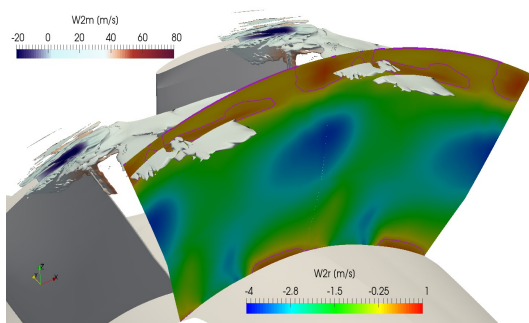
Figure 12-*Blade to blade passage; relative radial velocity and helicity iso-surface (h=40000 m/s^2) colored with relative meridional velocity.*

Relative velocity iso-contours on three surfaces at three different radial heights calculated using the 3D CFD are presented in Figure 13. The fluid is aligned with the blade profile along all the blade span; no flow separations occur along the profile and the wake is limited in a very small region at the

trailing edge of the blade. Taken together the above indicates a well-designed blade.

(a)

(b)

(c)

(d)
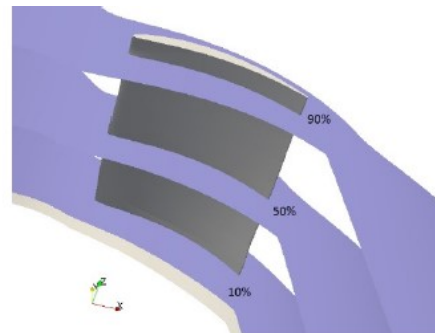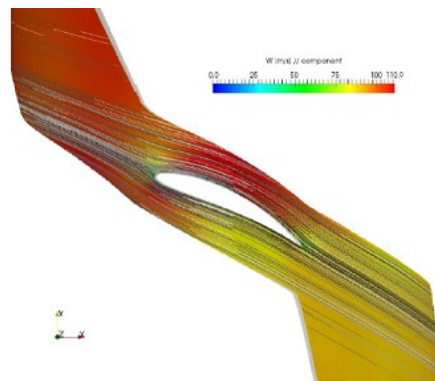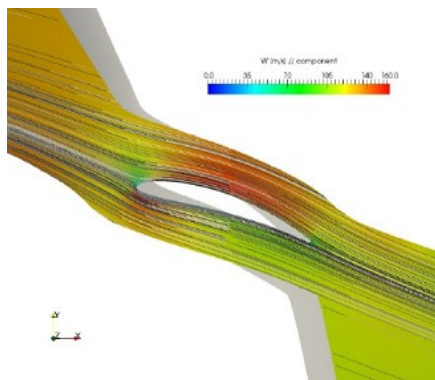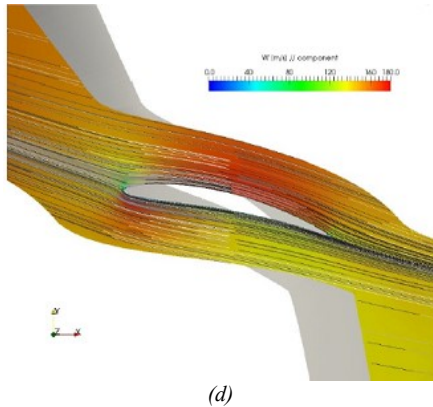
Figure 13 - *Relative velocity contours and streamlines on 3 surfaces (a) at 19% (b), 50% (c) and 90% (d) of rotor span.*

Helicity density iso-surface colored with absolute velocity are presented in Figure 14. The blade tip-to-casing leakage vortex is ejected from the blade pressure side 50% blade chord downstream of the blade leading edge. This location for ejection was expected as it corresponds to peak differential pressure across the blade tip. The absence of large vortical structures along all the blade suction surface is an indicator of well-conditioned flow through the blade-to-blade passage at the design duty point.
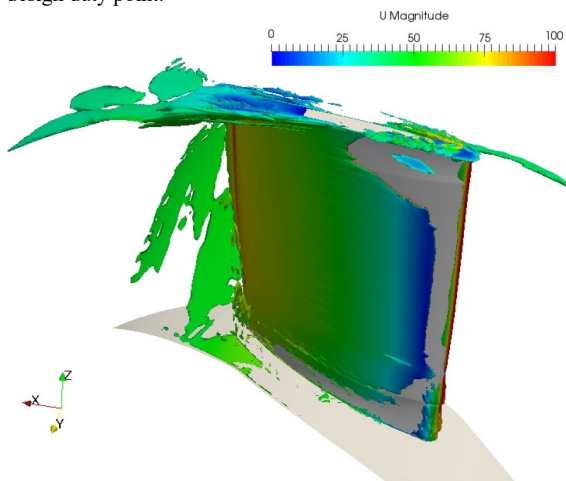
Figure 14 - *Helicity iso-surface (h=50000 m/s^2) colored with absolute velocity magnitude.*

To conclude, the aerodynamic flow conditions behind the rotor are reproduced with different accuracy by the numerical methods. The tangential velocity component is characterized by a similar trend, close to the free vortex radial distribution used for designing the fan stage. As mentioned before, the absolute

outlet flow angle $\alpha_2(r)$ predicted by the Actuator Disk is the input parameter for the stator design; the difference between the Actuator Disk and the 3D CFD distributions is relatively small (with a maximum value of 6° mainly due to a different predicted meridional component). In addition, the stator camber plate resulting from the 3D CFD $\alpha_2(r)$ profile would be louder, more difficult to manufacture and less "flexible", if compared to the smoother shape of the Actuator Disk $\alpha_2(r)$ profile.

Starting from a numerical approach as simple as AXLAB, and then progressively refining the methodology with the Actuator Disk model and then the 3D CFD, it was possible to reduce the uncertainty of the design as a designer progress through the methodology. By using each in progression as the new fan design was developed, it was possible to both minimize the time needed to design the fan and have confidence it would perform as intended when built and tested.

EXPERIMENTAL TESTS

The final fan design was built and experimentally tested in accordance with the requirements of the AMCA 210-07, standard chamber setup Figure 12-type B [27] for different blade angles. Inside the test chamber, flow straighteners and screens are installed to ensure uniform flow conditions. Flow rate is adjusted by means of a throttle and an auxiliary fan until the prescribed volume flow rate through the test system is obtained. Flow rate is derived from a measurement of differential pressure across a muzzle inside the chamber. Static pressure rise across the fan is the difference between static pressure in the test chamber and ambient pressure outside the chamber. The fan test setup is illustrated in Figure 15.
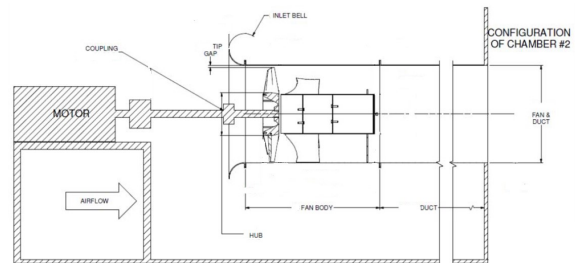
Figure 15 - *Fan test setup.*

The final design was tested with blade at nine angular positions from 15 degrees to 55 degrees, as measured at the blade hub. The nine fan characteristics were then transformed into a 'fan chart' by overlaying efficiency contours, Figure 16.

The fan chart presents a substantial portion of the operating envelope with a total efficiency above the target 60% from 7 to 24 m^3/s and a blade pitch range of 25 to 55 degrees. At the beginning of the design process a Balje chart was used to characterize the design point (Figure 1) indicating a maximum available efficiency slightly higher than 70%.

At the design point the achieved efficiency is around 60%, representing a good outcome for many different reasons; the first one concerns the technical manufacturing and testing differences between the present fan and those that populated the Balje chart. Specifically, the aerodynamic design was compromised by a requirement for stators to be manufactured from rolled-plate. Twisted and tapered airfoil stators would have resulted in both a higher peak fan efficiency, and better off-design efficiency. Furthermore, the gap in efficiency is explained by a sure and certain difference between the dimensional parameters (Q, Δp, ω, D_s) that define the dimensionless ω_s-d_s. Obviously, cinematic and geometric constraints (ω, D_s) force ω_s-d_s to a sub-optimal space. In addition, it is very critical to deal with such a direct efficiency comparison for a variable pitch fan; in fact, once the blade is designed, the fan can be identified in the Balje Diagram by the best efficiency operating point of its entire range of angular position, making the comparison with the design duty point meaningless.

The designed fan achieved a peak efficiency of just over 70% being able to ensure the required efficiency at off-design point in a wide range of angular position. This efficiency operating chart was considered by the authors to be a success for an industrial fan with rolled-plate stators, tested as a prototype. A production version of the fan can reasonably be expected to eliminate some aerodynamically undesirable features associated with the prototype, and may therefore be expected to perform slightly better than the prototype.
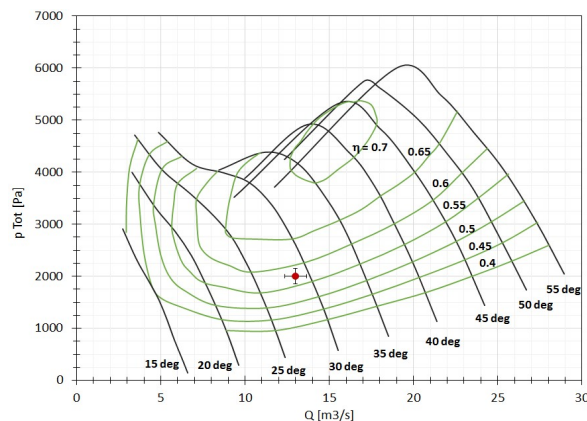
Figure 16 - *Fan operating chart.*

CONCLUSIONS

This paper presents the process used to design a pressure variable pitch axial fan, with target total efficiency above the 60%. The Balje chart characterizes the fan design point (Φ=0.066, Ψ=0.018) as theoretically capable of achieving a total efficiency of over 70%. When built, and tested the final

design did achieve a total efficiency of over 70% over a portion of its operating range.

The rotor design process is based on two steps; the first utilizes a *Hybrid Methodology* that directly links a designer-selected vortex distribution with the aerodynamic capability of designer-selected two-dimensional blade profiles. The hybrid design returns radial distributions of blade chord, pitch and twist and gives feedback on the practical feasibility of the selected blade profile to achieve the selected work distribution. The second step comprises a performance assessment of the selected two-dimensional blade profile when stacked into a three-dimensional blade using the step-one derived radial distributions of blade chord, pitch and twist. Performance is assessed using a quasi-three-dimensional axisymmetric throughflow code named AXLAB and a three-dimensional synthetic rotor simulation based on an Actuator Disk model within a virtual test rig. The AXLAB code is quick to setup and run. The Actuator Disk model takes more time to setup and run, however more accurately models the flow-field physics than the AXLAB code.

The stage design is completed with a fixed stator design; the stator was undertaken using the radial distribution of rotor exit flow angle, computed using the Actuator Disk model, as an input parameter.

The final design was validated through a full three-dimensional computational fluid dynamic (CFD) analysis of the blade-to-blade flow-field. The fluid-flow and the global performances were compared with design values and with those predicted by AXLAB and the Actuator Disk. These methods represent with different accuracy the fluid-flow spanwise distribution. Compared to the design target, the load coefficient is overestimated by 10% by the Actuator Disk model and underestimated by the 3D CFD at the design operating point. Both methods predicted efficiency would be above the 60% target at the design point.

The fluid flow comparison clarified that the differences between the 3D CFD fields and those computed by AXLAB and Actuator Disk are related to a different capability of each computational method to model three-dimensional vortical structures (i.e. the tip vortex) that characterize the blade-to-blade passage and distort the streamlines in the blades span. The 3D CFD analysis indicated that the *Hybrid Design Methodology* had facilitated creation of a blade design capable of working at the design point in accordance to the selected vortex distribution, with differences due to the different losses models implemented in the axisymmetric tools.

The achieved efficiency was considered by the authors to be good for a prototype industrial fan incorporating rolled plate stator blades.

The final fan design was built and tested in accordance with the requirements of AMCA 210-07. The fans characteristic was measured at nine blade angles from 15 to 55 degrees that were used to generate the new designs fan chart. The fan chart illustrates that the final fan design achieves a total efficiency of 60% over substantial portion of its operating range. These

achieved efficiency levels were concluded to be good for an industrial fan design utilizing rolled-plate stators.

The design process (design-analysis-design) presented in this paper allows a designer to assess the feasibility of achieving a target design point using a selected two-dimensional airfoil and vortex distribution. The use of a quasi-three-dimensional axisymmetric code and three-dimensional synthetic rotor simulation based on an Actuator Disk model minimize the need for three-dimensional CFD analysis. Even if the 3D CFD is still an essential analysis step, the presented design process considerably reduces the number of high time demanding 3D simulations, by defining the blade geometry and configuration in a previous cheap to run step. In so doing the time and cost associated with the design of a new industrial fan is also minimized, bringing it within reach of all industrial fan designers.

ACKNOWLEDGMENTS

NOMENCLATURE

Latin

c	Absolute velocity	[m/s]
C_l	Lift coefficient	[-]
C_d	Drag coefficient	[-]
D	Fan diameter	[m]
f	Momentum equation source term	[m/s²]
F	Aerodynamic component; $F = f(C_{l,d}, w_\infty)$	[-]
h	Helicity density; $h = u \cdot (\nabla \times u)$	[m/s²]
l	Chord length	[m]
L	Lift	[N/m]
n	Rotational speed	[rpm]
p	Total pressure	[Pa]
Q	Volume flow rate	[m³/s]
P	Mechanical power	[W]
Re	Reynolds number; $Re = wl / v$	[-]
r_{mid}	Midspan radius; $r_{mid} = 0.5(r_{shroud} + r_{hub})$	[m]
r [%]	Non-dimensional radius; $r\,[\%] = r / r_{hub}$	[-]
t	Blade spacing; t=2πr/z	[m]
U	Rotation velocity	[m/s]
w	Relative velocity	[m/s]
z	Blade count	[-]

Symbols

Δp_{tot}	Fan total pressure rise	[Pa]
α	Absolute flow angle	[-]

β	Relative flow angle	[-]
ζ	Pitch angle	[-]
Γ	Circulation	[m²/s]
χ	Hub to shroud ratio	[-]
ϑ	Camber	[-]
τ	Radius of curvature	[m]
ρ	Fluid density	[kg/m³]
σ	Solidity; σ= l / t	[-]
Φ	Global flow coefficient; $\Phi = Q/(\omega D^3)$	[-]
ϕ	Local flow coefficient; $\phi(r) = c_m(r)/U$	[-]
Ψ	Global load coefficient; $\Psi = \Delta p/\rho/(\omega D)^2$	[-]
ψ	Local load coefficient; $\psi(r) = \Delta p/\rho/U(r)^2$	[-]
ω	Angular velocity	[1/s]
ω_s	Specific speed; $\omega_s = \Phi^{1/2}/\Psi^{3/4}$	[-]
d_s	Specific diameter; $d_s = \Psi^{1/4}/\Phi^{1/2}$	[-]
ν	Kinematic viscosity	[m²/s]
η_{tot}	Fan total efficiency; $\eta_{tot} = \Delta p_{tot} Q / P$	[-]

Acronyms and subscripts

1	Upstream rotor section
2	Downstream rotor section
3	Downstream stator section
AoA	Angle of attack
AXLAB	Axial Laboratory
ESDU	Engineering Sciences Data Unit
d	Design value
m	Meridional direction
mid	Midspan
r	Radial direction
t	Target value
tg	Tangential direction
tot	Total
∞	Average vector

REFERENCES

[1]. Corsini A., Delibra G., Sheard A. G., (2013), ' A Critical Review of Computational Methods and Their Application in Industrial Fan Design', *ISRN Mechanical Engineering, vol. 2013, Article ID 625175, pag. 20.*

[2]. Mathson, T., Ganesh, R., Dikeman, S., Osborn, K. And Bublitz, M., (2015), 'Introducing Fan Efficiency Ratios', *An AMCA International Whitepaper, www.amca.org/whitepapers.*

[3]. Hauer A., Brooks J., (2012), 'Fan Motor Efficiency Grades in the European Market', *AMCA in motion (2), pp. 14-20.*

[4]. S. F. Smith, (1965), 'A simple correlation of turbine efficiency', *Proc. Seminar on Advanced Problems in Turbomachinery, Von Karman Institute.*

[5]. O. E. Balje, (1981), 'Turbomachines', *John Wiley.*

[6]. M. V. Casey, (1987), 'A mean line prediction method for estimating the performance characteristics of an axial compressor stage', *International Conference on Turbomachinery-Efficiency Prediction and Improvement, Paper C 264/87.*

[7]. O. Cordier, (1953), *Brennstoff-Wirme-Fraft, 5, 337.*

[8]. R. I. Lewis, (1996), 'Turbomachinery performance Analysis', *Butterworth-Hainemann.*

[9]. Wallis R. A., (1961), 'Axial flow Fans', *George Newnes Limited, London.*

[10]. Carter A. D. S., Hughes H. P., (1946), 'A Theoretical Investigation into the Effect of Profile Shape on the Performance of Airfoils in Cascade', *British Aeronautical Research Counsil.*

[11]. Howell A. R., (1942), 'The present basis of Axial Flow Compressor Design', *British Aeronautical Research Council.*

[12]. S.L. Dixon, C.A. Hall, (2010), 'Fluid Mechanics and Thermodynamics of Turbomachinery', *Butterworth-Heinemann, Oxford OX2 8DP.*

[13]. ESDU, (1980), 'A guide to fan selection and performance', *ESDU Item No. 79037.*

[14]. Mellor, G., (1957), 'The aerodynamic Performance of Axial Compressor Cascades with Applications to Machine Design', (sc.D.Thesis), *M.I.T. Gas Turbine Lab, M.I.T. Rep. No. 38.*

[15]. J. Horlock, (1958). 'Axial Flow Compressors-Fluid Mechanics and Thermodynamics, *Butterworths Scientific Publications.*

[16]. Drela, Mark, and H. Youngren. 'X-Foil 6.96' *Software December (2001).*

[17]. Bonanni T., Cardillo L., Corsini A., Delibra G., Sheard A. G., Volponi D., (2016), 'Derivative Design of Axial Fan Range: from Academia to Industry' *GT2016-57469.*

[18]. Bonanni T., Corsini A., Delibra G., Sheard A. G., Volponi D., (2016), 'Modeling of Axial Fan and Anti-stall Ring on a Virtual Test Rig for Air Performance Evaluation', *GT2016-56862.*

[19]. Viterna, L. A., Janetzke D. C., (1982) 'Theoretical and Experimental Power from Large Horizontal-Axis Wind Turbines', *NASA TM-82944.*

[20]. Vavra M. H., (1960), 'Aero-Thermodynamics and Flow in Turbomachines',. *John Wileys Sons, 380.*

[21]. Weller H. G., Tabor G., Jasak H., Fureby C., (1998), 'A Tensorial Approach to Continuum Mechanics using Object-oriented Techniques', *Journal of Computational Physics, vol. 12(6), pp. 620-631.*

[22]. Leonard, B. P., (1979), 'A stable and accurate convective modelling procedure based on quadratic upstream interpolation', *Computer Methods in Applied Mechanics and Engineering Vol. 19 (1).*

[23]. Patankar, S. V. and Spalding, D.B. (1972), 'A calculation procedure for heat, mass and momentum transfer in three dimensional parabolic flows', *Int. J. of Heat and Mass Transfer, Volume 15, Issue 10, October 1972, Pages 1787-1806.*

[24]. Jemcov, A., Maruszewski, J.P. and Jasak. H., (2007), 'Performance improvement of algebraic multigrid solver by vector sequence extrapolation', *CFD 2007 Conference, CFD Society of Canada.*

[25]. Lien, F.S. & Leschziner, M.A. (1994), 'Assessment of Turbulence-transport Models Including Non-linear RNG Eddy-viscosity Formulation and Second-moment Closure for Flow over a Backward-facing Step'. *Computers & Fluids, vol. 23, pp. 983-1004.*

[26]. Durbin B. (2011), 'Review: Adapting Scalar Turbulence Closure Models for Rotation and Curvature'. *Transactions of the ASME, Journal of Fluids Engineering, vol. 133, Paper No. 061205, pp. 1-8.*

[27]. ANSI/AMCA 210-07, *2008.*

GT2018-76363

A META-MODEL FOR AERODYNAMIC PROPERTIES OF A REVERSIBLE PROFILE IN CASCADE WITH VARIABLE STAGGER AND SOLIDITY

Gino Angelini, Tommaso Bonanni, Alessandro Corsini,
Giovanni Delibra, Lorenzo Tieghi, David Volponi

Department of Mechanical and Aerospace Engineering, Sapienza University of Rome
Via Eudossiana 18, 00184 Rome, Italy

ABSTRACT

In this paper, a systematic CFD work is carried out with the aim to inspect the influence of different cascade parameters on the aerodynamic performance of a reversible fan blade profile. From the obtained results, we derive a meta-model for the aerodynamic properties of this profile. Through RANS simulations of different arrangements in cascades, the aerodynamic performance of airfoils are analyzed as Reynolds number, solidity, pitch angle and angle of attack are varied. The definition of a trial matrix allows the reduction of the minimum number of simulations required. The computed CFD values of lift and drag coefficients, stall margin and the zero-lift angle strongly depend on cascade configuration and differ significantly from standard panel method software predictions. In this work, X-Foil has been used as a benchmark. Particularly, the high influence of pitch angle and solidity is here highlighted, while a less marked dependence from the Reynolds number has been found.

Meta-models for lift and drag coefficients have been later derived, and an analysis of variance has improved the models by reducing the number of significant factors. The application of the meta-models to a quasi-3D in-house software for fan performance prediction is also shown. The effectiveness of the derived meta-models is proven through a spanwise comparison of a reversible fan with the X-Foil based and meta-model based versions of the software and 3D fields from a standard CFD simulation. The meta-model improves the software prediction capability, leading to a very low global overestimation of the specific work of the fan.

INTRODUCTION

A significant part of the design and performance prediction of axial flow compressors and fans is based on measurements of the flow through two-dimensional cascades. Among the first scientific investigations on the influence of solidity, we report on experiments conducted by Howell [1], Carter [2] and Kantrowitz [3], with many further studies highlighting the importance and the sensitivity of the topic. In addition, systematic works on NACA 65-series compressor blade sections indicate a continuous variation of blade-section performance as the major cascade parameters (blade camber, inlet angle and solidity) are varied [4]. These works are of fundamental importance for compressor designers to select the proper blade camber and angle of attack when compressor velocity diagram and desired solidity have been selected.

In order to successfully satisfy design requirements and provide a reliable performance analysis, designers require accurate cascade data not only in the design point, but also over a wide range of angle of flow conditions and cascade geometry parameters [5]. Unfortunately, this kind of data is seldom available for target fan design conditions and in particular for reversible profiles that are commonly used in tunnel and metro applications. Nowadays design procedure, which always relies more on optimization procedures, overcome this problem by the massive use of simulation processes, that require to be easy to compute and of a comparable level of accuracy as physical testing data. To address such a challenge, approximation or metamodeling techniques are often used providing an accurate solution with a comparable degree of accuracy.

Meta-models have been found to be a valuable tool to support a wide scope of activities in modern engineering design,

especially design optimization [6][7]. The pivotal concept of several recent works is, in fact, the development of CFD-based metamodels to solve very specific problems as the design of a machine in a specific work condition or in a particular configuration [8]. Very little effort in the last years was devoted to the implementation of CFD-based metamodels in older design or performance analysis procedures, providing the designer with new and more reliable instruments.

The main objective of this paper is the creation of a metamodel for deflection, lift and drag coefficient based on these geometric, cinematic and dynamic factors. In particular, response surface methodology and Central Composite Design (CCD) [9] are used to develop a second-degree polynomial regression model of the aerodynamic response of the blade profile. The CCD trials matrix is obtained by two-dimensional CFD simulations of the cascade configuration; data for deflection and aerodynamic coefficients when varying the four input factors are obtained with OpenFOAM 2.4.x solver.

The obtained meta-models are compared with results obtained by X-Foil software [10].

NUMERICAL METHODOLOGY

Computations were carried out with the C^{++} open-source code OpenFOAM 2.4.x [12] using the *simpleFoam* solver for steady computations of incompressible flows. Generalized Algebraic Multi-Grid solver was used for pressure equation, while U and $\tilde{v}$ equations were solved with a *smoothSolver*. Convergence threshold was set to 10^{-3} for lift and drag coefficients. The same numerical approach has been applied to all the simulations.

RANS closure

Turbulence modelling relied on the Spalart-Allmaras turbulence model [12], commonly used for external aerodynamics.

Grid

The fully hexahedral computational domain entails a single 2D blade-to-blade passage, with periodic boundary conditions imposed in the pitch-wise direction. The domain extends 30 chords up- and 60 down-stream of the blade leading and trailing edge. Grid dimensions vary between a minimum of 210k cells to a maximum of 600k, depending on the solidity of the case. A y+ value of y+ ≈ 1 is obtained by setting wall spacing to 0.02 mm for all the grids. Mesh quality indicators (Table 1) are very similar between all the grids.

Table 1 - Mesh quality indicators

	Min	Max	Average
Area ratio	1	1.7	1.03
Aspect ratio	1	106	17
Skewness	0	0.58	0.03
Min incl. angle	25	90	82
y+	0.02	0.79	0.3

The correct inlet fluid angle for every simulation is achieved by specifying a constant velocity vector at the inlet. The v inlet value is adjusted case by case in order to obtain the desired Re number, and $\tilde{v}$ inlet value is set to $\tilde{v} = 3v$. At the outlet of the domain convective boundary conditions are specified. Over blade walls, the no-slip conditions for velocity is imposed, while $\tilde{v}$ treatment in the boundary layer relies on *nutUSpaldingWallFunction* [14].

Validation

Validation of the approach has been achieved through a comparison between numerical results and experimental data from Emery et al. [4].
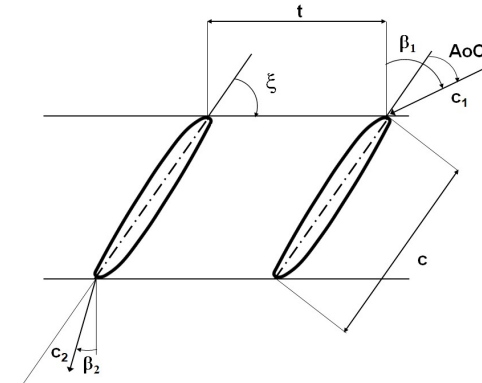
Figure 1 – Geometrical definition of the cascade.

Available data refers to performance analysis of different NACA profiles with combinations of inlet air angle, solidity and cambers over the useful angle of cascade. Figure 1 shows the cascade geometry, where angle of cascade (AoC) is defined as the angle between the pitch angle ζ and the flow inlet velocity c1, and t the blade spacing. Five configurations of the NACA 65-010 profile are here used for the validation (Table 2), with constant value of solidity σ =1, chord c = 0.973 m and Re = 245000. This profile has been chosen because literature lacks on experimental data on reversible cascades, and among the families of the available NACA profiles, 65-010 is geometrically more similar to a reversible blade (straight chord and high thickness).

Table 2 – Geometrical parameters and flow characteristics

Case	Pitch	AoC	β_1
1	34	4	60
2	57	-3	30
3	57	12	45
4	63	15	45
5	57	17	60

A sensitivity analysis has been carried out, testing the same configurations for three different cells numbers (45k, 200k and 350k). The sensitivity analysis shows results independency from 200k to 350k cells. For the reversible profiles further analyzed a grid refinement near the leading and trailing edge of the blade has been required in order to maintain the same mesh quality indicators. The numerical methodology here presented shows a good capability of predicting the aerodynamic performance of the blade (Table 3).

Table 3 - Validation Results

Cells	45k		200k		350k		Emery	
Test	β_2	CI	β_2	CI	β_2	CI	β_2	CI
1	34.71	-0.180	33.59	-0.152	33.6	-0.153	33.4	-0.15
2	58.73	0.064	59.08	0.028	59.1	0.028	59.2	0.03
3	36.15	0.334	36.00	0.331	36.0	0.331	35.6	0.34
4	37.43	0.418	37.15	0.397	37.1	0.397	36.3	0.4
5	44.2	0.494	45.05	0.469	45.0	0.468	45.1	0.475

CENTRAL COMPOSITE DESIGN

In statistical modeling, regression analysis is a process for estimating how variables are connected, either focusing on the relationships between dependent and one or more independent variables, or to find which among the independent variables explain the higher variability. Among all the methods for carrying out regression analysis, Response Surface Methodology (RSM), introduced by Box and Wilson in 1951 [11], uses a sequence of designed experiments to obtain an optimal response. Here a second-degree polynomial is used to estimate the response surface. This polynomial is easy to estimate, and it is suitable for optimization processes.

Within the theory of optimization, an experiment is a series of tests in which the input variables are changed according to a given rule in order to identify the reasons for the changes in the output response [9]. Design Of Experiments (DOE) is inherently a multi-objective optimization problem regarding the selection of the points that maximize the accuracy of the information obtained by experiments (whether numerical or physical). In order to perform a DOE it is necessary to define the problem, choose the variables (which are called *factors* by the experimental designer) and define the design space, or *region of interest*, which is the range of variability for each factor. Each factor can assume different values, or *levels*, according to its discretization within the design space. The DOE technique and the number of levels are to be selected according to the number of experiments which can be afforded. A full factorial design of experiment is commonly used to test all possible combinations of various factors, leading to a large number of experimental trials. Indeed, when using quadratic polynomial for modelling a response surface, (k+1)(k+2)/2 coefficients, or *regressors* are required, being *k* the number of factors; to fit quadratic response surfaces, at least the same

number of points and three levels for each design factor are required. In most cases it is impossible to have a full-factorial 3-level design with 3^k experiments.

A popular compromise which reduces the number of experiments close to a 2-level full factorial design is the Central Composite Design (CCD), a 2^k full factorial to which $2k$ axial trials (or star points) and n_c center point trials are added [9]. In CCD, factors are tested at minimum of three levels: minimum, middle and maximum, equivalent to levels -1, 0 and 1, which are called *coded units*.

The placement of the axial points is based on the concept of *rotatability*, a property that ensures that the prediction variance is dependent only on the distance from the origin and not on the orientation with respect to the coordinate axes. It therefore provides equal precision of response estimation in any direction of the design. To obtain rotatability of a design, each experimental factor must be represented at five levels of coded units $-\alpha, -1, 0, 1, \alpha$. As shown by [15], for a full factorial CCD, a design is rotatable if:

$$\alpha = \left(2^k\right)^{0.25} \qquad (1)$$

Here a *Central Composite Inscribed* (CCI) is used: axial points are located at factors levels -1 and 1, while factorial points are brought into the interior of the design space and located at distance $1/\alpha$ from the center point (Figure 2). The method requires three levels for each factor.
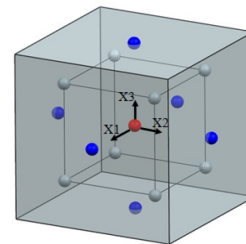
Figure 2 - Visualization of CCI for three factors X_1, X_2, X_3.

Levels for the investigated factors Re (X_1), σ (X_2) ξ (X_3) and AoC (X_4) were specified by the application and available experimental data set. In particular, the coupling between chord and twist radial distribution of the blade and the global information of the tested fans (blade count, reference pitch, rpm and characteristic curve), automatically leads to the definition of the entire design space.

All the tested factors affect the flow field, and consequently the lift and drag coefficients, in the cascade. The interaction between the tested parameters and quadratic effects cannot be easily described or predicted using theoretical analysis only. In this case, response surface methodology and CCD were used to identify the significance of each of these factors and develop a second-degree polynomial correlation for lift and drag coefficient prediction. A rotatable CCI was used as the experimental design. Four factors were studied in the simulations, at which corresponds a number of factorial runs

equal to $2^4 = 16$, and to maintain rotatability in accordance with (2), with $\alpha = 2$. The operating ranges for all the factors and the levels at which they were tested are shown in Table 4.

Table 4 - Tested levels of design factors X_1, X_2, X_3 and X_4

Factors	Coded Levels and Corresponding Absolute Levels				
	-1	-1/α	0	1/α	1
X_1	500000	863000	1230000	1590000	1950000
X_2	0.155	0.454	0.752	1.051	1.350
X_3	15.0	24.85	34.7	44.55	54.4
X_4	-3.0	2.5	8.0	13.5	19.0

The total number of experimental trials is equal to $N=2^k+2k+n_c=25$. Full factorial design represents a possible alternative approach, but it is computationally more expensive due to the requirement of a minimum of $3^4=81$ numerical trials. The CCI design for the considered factors results in the trial matrix presented in Table 5. In the same table Cl and Cd values calculated by CFD simulations are presented as well.

Table 5 - Design of experiment matrix

Trial	X_1	X_2	X_3	X_4	C_l	C_d
1	8.63E+05	0.454	24.85	2.5	0.201	0.0130
2	1.59E+06	0.454	24.85	2.5	0.202	0.0122
3	8.63E+05	1.051	24.85	2.5	-0.106	0.0129
4	1.59E+06	1.051	24.85	2.5	-0.106	0.0113
5	8.63E+05	0.454	44.55	2.5	0.132	0.0136
6	1.59E+06	0.454	44.55	2.5	0.132	0.0132
7	8.63E+05	1.051	44.55	2.5	-0.077	0.0149
8	1.59E+06	1.051	44.55	2.5	-0.072	0.0137
9	8.63E+05	0.454	24.85	13.5	0.878	0.0182
10	1.59E+06	0.454	24.85	13.5	0.880	0.0168
11	8.63E+05	1.051	24.85	13.5	0.500	0.0136
12	1.59E+06	1.051	24.85	13.5	0.500	0.0133
13	8.63E+05	0.454	44.55	13.5	0.771	0.0143
14	1.59E+06	0.454	44.55	13.5	0.770	0.0135
15	8.63E+05	1.051	44.55	13.5	0.417	0.0105
16	1.59E+06	1.051	44.55	13.5	0.415	0.0098
17	5.00E+05	0.753	34.7	8.0	0.394	0.0122
18	1.95E+06	0.753	34.7	8.0	0.379	0.0131
19	1.23E+06	0.155	34.7	8.0	0.712	0.0156
20	1.23E+06	1.350	34.7	8.0	0.100	0.0113
21	1.23E+06	0.753	15.0	8.0	0.595	0.0117
22	1.23E+06	0.753	54.4	8.0	0.294	0.0137
23	1.23E+06	0.753	34.7	-3.0	-0.335	0.0190
24	1.23E+06	0.753	34.7	19.0	0.612	0.0308
25	1.23E+06	0.753	34.7	8.0	0.383	0.0114

These trials are sufficient to derive a meta-model with a least square method, however, to have a more exhaustive comprehension, several additional points have been computed. In particular, for a given triplet of factors X_1, X_2 and X_3, different value of X_4 (AoC) were investigated. These aerodynamic conditions have been simulated in order to detect the curvature of the C_l and the slope increase of the C_d in the near stall region and the minimum value of the C_d in the linear range of the polar curve.

RESULTS AND DISCUSSION

Figure 3 shows the lift and drag coefficient curves of the tested configurations versus the one computed by X-Foil, a

program commonly used to calculate lift and drag characteristics. Different line styles (i.e. dotted vs dashed lines) denote different solidity for the same pitch, and every symbol refers to a different pitch angle. The trial points of the CCI matrix are marked with empty symbols. The polar curves obtained from X-Foil show a very low dependence from the Re numbers, so only the curve at the intermediate Reynolds is reported. The X-Foils curves mismatch with the trials predictions in term of C_l and C_d values, curve slope, stall margin and the zero-lift angle. This behavior is fully justified by the fact that X-Foil only simulates isolated airfoils. X-Foil predictions are still useful as a term of comparison. The most interesting relations found by the authors are listed below.

The Reynolds number is not affecting the C_l curves, while the C_d distributions slightly decrease as the Re number increases. Figure 3 reports the Cl distribution for a single Reynolds number, as all the curves would be overlapping.
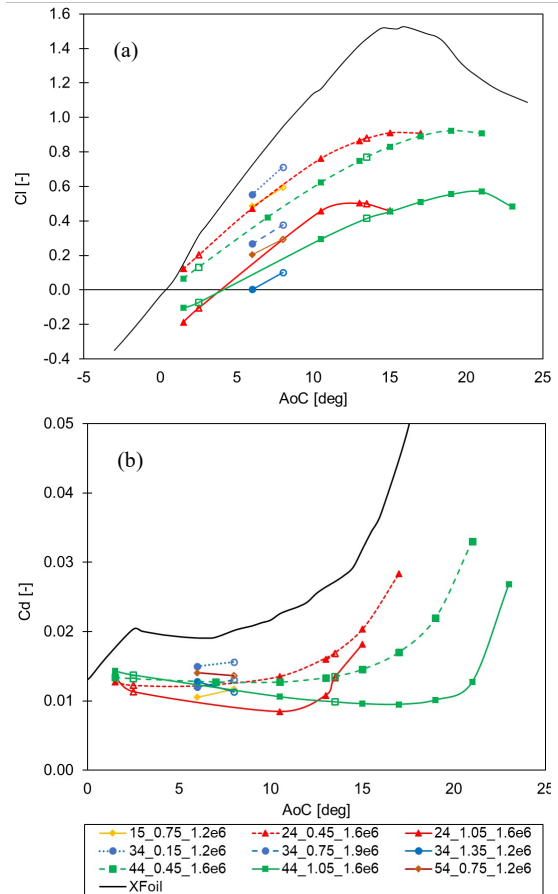
Figure 3 - Lift (a) and drag (b) coefficient distributions of selected cascades configurations among those tested. Key: ξ_σ_Re.

It is evident that the computed curves differ substantially when changing the geometrical configuration. With an accurate analysis, it is possible to detect a clear logic in the mechanism that affects the changes in the curves, by isolating the pitch (ξ) and solidity (σ) effects on the deflection capability of the cascade.

Effect of pitch angle

For a fixed σ, an increase of the cascade pitch increases the stall margin of the polar curves, while maintaining approximately the same deflection capability (C_l). An increase in ξ modifies C_l curves and extend the stall margin, that is defined as the delta between the zero lift and the maximum lift angle of cascade (triangle dashed line to square dashed line and triangle solid to square solid in Figure 4); the higher the pitch, the lower the angular coefficient of the stable range of the polar curve, while the zero-lift AoC approximately remain unchanged. The pitch effects on the aerodynamic characterization of the cascade are shown in Figure 5. These geometrical configurations have the same C_l at 17° but present a completely different aerodynamic. At a pitch angle of 24° the cascade is in stall, presenting a big recirculation zone on the suction surface, while at ξ=44° the cascade still operates in the stable range. For a fixed solidity and AoC, a lower pitch results in a more blocked configuration that leads to anticipated stall. For a fixed pitch angle, an increase of the cascade solidity deeply affects the polar curves which are shifted at lower C_l values. This behavior is highlighted in Figure 5, where an increase in σ (dashed to solid for every line) reduces the deflection capability and the stall margin of the cascade.

Figure 5 - Streamlines over velocity contours for Re=8e5, AoC = 17 deg, σ = 0.45, ξ = 24 deg (a) and ξ = 44 deg (b).

Effect of solidity

The solidity effects on the aerodynamics of the cascade are shown in Figure 7 and Figure 8, where velocity streamlines and velocity contours at two different configurations are reported. Figure 7 refers to a high deflection condition (triangle dotted/solid lines in Figure 6). The high solidity cascade is in stall, while at σ = 0.45 the cascade is still in the stable range in a near-stall situation.

The high influence of the solidity on cascade deflection capability is also highlighted in Figure 8 (light blue and dark blue curves in Figure 6) where the blade interaction due to the high solidity leads from an higher lift coefficient (C_l = 0.55 in Figure 8 (a)) to a zero-lift situation (Figure 8 (b)). In conclusion, the blockage due to high solidity (similarly to the blockage due to low pitch values) affects the aerodynamic of the cascade, reducing the deflection capability and the stall margin.

Figure 4 - Pitch influence on the lift coefficient curves.
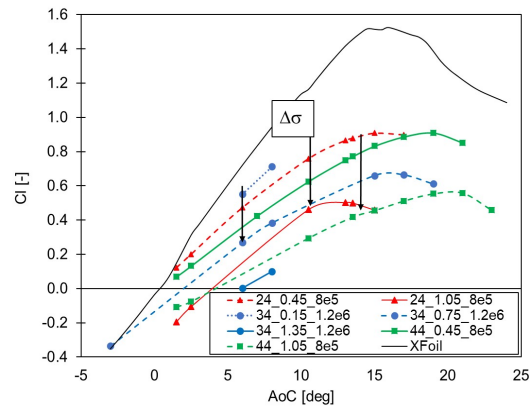
Figure 6 - Solidity influence on the lift coefficient curves.
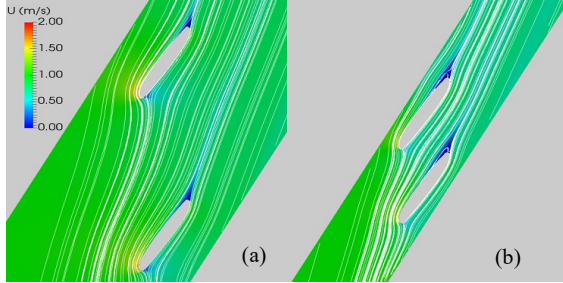
Figure 7 - Streamlines over velocity contours for Re=1.2e6, AoC =13 deg, ξ = 24 deg, σ = 0.45 (a) and σ =1.05 (b).
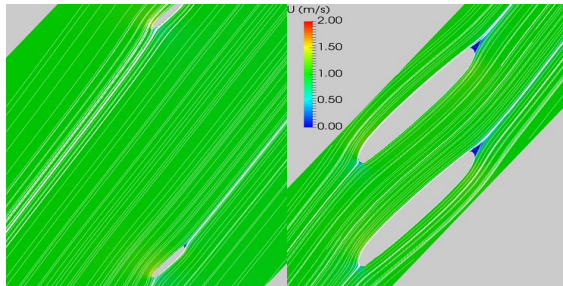
Figure 8 - Streamlines over velocity contours for Re=1.2e6, AoC = 6 deg, ξ = 34 deg, σ= 0.15 (a) and σ = 1.35 (b).

Also, the drag coefficient curves in Figure 3b are affected by the blockage effects on the cascade and follow the same logic. At low pitch angles the growing portion of the Cd curves have higher gradients, while, for high solidity values, the curves are slightly shifted, and the minimum drag coefficient point approaches the high gradient zone of the curve leading to a stall margin reduction.

META-MODEL AND STATISTICAL ANALYSIS

Lift and drag coefficients at specific points of the design matrix (Table 5) were used to build the meta-models. A least square method [16] was applied to derive a mathematical correlation by fitting a response surface to the computed values of C_l and C_d at the CCI points. As suggested from the results reported in the previous section, the independence of the lift coefficient curves from the Reynolds number (X_1), suggested to neglect this factor from the C_l regression analysis. The full quadratic models are given by (2) and (3):

$$C_l = 0.543$$
$$-0.6537X_2 - 0.0161X_3 + 0.1087X_4$$
$$+0.0559X_2^2 + 0.00015X_3^2 - 0.00205X_4^2 \quad (2)$$
$$+0.00534X_2X_3 - 0.0168X_2X_4 - 0.00036X_3X_4$$

$$C_d = 0.01102$$
$$+4.82\cdot10^{-10}X_1 - 2.54\cdot10^{-3}X_2 + 1.46\cdot10^{-4}X_3 - 1.29\cdot10^{-4}X_4$$
$$-7.32\cdot10^{-16}X_1^2 + 1.24\cdot10^{-3}X_2^2 - 8.61\cdot10^{-7}X_3^2 + 9.85\cdot10^{-5}X_4^2 \quad (3)$$
$$-1.54\cdot10^{-10}X_1X_2 + 1.87\cdot10^{-11}X_1X_3 + 2.25\cdot10^{-11}X_1X_4$$
$$+7.36\cdot10^{-5}X_2X_3 - 6.21\cdot10^{-4}X_2X_4 - 2.27\cdot10^{-5}X_3X_4$$

Both models consider linear effects, quadratic effects and two-way interactions between the factors. The empirical correlation represented into (3) and (4) must use factors in uncoded units, i.e., actual values of these factors. Coding of factors removes any pseudo effects due to the use of different scales. In this way, coefficients in the model equations become a measure of the magnitude of the response of linear effects, resulting from one-unit change in a factor in one specific term, with all other terms held constant. Whenever two factors (X_iX_j) are involved, the effect of a change in one factor associated with the interaction term varies depending on the value chosen for the other factor. In the case of quadratic terms, the response to a change in the value of a factor depends on the value of the factor itself.

A perfect fit between the model and the training data cannot be achieved because a second order polynomial cannot describe all the relationships between factors response. Coefficients of determination R^2, *adjusted R^2* and *predicted R^2* are commonly used to assess the quality of the model. R^2 is a statistic which indicates the response variation explained by a model, being a pure correlation between measured and predicted values; in regression R^2 measures how the regression surface approximates the real data set. However, being R^2 monotone in the number of variables when dealing with ordinary least square, a meaningful comparison between two models can be performed with the *adjusted R^2* [17]. This statistic is used to compare the explanatory power of models and its value increases only when an added term improves the model more than by chance [18]. These coefficients are calculated using data that were themselves used for model development.

Predicted R^2 is used to assess the model prediction capability for new observations. It is calculated by systematically removing each observation from the data set, estimating the regression equation and determining the model's capability in predicting the removed observation. The predictive residual sum of squares statistic is used to calculate the value of predicted R^2 [19]. The coefficients of determination R^2, (Table 6), show that the C_l model accurately approximates the data at the design points, while the C_d model is much less accurate.
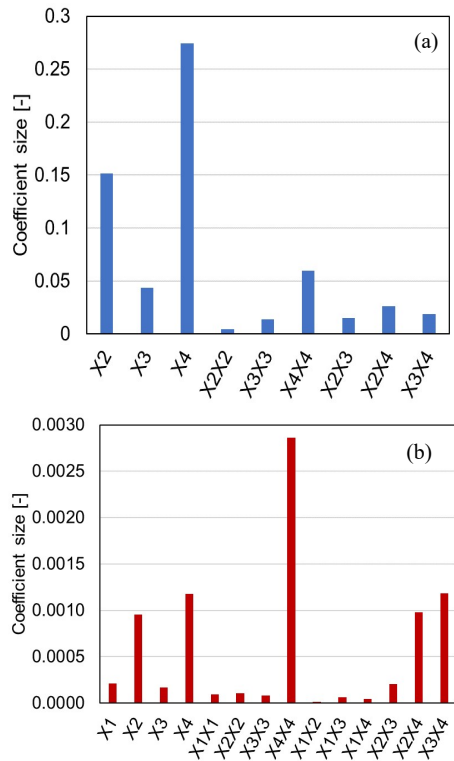
Figure 9 - Comparison of the absolute values of the coefficients in coded units for each term of the full C_l (a) and C_d (b) model.

The predictive capability of the developed C_l model for new observations may be 94%, based on the predicted R^2 value, which is computed by removing from the DOE matrix the trial points with the same X_2, X_3, X_4. The C_d model presents a not acceptable value of 9%, but this high value is caused by the alteration of the predictive capability and the related statistics of the model when dealing with two-way interaction terms of factors at several different orders of magnitude (as X_1X_3). Fortunately, these factors have usually very low coded coefficients (Figure 9) and are statistically not significant.

Table 6 - Full model fitting test results.

Model Parameter	C_l Full Model	C_d Full Model
R^2	98.67%	80.61%
Adjusted R^2	97.87%	64.20%
Predicted R^2	94.07%	9.32%

The statistical significance of the terms of the models defined by equations (3) and (4) can be evaluated using the *analysis of variance* (ANOVA) [19], that is a collection of statistical model used to analyze the differences among group means and their associated procedures. The observed variance in a particular variable is partitioned into components attributable to different sources of variation. For all terms of the model equation, values characteristic of a so-called ANOVA table are calculated individually. These values will be important in subsequent discussions and are thus defined here.

The Adjusted Sum of Square is computed term by term and estimates the reduction in residual sum of square when including the considered term in the model. The Adjusted mean squares (Adj MS) is obtained by dividing Adj SS by the number of degrees of freedom (DF). These statistics are of primary importance when comparing the full model with the reduced model obtained by omitting the variable in question. Variation in the data unexplained by the model is represented by the Residual Error (RE).

Ratios of the Adj MS for all terms of the model equation and Adj MS of the RE are calculated. Because the ratios of variances follow an F-distribution [15], an F-test [20] is employed to identify statistically significant terms of the model. An F-test is a statistical test in which the test statistic has an F-distribution under the null hypothesis. It is used when comparing models that have been fitted to a data set, in order to identify the model that best fits the population from which the data were sampled, or, in other words, to identify statistically significant terms of the model. By performing an F-test for each term of the model, it is possible to obtain the specific p-values. Under the null hypothesis [20], i.e. the inclusion of the specific term does not have significative effect on the model [21], this statistics measure the probability of obtaining data at least as extreme as the data from the model. Therefore, a low p-value indicates a great dependency of the predicted response from the specific term.

Results of ANOVA for the full C_l quadratic model are shown in Table 7, while Table 8 reports the ANOVA for a partially-reduced C_d quadratic model. This table is obtained by removing some two-way interaction terms and one quadratic term that have be found to affect all the statistics; these terms have the lower coded coefficients (Figure 9b).

Table 7 - ANOVA table for the full Cl quadratic model.

Source of Variation	DF	Adj SS	Adj MS	F-Ratio	*p*-Value
Regression	9	2.645	0.294	123.3	2.0E-12
X_2	1	0.576	0.576	241.8	1.2E-10
X_3	1	0.047	0.047	19.8	4.7E-04
X_4	1	1.881	1.881	789.5	2.2E-14
X_2X_2	1	5E-04	5E-04	0.2	0.66
X_3X_3	1	0.004	0.004	1.7	0.21
X_4X_4	1	0.075	0.075	31.3	0.0001
X_2X_3	1	0.004	0.004	1.7	0.22
X_2X_4	1	0.012	0.012	5.1	0.04
X_3X_4	1	0.006	0.006	2.5	0.13
Residual Error	15	0.036	0.002		
Total	24	2.680			

Table 8 - ANOVA table for a partially-reduced Cd quadratic model.

Source of Variation	DF	Adj SS	Adj MS	F-Ratio	*p*-Value
Regression	11	0.0003	3.0E-05	4.9	0.004
X_1	1	1.1E-06	1.1E-06	0.2	0.67
X_2	1	2.3E-05	2.3E-05	3.8	0.07
X_3	1	6.9E-07	6.9E-07	0.1	0.74
X_4	1	3.5E-05	3.5E-05	5.7	0.03
X_2X_2	1	5.8E-07	5.8E-07	0.1	0.76
X_3X_3	1	8.7E-09	8.7E-09	0.001	0.97
X_4X_4	1	1.8E-04	1.8E-04	29.8	0.0001
X_1X_4	1	3.2E-08	3.2E-08	0.005	0.94
X_2X_3	1	7.5E-07	7.5E-07	0.1	0.73
X_2X_4	1	1.7E-05	1.7E-05	2.8	0.12
X_3X_4	1	2.4E-05	2.4E-05	4.0	0.07
Residual Error	13	7.8E-05	6.0E-06		
Total	24	0.0004			

Improved meta-models

Based on the results of ANOVA shown in the previous Tables, the models were improved by removing terms (one-by-one) with *p*-values greater than 0.05, considered as statistically insignificant at a 95% confidence level. The removed terms were not taken into account in the regression analysis. The improved models are defined by:

$$C_l = 0.3028$$
$$- 0.3843X_2 - 0.0045X_3 + 0.0992X_4 \quad (4)$$
$$- 0.0022X_4^2$$
$$- 0.0168X_2X_4$$

$$C_d = 0.00961$$
$$- 5.99 \cdot 10^{-10}X_1 + 1.7 \cdot 10^{-3}X_2 + 1.65 \cdot 10^{-4}X_3 \quad (5)$$
$$- 1.11 \cdot 10^{-4}X_4 + 9.91 \cdot 10^{-5}X_4^2$$
$$- 6.21 \cdot 10^{-4}X_2X_4 - 2.27 \cdot 10^{-5}X_3X_4$$

Absolute values of the coefficients for each term of the second-degree polynomials based on factors expressed in coded units are shown in Figure 10.
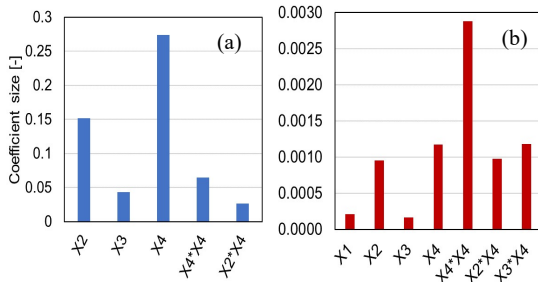
Figure 10 - Comparison of the absolute values of the coefficients expressed in coded units for each term of the enhanced C_l (a) and C_d (b) model.

The most significant factor for both C_l and C_d enhanced model is clearly the AoC (X_4), which has high coefficient values for both the linear and quadratic terms. A second important term is the solidity (X_2), that, as explained in the previous section, considerably shifts the polar curve. Linear term related to pitch (X_3) is less significant than the other terms. The effects of the interaction terms vary depending on the values of these factors; in the C_l model, for all values of solidity, the interaction X_2X_4 affects the response less than the AoC linear term. Because the AoC is the most important factor, the value of X_4 was always taken into account while evaluating the influence of the other variables on C_l and C_d values.

Regarding the C_d regression, some terms that in Table 5 are characterized by *p*-values higher than 0.05 are included in the enhanced model. The terms X_2 and X_3X_4, after removing one-by-one the higher *p*-values factors, became statistically significant; the terms X_3 and X_2X_4 have been included in the model, even if characterized by high *p*-values, because both the R^2 and the predicted R^2 have been found to substantially decrease for a model not including these terms. In order to maintain acceptable model fitting test results, we opted for including X_3 and X_2X_4 in the C_d model; this combination of terms has been found to guarantee the higher *adjusted R^2* value.

Although R^2 and *adjusted R^2*, shown in Table 9, decrease if compared with those of the full quadratic models (Table 6), the enhanced models offer a higher prediction capability of 94.7% and 33.6% for new observations. The higher value of predicted R^2, combined with the reduced computational time required whenever the meta-models are adopted in a software, fully justifies the model improvement.

Table 9 - Improved model fitting test results.

Model Parameter	C_l Improved Model	C_d Improved Model
R^2	98.14%	80.23%
Adjusted R^2	97.65%	72.09%
Predicted R^2	94.70%	33.64%

A summary of ANOVA applied to the enhanced model are presented in Table 9 (C_l) in Table 10 (C_d).

Table 10 - ANOVA table for the enhanced Cl quadratic model.

Source of Variation	DF	Adj SS	Adj MS	F-Ratio	*p*-Value
Regression	5	2.631	0.526	200.8	9.3E-16
X_2	1	0.576	0.576	219.9	6.7E-12
X_3	1	0.047	0.047	18.0	4.4E-04
X_4	1	1.881	1.881	717.9	1.5E-16
X_4X_4	1	0.114	0.114	43.4	2.7E-06
X_2X_4	1	0.012	0.012	4.6	0.04
Residual Error	19	0.05	0.003		
Lack-of-fit	9	0.050	0.006	480.1	5.6E-12
Pure error	10	0.0001	1.15E-05		
Total	24	2.68			

8

Table 11 - ANOVA table for the enhanced Cd quadratic model.

Source of Variation	DF	Adj SS	Adj MS	F-Ratio	*p*-Value
Regression	7	0.0003	4.6E-05	9.9	6.4E-05
X_1	1	1.1E-06	1.1E-06	0.2	0.63
X_2	1	2.3E-05	2.3E-05	4.9	0.04
X_3	1	6.9E-07	6.9E-07	0.1	0.71
X_4	1	3.5E-05	3.5E-05	7.3	0.015
X_4X_4	1	2.2E-04	2.2E-04	47.7	2.5E-06
X_2X_4	1	1.7E-05	1.7E-05	3.5	0.077
X_3X_4	1	2.4E-05	2.4E-05	5.2	0.036
Residual Error	17	8.0E-05	4.7E-06		
Total	24	0.0004			

Significant changes in the lift coefficient were observed when increasing the solidity of the cascade. As illustrated in Figure 11, for a fixed AoC, the higher the solidity, the lower the C_l; in addition, a high-solidity configuration decreases the maximum achievable lift coefficient, even at high AoC. This trend is more pronounced at high X_3 value, Figure 11 (b). The solidity effects on the aerodynamic efficiency (C_l / C_d) are illustrated in Figure 11 (c) and (d), that presents high efficiency regions at low solidity. At higher pitch values, the regions are shifted to higher AoC and are more affected by solidity increase.

As explained in the previous section (discussion of Figure 4), for a fixed solidity, a pitch increase tends to slightly decrease the cascade deflection capability for a given AoC. Figure 12 shows this dependence at two solidity levels, with the C_l contour being not perfectly parallel to the vertical axis. This effect is less important if compared to the solidity effect and is confirmed by the X_3 coefficient size of Figure 10. Aerodynamic efficiency contours are illustrated in Figure 12 (c) and (d).

META-MODEL ASSISTED PERFORMANCE PREDICTION

It is necessary to develop and optimize robust, fast and reliable numerical tools for fan performance prediction. It is particularly important to have numerical tools that are able to verify designer choices, with cheap computational time and within a known range of confidence. Here we show the predicting capability enhancement whenever the derived meta-models are applied to an in-house developed software, the quasi-3D *AxLab* solver. This is achieved through comparison with 3D fields of a standard k-ε simulation. The meta-model implementation in AxLab leads to a far better prediction of 3D statistics and spanwise distributions, especially in term of specific work. It must be stressed the extreme gain using this approach, thanks to the computational time savings (in this case few seconds for an AxLab run versus days of computing time).

AxLab software is a python program for performance analysis of ducted axial fans [22]. It is based on a blade element axisymmetric principle whereby the rotor blade is divided into a number of streamlines. For each among these, relationships for velocities pressure are derived from incompressible

conservation laws for mass, tangential momentum and energy. The complexity of 3D flows inside the vane is partially reproduced using a quasi-3D approximation, obtained by the juxtaposition of the flow conditions on the meridional plane and the circumferential plane.

Two alternative versions of AxLab software are here analyzed; they differ from each other on the way β_2 is computed. The standard AxLab derives profile deflection from the C_l polar curves from X-Foil software (X-Foil based - XB), while an enhanced version uses the derived meta-model (meta-model based - MB). Both are applied for the performance prediction of a reversible fan. The fan is simulated at the duty point $\Phi = 0.072$ and $\Psi = 0.0092$ with ξ=20 deg. Validation of the model has been achieved through comparison with experimental data ($\Phi = 0.072$, $\Psi = 0.009$). Table 12 shows the variation of the factors included in the meta-model over the span of the blade. They are all fully included in the initial DOE space.

Table 12 - Features of the simulated fan.

Normalized span	Reynolds number	Solidity	Pitch angle
0.1	1000861	0.985	39.36
0.2	1055204	0.859	36.78
0.3	1085536	0.742	34.34
0.4	1095647	0.638	32.05
0.5	1091150	0.548	29.89
0.6	1079369	0.472	27.88
0.7	1069073	0.411	26.02
0.8	1070307	0.365	24.30
0.9	1094293	0.333	22.72
1.0	1259222	0.310	20.00

The introduction of the meta-models is responsible for an overall improvement of the solver. An analysis of significant outlet flow feature over the normalized span of the blade (r/r$_{tip}$) is reported below. Along all the span, enhanced AxLab grants a perfect fit in term of axial outlet velocity, apart from a small deflection in the mid span of the blade (Figure 13a). The tangential velocity profile still remains slightly different from the one from the 3D simulation, especially in the tip leakage region, but we observed a reduction in the prediction error (Figure 13b). In the end, the profile deflection that results from a better prediction of velocity profiles follows accurately the trend indicate by the 3D simulation (Figure 13c).
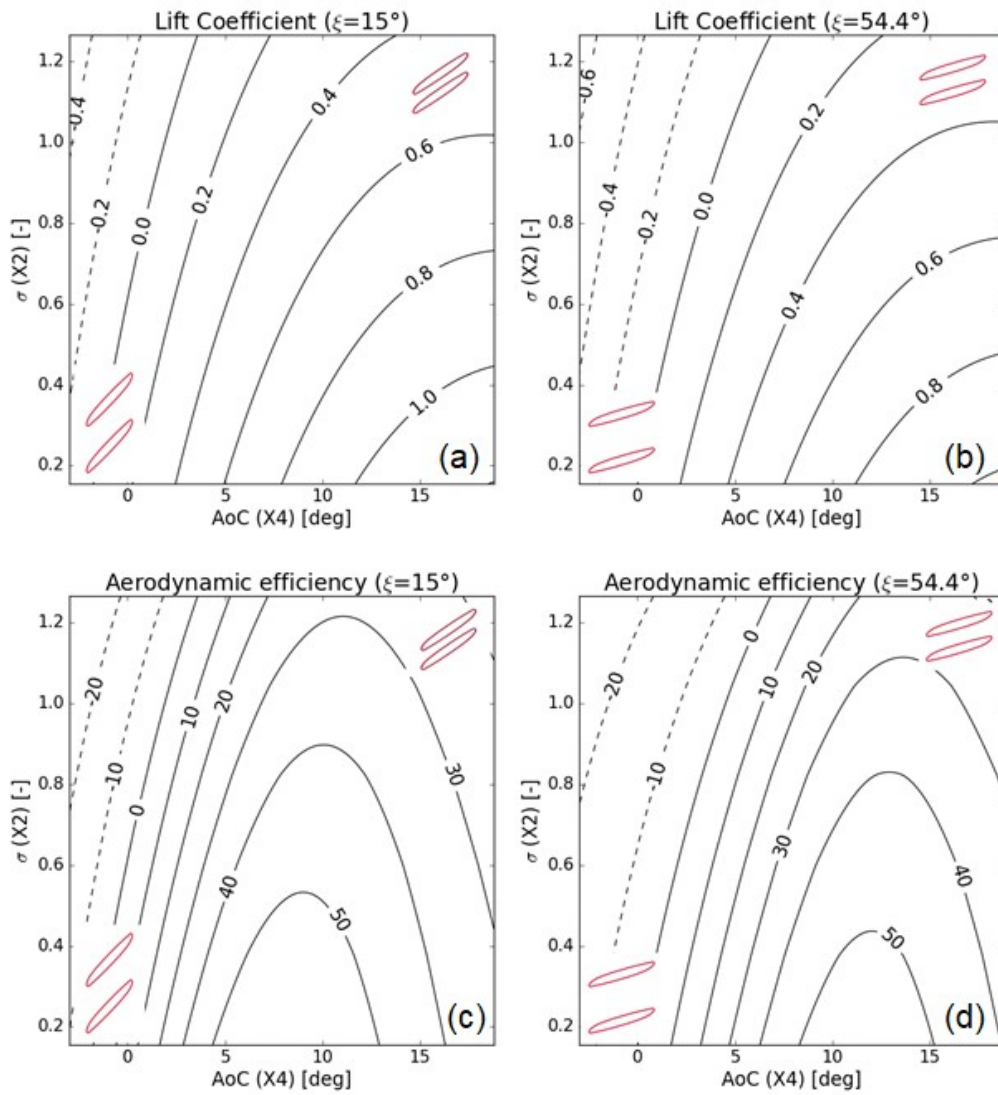
Figure 11 – Contour lines of lift coefficient (a-b) and aerodynamic efficiency (c-d) as function of solidity and AoC for two different configuration of pitch angle (a,c vs b,d).
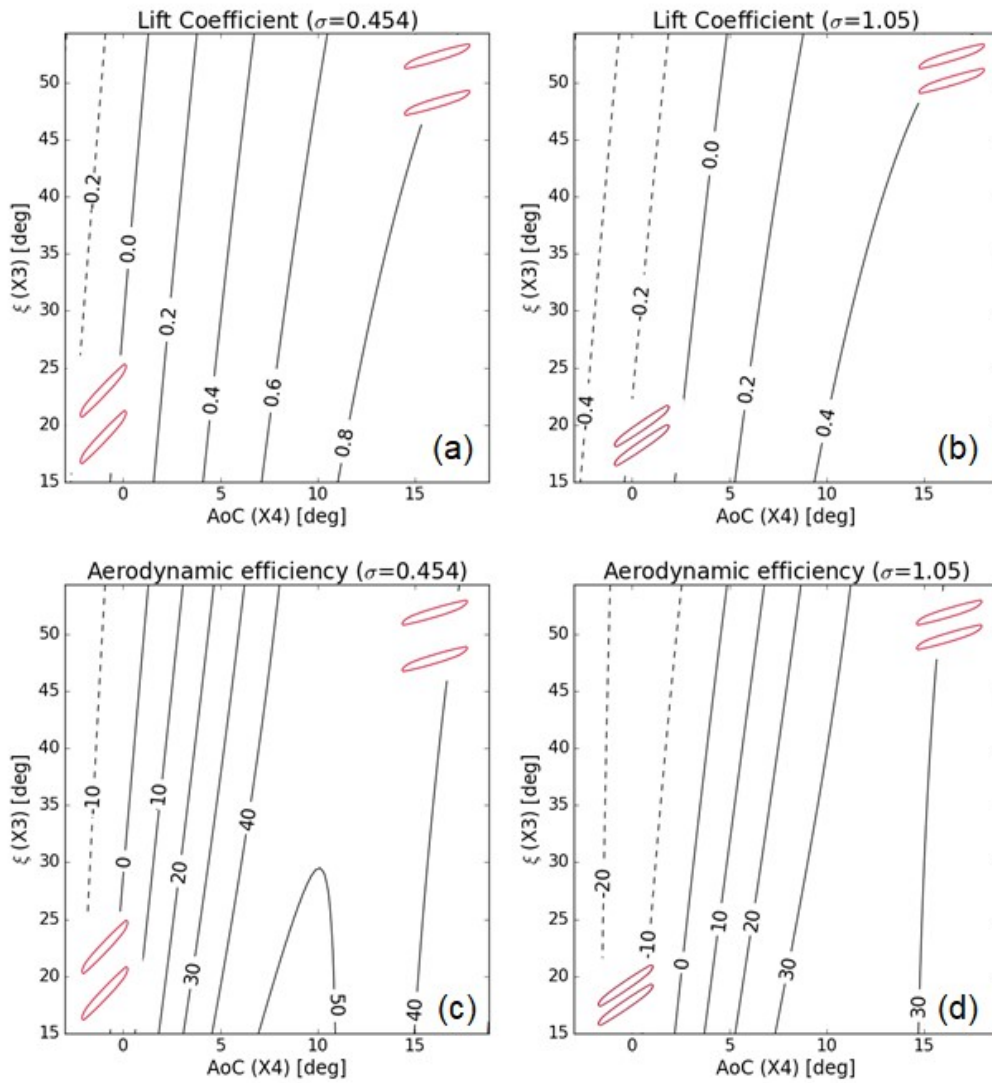
Figure 12 - Contour lines of lift coefficient (a-b) and aerodynamic efficiency (c-d) as function of pitch and AoC for two different solidities (a,c vs b,d).

11
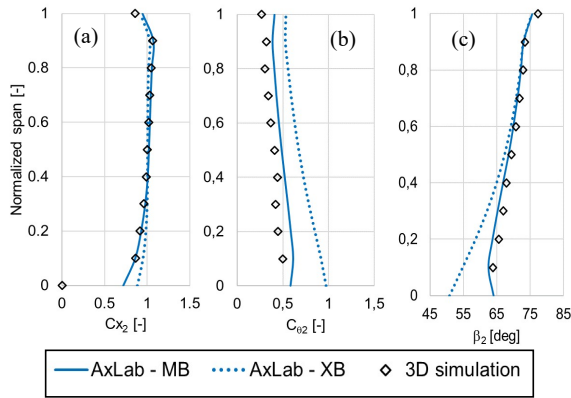
Figure 13 - Spanwise distributions of – normalized axial velocity (a), normalized tangential velocity (b), deflection β_2 (c) at the fan outlet section

Figure 14 highlights the benefits of the meta-models in terms of the local load coefficient ψ prediction. The quasi-3D approximation of the flow still suffers from a slight overrating of the total specific work, but globally this overprediction remains in an error range of 15%, extremely smaller than the one computed on the classical approach (50%), and such difference must be ascribed to the overestimation of outlet tangential velocity.
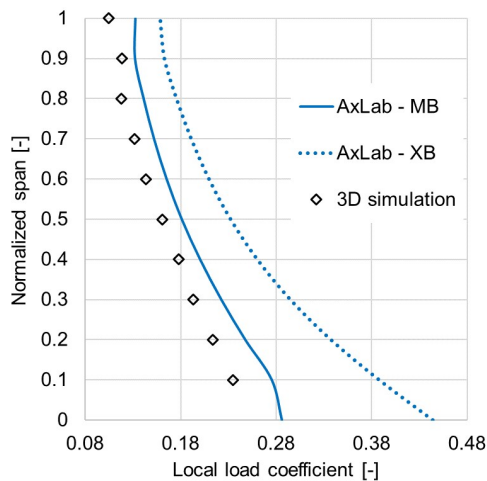
Figure 14 - Spanwise load coefficient distribution.

CONCLUSIONS

This paper presents a systematic study on cascades of a reversible blade profile that are commonly used in fan industry.

Similar studies were traditionally carried out for compressor airfoils, but a similar application to this methodology has been here used for reversible fans. A CFD numerical investigation over the influence of four factors, i.e. solidity, pitch, angle of attack and Reynolds number, in aerodynamic performance of the blade profiles is here performed. Meta-models for lift and drag coefficients are developed and further improved through an ANOVA analysis. The improved meta-models are later on applied to a quasi-3D solver and spanwise fields are compared.

The work has been carried out to gain knowledge on non-evident phenomena and to discover hidden relations between the chosen factors, that can have huge impact on the fan performance. As a direct consequence, numerical tools used in fan design process can be improved in term of prediction capability.

The creation of a DOE matrix allows the reduction of the numbers of required trials, from 81 simulations for a full factorial analysis to the 25 of the paper; however, further simulations have been run to have a more detailed description of the cascade effects on the aerodynamic performance. The authors report here a marked mismatch between the polar curves in cascade arrangement and the curves computed by XFoil software, in term of C_l and C_d values, curve slope, stall margin and the zero-lift angle. C_l curves are not affected by Reynolds number, while the C_d distributions slightly decrease as Re increases. The work shows that for a fixed solidity and AoC, a lower pitch results in a more blocked configuration that leads to anticipated stall. For a fixed pitch angle, the polar curves shift at lower C_l values as the solidity increases. A high influence of the solidity of the cascade on the deflection capability is also highlighted by the trials. The deflection capability and the stall margin are drastically reduced by the blockage due of the high solidity.

A least square method has been applied to derive meta-model for lift and drag coefficient calculation; such meta-models can consider linear effects, quadratic effects and two-way interactions between the studied factors. An initial formulation includes all the four factors, which is later simplified by a weight analysis that reduces the number of included factor to significative terms only.

The derived meta-models are also applied to a quasi 3D in-house solver AxLab, here used for fan performance prediction. The derived meta-models are found to drastically improve the solver capabilities. Results from AxLab are compared with fields from a full 3D CFD simulation. A spanwise analysis shows how the models affect the radial distribution of cinematic fields. The error in tangential and axial outlet velocities is greatly reduced, bringing to a smooth fit of β_2 angle 3D profile. This has been found to have serious benefit in the estimation of the specific work of the blade, that is overpredicted by 15%.

The authors have found high influences of pitch, AoC and solidity in the aerodynamical performance of the reversible profiles. Similar effects are not usually taken in account in the standard approaches to polar curve calculation, so a meta-model

for aerodynamical properties has been created. The meta-model has been proved to be really effective when applied to a quasi 3D solver for the performance prediction of reversible fans.

In this the methodology used for the derivation of a meta-model for a single blade profile has been shown. However, the same kind of analysis can be extended and replicated to other different reversible profiles, obtaining an overview on all the phenomena involved in reversible airfoils.

NOMENCLATURE
Latin

AoC	angle of cascade	[deg]
c	chord	[m]
c_1	inlet velocity magnitude	[m/s]
c_{x2}	normalized outlet axial velocity	[-]
$c_{\theta2}$	normalized outlet tangential velocity	[-]
c_2	outlet velocity magnitude	[m/s]
C	absolute velocity	[m/s]
C_D	drag coefficient	[-]
C_L	lift coefficient	[-]
D	fan diameter	[m]
Q	volume flow rate	[m³/s]
t	blade spacing	[m]
R^2	coefficient of determination	[-]
Re	Reynolds number; Re = U(r)*c / ν	[-]
U	tip speed of the blade	[m/s]
U_b	bulk velocity	[m/s]
$X_{1,2,3,4}$	coded factors	[-]
y^+	wall distance	[-]

Greek

α	rotatability coefficient	[-]
β_1	angle between c_1 and axial direction	[deg]
β_2	angle between c_2 and axial direction	[deg]
σ	solidity	[-]
ν	kinematic viscosity	[m²/s]
$\tilde{\nu}$	Spalart-Allmaras variable	[m²/s]
ξ	pitch angle	[deg]
Φ	global flow coefficient; $\Phi = Q/(\omega D^3)$	[-]
ψ	local load coefficient; $\psi(r)=\Delta p_{tot}/(U(r)^2\rho)$	[-]
Ψ	global load coefficient; $\Psi =\Delta p_{tot}/((\omega D)^2\rho)$	[-]

Acronyms

Adj MS	adjusted mean square
Adj SS	adjusted sum of square
ANOVA	analysis of variance
CCD	central composite design
CCI	central composite inscribed
CFD	computational fluid dynamic
DF	degrees of freedom
DOE	design of experiments
MB	meta-model based
RANS	Reynolds averaged Navier Stokes
RE	residual error

RSM	response surface methodology
XB	X-Foil based

REFERENCES

[1].   A.R. Howell. "Fluid dynamics of axial-flow compressors." In Proceeding of Institution of Mechanical Engineers, volume 153, pages 441-452, 1946.

[2].   A. D. S. Carter. "The low speed performance of related aerofoils in cascade." Technical paper R.55, NGTE, September 1949.

[3].   Kantrowitz, A., and Daum F.. "Preliminary Experimental Investigation of Airfoils in Cascade.", No. NACA-WR-L-231, 1942.

[4].   J. C. Emery, L. J. Herrig, J. R. Erwin, and A. R. Felix, "Systematic two-dimensional cascade tests of NACA 65-series compressor blades at low speeds.", 1958.

[5].   Bullock, R. O., and I. A. Johnsen. "Aerodynamic design of axial flow compressors.", 1965.

[6].   J.-F. Barthelemy and R. T. Haftka, "Approximation concepts for optimum structural design—a review.", Structural optimization, vol. 5, no. 3, pp. 129–144, 1993.

[7].   R. T. Haftka, E. P. Scott, and J. R. Cruz, "Optimization and experiments: A survey.", Applied Mechanics Reviews, vol. 51, no. 7, pp. 435–448, 1998.

[8].   K. Bamberger and T. Carolus, "Performance prediction of axial fans by cfd-trained meta-model.s", in ASME Turbo Expo 2014: Turbine Technical Conference and Exposition, American Society of Mechanical Engineers, 2014, V01AT10A028–V01AT10A028.

[9].   Montgomery D.C. "Design and Analysis of Experiments.", John Wiley & Sons, Inc.: Hoboken, NJ, USA, 2001, p. 456.

[10].   Drela, Mark, and H. Youngren. 'X-Foil 6.96' *Software December (2001).*

[11].   W.K. B. Box G. E. P., "Experimental attainment of optimum conditions.", Journal of the Royal Statistical Society, 1951.

[12].   OpenFoam User Guide v5

[13].   Spalart PR, Allmaras SR. "A one-equation turbulence model for aerodynamic flows." Reno: AIAA, 1992, Report No.: AIAA-92-0439.

[14].   Spalding D. B., "A Single Formula for the Law of the Wall", 1961.

[15].   Box G.E.P., Hunter J.S., Hunter W.G. "Statistics for Experimenters: Design, Innovation, and Discovery.", Wiley-Interscience: Hoboken, NJ, USA, 2005, pp. 47, 455.

[16].   R. H. Myers, D. C. Montgomery, and C. M. Anderson-Cook, "Response surface methodology: process and

product optimization using designed experiments.",
John Wiley & Sons, 2016.

[17]. Mason R.L., Gunst R.F.; Hess J.L. ″Statistical Design
and Analysis of Experiments.", 2nd ed.; John Wiley &
Sons: New York, NY, USA, 2003, pp. 194–195, 504–507.

[18]. Allen D.M. "The Relationship between variable
selection and data argumentation and a method for
prediction.", Technometrics 1974, 16, 125–127.

[19]. Doncaster C.P.; Andrew J.H.D. "Analysis of Variance
and Covariance: How to Choose and Construct Models
for the Life Sciences.", Cambridge University Press:
Cambridge, UK, 2007; pp. 1–14, 238.

[20]. Wasserstein Ronald L.; Lazar Nicole A, "The ASA's
Statement on p-Values: Context, Process, and
Purpose". The American Statistician. 70 (2): 129–133.
doi:10.1080/00031305.2016.1154108.

[21]. Andersson O., "Experiment: Planning, Implementing
and Interpreting", John Wiley & Sons: Chichester,
UK, 2012, p. 164.

[22]. Bonanni T., Cardillo L., Corsini A., Delibra G., Sheard
A. G., Volponi D., (2016), "Derivative Design of
Axial Fan Range: from Academia to Industry"
GT2016-57469.

Gino Angelini, Tommaso Bonanni, Alessandro Corsini, Giovanni Delibra, Lorenzo Tieghi, David Volponi

A preliminary investigation on surrogate-based optimization of truly reversible profile family for axial fans.

Nowadays open literature offers a wide canvas of different techniques for surrogate-based multi-objective optimization. Great part of those works, in order to give a specific focus on methodological and theoretical aspects, are applied to simple mathematical functions. Techniques validated and discussed in those works are then extended to more specific and complex problems like the aerodynamic optimization of an aerofoil. Currently, very few studies are focused on the impact that different optimization frameworks and meta-models have on the replacement of the specific fitness function. In this paper a preliminary study on surrogate-based optimization of truly reversible profiles family for axial fans with a focus on how two different meta-model techniques and use affect results of the multi-objective optimization problem is presented. After the definition, the Multi-Objective Optimization Problem (MOOP) is solved by means of genetic algorithms (MOEA) that were demonstrated to be effective tools for the solution of arbitrary complex functions. Algorithm used for genetic optimization was NSGA II. In the second part of the paper authors explored the possibility to reduce the computational cost of MOEA by means of two different surrogate models (SMs): a polynomial obtained by a least square method (LSM) and an artificial neural network (ANN). SMs were tested in two different optimization approaches with different levels of computational effort. Results obtained demonstrate that it is possible to reduce the computational cost in this specific problem. In the end, the paper provides a critical analysis of results obtained with different methodologies and the effective impact of different SMs on the MOEA.

INTRODUCTION

Reversible single-stage axial fans are largely employed in tunnel and metro ventilation systems, where they are intended to supply and extract air from the tunnels. Historically selected solutions to produce the same flow and pressure in both supply and extract modes included different impellers configurations or the use of a reversible fan blade aerofoil section, that resulted to be the less expensive [1].

Traditionally, truly reversible aerofoil have been generated by flipping the pressure side of a symmetrical non-cambered aerofoil and joining the suction side trailing edge with the pressure side leading edge and vice versa. In so doing, the aerofoil has periodic aerodynamic features every 180 degrees of angle of attack. However, the unnecessary thickness in the trailing edge created by the reversed surface, reduces the performance if compared to other aerofoils generally used for turbomachinery blades; as a global effect, the average efficiencies of reversible fans reach just 95% of the correspondent non-reversible geometry [3].

From 2012 the new trend in mandating minimum efficiency grades asked fan designers for always more attention to efficiency constraints during the design of a new reversible fan, pushing their interest in revised aerofoil concepts that can increase fan efficiency.

In the past, this process relied mainly on three data sources: (i) numerical solutions of the two-dimensional flow past a single aerofoil or cascade, (ii) two-dimensional cascades wind tunnel data [4] or (iii) fully three-dimensional annular cascades data [5]. Nevertheless, experimental reversible cascade data are seldom available to industrial fan designers because there was very little effort to find a selection of optimized reversible aerofoils, since it is very hard to find such an application in the aerospace industry.

A variety of optimization strategies is available in literature to solve Multi-Objective Optimization Problems (MOOPs) and the choice depends upon various aspects, in particular the level of knowledge of the objective function and the fitness landscape [6]. Among these methods, Evolutionary Algorithms (EAs) often perform well approximating solutions to all types of problems because they ideally do not make any assumption about the underlying fitness landscape and they are able to find a good spread of solutions in the obtained set of solutions. Over the past decade, a number of Multi-Objective Evolutionary Algorithms (MOEAs) have been suggested [7-11], primarily because of their ability to find multiple Pareto-optimal solutions in one single simulation run. Different EAs were suggested to solve optimization problems: among them, Genetic Algorithms (GAs) and their variant NSGAII [12] are the most popular.
However, when dealing with real-world optimization problems, the number of calls of the objective function to find a good solution can be high, even with these approaches. Furthermore, in optimization problems based on computer

1

experiments, where the simulation acts as the objective function, the computational cost of each simulation run can severely restrict the number of available calls to the fitness function.

Traditionally, the number of proposals that make use of SMs in MOEAs have been classified according to the type of SM at hand [12], [15]. However, both works have shelved MOEA's point of view (i.e., how the SM is incorporated into MOEA's evolutionary process). Jin [16] and Manríquez [17] proposed a classification based on the way EAs or MOEAs incorporate the SMs (how they are employed in the optimization loop). This kind of taxonomy is called working style classification and allows finding easily similar optimization problems, placing greater emphasis on the methodology followed and not on the SM used. According to such a classification, the approaches are divided into Direct Fitness Replacement (DFR) methods and Indirect Fitness Replacement (IFR) methods [17].

In this paper a preliminary study on the methodology to obtain a set of optimized aerofoil shapes for the use of reversible fan blading is presented. In particular the possibility to speed up the MOOP resulted from a non-dominated sorted genetic algorithm proposed by Deb [12] (NSGA II) by means of SMs is investigated. Metamodels, created by a least square interpolation surface and artificial neural network, were used to replace a virtually expensive numerical simulation represented in this work by XFoil software developed by Drela [13]. Each metamodel was used in two different optimization strategies: a simple-level characterized by a NEC approach and a IFR bi-level. In order to have the maximum control on each step of the MOOP solution, the entire optimization framework and the meta-models development were in-house coded in Python.

Even if the use of a potential solution of an isolated aerofoil can lead to non-optimal solutions, it is still a good replacement of an expensive tool such as CFD to perform a preliminary study on this topic and to define guidelines to replicate the study in cascade configuration by means of CFD, and to pursue the work started by Angelini et al. [18].

MULTIOBJETIVE OPTIMIZATION WITH EVOLUTIONARY ALGORITHMS (MOEA)

Whether a MOEA is assisted or not from surrogated models, there are some main aspects that are common to both approaches: the choice of the objective functions, the aerofoil parametrization and the optimization algorithm. In this paragraph common elements that were used during the optimization task are described.

Objective Functions

The selected objective functions for the multi-objective optimization problem (MOOP) were the aerodynamic efficiency (ε) and the stall margin (α), defined as:

$$\varepsilon = \frac{C_{LS}}{C_D} \, , \; \alpha = \frac{AoA\big(\max(C_L)\big) - AoA(C_{LS})}{AoA\big(\max(C_L)\big)} \tag{1}$$

According to the given definition of stall margin α, each aerofoil polar has to be computed between 0° and the angle of attack where the C_L reaches its maximum. In (1) $AoA(C_{LS})$ is the angle of attack where lift coefficient reaches a specified lift coefficient C_{LS}.

Aerodynamic efficiency was selected in this study to represent a useful parameter for a designer to estimate profile losses in relation to aerodynamic blade section loading. Stall margin provides a measure of how stable working conditions of the profile are, before occurring of unstable phenomena. When optimized elements data are used in a quasi 3D axisymmetric code for design or performance prediction of an axial fan, as in the work of Angelini et al. [18] or Drela et al. [20] stall margin is also a measure of solution reliability. The α objective function has the additional purpose to prevent tendency that optimized elements have to move their maximum aerodynamic efficiency in proximity of $AoA(max(C_L))$.

Aerodynamic efficiency, lift coefficient and therefore stall margin are not only functions of aerofoil geometry (g) but also of Reynolds (Re) and Mach numbers. In this study, the dependency from Mach number is neglected since for fans applications the Mach number is generally lower than 0.3 and there are no compressibility effects [16]. On the contrary, Reynolds number plays a determinant role, and so the following dependencies must be considered:

$$\varepsilon = \varepsilon(Re, C_{LS}, g) \; , \; \alpha = \alpha(Re, C_{LS}, g) \tag{2}$$

The objective is to get a set of optimized geometries under specified Re and C_{LS} that can be used to replace current aerofoils sections of an existing blade geometry. Such new set of geometries, g' is considered optimized under said Re and C_{LS} if aerodynamic efficiency ε' and/or stall margin α' results higher than the ε and α of the current set:

$$\varepsilon(Re, C_{LS}, g') = \varepsilon' \ , \ \alpha(Re, C_{LS}, g') = \alpha' \text{ and } C_L(Re, AoA', g') = C_{LS} \tag{3}$$

Such aerofoil collection can be used to re-stagger an existing fan blade in order to obtain better fan efficiency or more stable working conditions at a given design point. In fact when velocity diagrams, aerodynamic loading ($C_{L,i}$), Reynolds number (Re_i) and blade solidity (σ_i) are prescribed at each blade radius, it is possible to determine the aerofoil stagger (γ_i) (Figure 1) that results in the blade working at optimized conditions ε' and α':

$$\gamma_i = \beta_{\infty,i} - AoA'_i \tag{4}$$
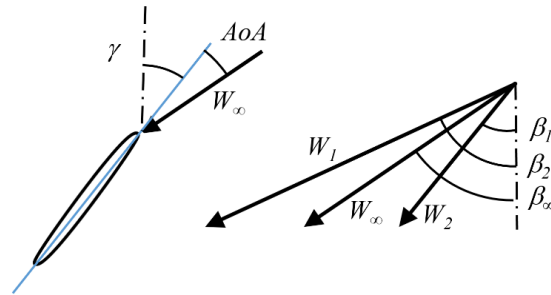
Figure 1 - Schematics of blade angle of attack (AoA) stagger (γ) and relative velocities.

where "i" identifies the generic blade section along the span. The restaggered blade with optimized aerofoils will result in a deflection ($\theta = \beta_1 - \beta_2$) close to the design deflection.

Since it was not possible to find the relative set of optimized solutions for all Re and C_{LS}, we decided to select a series of operating conditions on the envelope of reversible fans for tunnel and metro applications [19]. A matrix of 25 optimization cases was defined by means of the selection of 5 values for Re, and five values of C_{LS} reported inmTable 1. Each optimization starts from the same initial population (P_t) of N=40 reversible aerofoils selected between the most commonly used in ventilation industry, or generated by a simple rearrangement of the suction side of several generic non-cambered aerofoils.

Table 1 - Re and C$_{LS}$ values used in the test matrix.

Re	300000	675000	1050000	1425000	1800000
C$_{LS}$	0.1	0.3	0.5	0.7	0.9

Aerofoil Parametrization

As the optimization concerns truly reversible aerofoils, only the parametrization of the suction side of the profile is needed to univocally define aerofoil geometry. Selection of the parametrization scheme among all methods nowadays available represents a crucial issue because it has a strong influence on the whole optimization process as described by Wu [25], Kulfan [26] and Samareh [27]. For optimization purposes the most important features of a parametrization scheme are: (i) to provide consistent geometry changes and (ii) to produce an effective and compact set of design variables [27]. These two features are in fact fundamental during all the optimization process because they simplify the generation and simulation of geometries and also are responsible for avoiding data overfitting in the metamodel. Two different parametrization schemes were tested, one suggested by Sobieczky [28] and the B-Splines parametrization. These schemes were chosen for their simplicity and the reduced amount of design variables required to reproduce a set of given aerofoil geometries. The most suitable parametrization scheme was selected by means of its capability to reproduce the suction side of the set of 40 reversible aerofoils discussed above. In both cases a curve fitting algorithm, based on fitting technique developed by Schneider [29], automatically finds values of the parametrization coefficients for the given profiles to obtain

3

the minimum deviation between a selected reversible aerofoil and the resulting parametrization. The best combination of parameters was found with Nelder-Mead search algorithm.

In the end, the most successful resulted to be a 6th degree B-Spline parametrization, which guarantees a good balance between aerofoil geometrical features that can be reproduced and the number of design parameters.

B-Spline parametrization uses the coordinates of 6 points: two points define the beginning and the end of the aerofoil suction side and are forced to have coordinates (0,0) and (1,0). A second set of points indicates the direction of the surface at the leading edge and at the trailing edge. For those points, *x* was again forced to 0 and 1 respectively, while *y* coordinates are the first two degrees of freedom (Y_{a1} and Y_{a4}). Third couple of points are used to control the suction surface between leading and trailing edge adding other 4 degrees of freedom (X_{a2}, Y_{a2} and X_{a3}, Y_{a3}). Figure 2 shows the set of control points and relative parametrization (blue dashed line) after the curve fit in order to reproduce the given geometry (black line).
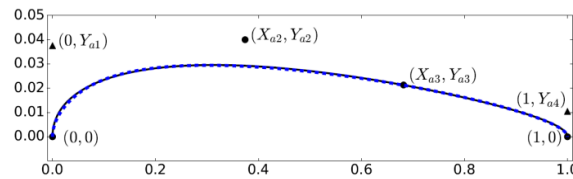
Figure 2 - Control points used to reproduce the given geometry (solid line) with a 6th degree B-Spline parametrization (dashed line)

NSGA II Algorithm

The MOOP has been solved using the non-dominated sorting genetic algorithm (NSGA-II) proposed by Deb [4]. NSGA-II has demonstrated to be able to find much better spread of solutions and better convergence near the true Pareto-optimal front compared to the Pareto achieved with different evolutionary algorithms. NSGA II is a non-dominated sorting-based multi-objective evolutionary algorithm (MOEA) combining the concept of non-dominated sorting together with an explicit diversity-preserving mechanism, based on crowding distance. Starting from the parent population P_t , taken as an initial set of $N = 40$ individuals (geometries), the algorithm generates an offspring population Q_t of the same size N. Then the two populations are combined together to form an R_t population of size $2N$. The offspring Q_t is generated using the following criterion: four elements are generated using crossover, mutation and breed interpolation from first two most promising elements in P_t. Of those four elements, first two are a random mutation, a third element is generated by scattered crossover and the genes of the last element are a simple average between parents' genes. Remaining 36 elements of Q_t population are randomly obtained by scattered crossover or mutation of random selected elements in P_t. A non-dominated sorting approach, as suggested by Deb, is used to pick individuals from the last non-dominated front. An advantage of this approach is that solutions compete each other also in terms of how dense they are in the fitness space. Thus, diversity is explicitly considered when forming the offspring population. Furthermore, elitism is ensured by non-dominated sorting of both parents and offspring and inclusion of non-dominated fronts in the new set of elements.

SURROGATE MODEL-BASED OPTIMIZATIONS

Main intent of this paper is the preliminary search of which is the best optimization framework for solving the MOOP previously described. MOEA optimization revealed to be a good tool to produce an approximate solution. Anyway, the number of calls of the objective function (XFoil in this case) to locate a good solution can be high.
If the final objective is to compute a solid solution for the MOOP, more accurate and computationally expensive fitness estimators need to be deployed into the MOEA framework, drastically increasing the time required to obtain a satisfying solution. An established framework for addressing such challenging optimization problems is that of Surrogate-based optimization, in which a metamodel approximates the true expansive fitness function and provides the optimizer with predicted objective values at a much lower computational cost [7, 8] . Surrogate-based optimization represents a class of optimization methodologies that make use of meta-modeling techniques to quickly find the local or global optima.
In this work, a Least Square Method (LSM) and an Artificial Neural Network (ANN) have been used as Surrogate Models (SM) of the true and virtually expansive function (XFoil) in the MOOP.
Two different metamodel optimization approaches were tested: (i) Simple-level framework, in which the optimization is entirely driven by the SMs and (ii) Bi-level framework, where the true function is used to evaluate the surrogate optimum designs. Simple-level framework (Figure 3), in which all the solutions have been assessed in the SM are assumed to be comparable to that assessed by the real function, is commonly seen in literature [9-11] and is considered the most straightforward SM approach. However, this approach can converge to false optimum, which in a MOOP is a Pareto front

4

not corresponding to the Pareto front estimated in the real function. A bi-level framework (or infill criterion) calls the true functions to validate the optimum solutions of the SMs and to enhance the accuracy of the SMs itself, by adding new sample points to the current data set (see Figure 4). The main optimization concerns the creation and refinement of the SMs and, therefore, calls of the true functions are necessary to this scope. The sub-optimization uses the current SMs to determine the new sample sites by using any optimization algorithm, such as gradient-based or EA. In this work, both a simple and bi-level optimization framework have been tested to solve the MOOP.

Following paragraphs describes operations that are common to the two approaches investigated and in general are part of metamodeling techniques: (i) design space sampling where examples are generated to train the meta-model, and (ii) surrogate model construction.
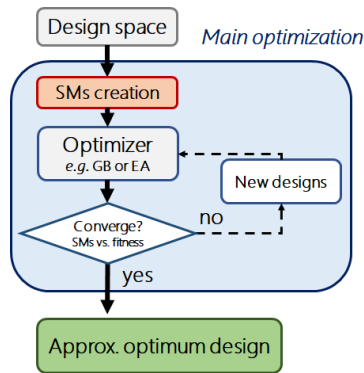
Figure 3 – Simple level surrogate model
optimization framework
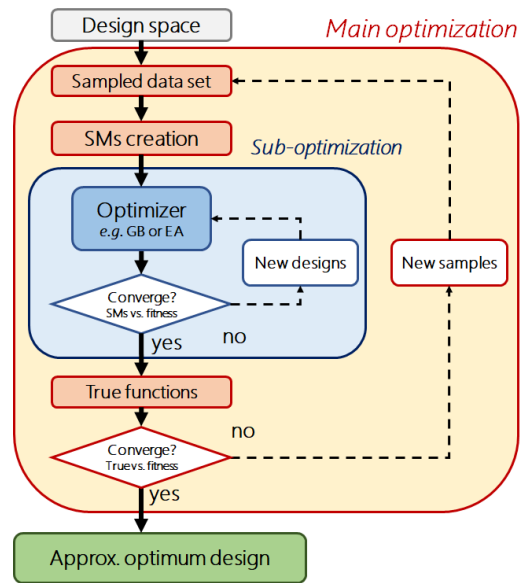
Figure 4 – Bi-level surrogate model optimization
framework

Sampling

Simple level optimization framework requires the construction of a surrogate model that is not going to be updated during optimization and so it must reproduce as far as possible the true expensive function. The metamodel was trained by means of selected samples inside the design space. In such cases, usually full factorial design of experiment is used to test all possible combinations of various factors h. Full factorial design is often the only choice when one is interested in accurate measurement results under various operating conditions or when the response is expected to change in unforeseen ways. However, this approach often requires a large number of experimental trials, as the number of trials increases geometrically with the number of factors to be tested.

A popular compromise which reduces the number of experiments to close a 2-level full factorial design is the Central Composite Design (CCD), that is a $2h$ full factorial to which $2h$ axial trials (or star points) and nc center point trials are added [32]. Having more samples than those strictly necessary for a bilinear interpolation (which are $2h$), allows the curvature of the design space to be estimated.

In this work, a rotatable Central Composite Inscribed (CCI) was used as the experimental design; axial points are located at factors levels -1 and 1, while factorial points are brought into the interior of the design space and located at distance $1/v$ from the centre point. In order to ensure the rotatability of the design, [33] v has been set to:

$$v = (2^h)^{0.25}$$

(5)

Being the design space parametrized by four factors, the number of factorial runs was equal to $2^8=256$, and to maintain rotatability in accordance with (5), v was set to 4. The operating ranges for all the factors and the levels at which they were tested are shown in Table 2.

Table 2 – Tested levels of design variables

Factor Name	Coded Levels and Corresponding Absolute Levels				
	-1	**-1/v**	**0**	**1/v**	**1**
X_{a2}	0.0140	0.0282	0.0330	0.0377	0.0519
Y_{a2}	0.0217	0.0423	0.0491	0.0560	0.0765
Y_{a1}	0.0126	0.0332	0.0401	0.0470	0.0676
X_{a3}	0.0049	0.0136	0.0164	0.0193	0.0280
Y_{a3}	0.2761	0.3430	0.3653	0.3876	0.4545
Y_{a4}	0.0265	0.0599	0.0710	0.0821	0.1155
Re	300000	862500	1050000	1237500	1800000
C_{LS}	0.1	0.4	0.5	0.6	0.9

The total number of experimental trials, based on the number of design factors $h=8$, was equal to $N=2^h+2h+1=273$. Full factorial design represents a possible alternative approach, but it would require a minimum of $3^8=6561$ numerical trials. All 273 examples were tested by means of XFoil on a simple laptop in order to calculate objective functions α and ε. The entire sampling task required approximately 1.5 hours on a 4 cores i7 laptop.

Polynomial response surface

A second-degree polynomial response surface was selected to create the first surrogate model, being still easy to estimate and suitable for optimization processes. An additional feature of polynomial response surface is the ability to handle noisy optimization landscapes [34, 35].

A CCD sample, enables estimation of the regression parameters to fit a second-degree polynomial regression model to a given response. The polynomial (6) quantifies relationship among the measured response (the dependent variable) and a number of experimental variables $X_1, ..., X_s$, where s is the number of factors considered, $\zeta_{s,s}$ are regressors (the unknown parameters) and q is an error associated with the model:

$$
\begin{aligned}
Y = \zeta_0 + \zeta_1 X_1 + \zeta_2 X_2 + ... + \zeta_s X_s + \\
\zeta_{1,1} X_1^2 + \zeta_{2,2} X_2^2 + ... + \zeta_{s,s} X_s^2 + \\
\zeta_{1,2} X_1 X_2 + ... + \zeta_{s-1,s} X_{s-1} X_s + q
\end{aligned}
\tag{6}
$$

The regressors (ζ_s, $\zeta_{s,s}$, $\zeta_{s-1,s}$) provide a quantitative measure of the significance of linear effects, curvilinear effects of factors and interactions between factors. A least square method was used to derive mathematical correlations for lift and drag coefficient by fitting a response surface to the computed values at the CCI points.

Artificial neural network

Structure of the neural network used in this work is the typical one used in regression problems [36], that is a multilayer perceptron. A *logsig* transfer function was preferred over the *tansig* in the hidden layers while in the output layer was used a linear neuron. After a series of tests made to select the best architecture, only one hidden layer with 25 neurons was used since the gain in precision of the more complex networks was not considered worth the increase in computational effort. Tests were made by using 10 to 60 neurons, 1 and 2 hidden layers for a total of 6 tests on a single layer network and 36 tests on a double layer network. The layout of the neural network is reported in Figure 5 where i represents the number of training examples, j is the number of independent variables, k is the neuron number and m is the number of predicted dependent variables. Following relations between network elements were considered

$$
z_{ik}^{(1)} = X_{ij} w_{jk}^{(1)} + b_{1k}^{(1)}
\tag{7}
$$

$$
a_{ik}^{(1)} = \sigma(z_{ik}^{(1)})
\tag{8}
$$

$$z_{im}^{(2)} = a_{ik}^{(1)} w_{km}^{(2)} + b_{1m}^{(2)} \tag{9}$$

$$Y_{im} = \lambda(z_{im}^{(2)}) \tag{10}$$

In (7) to (10) with w are indicated the weights of each synapse, b are biases of each neuron, z and a represent respectively activities of synapse layers, λ and σ are respectively a linear and sigmoid activation functions, and X and Y are training inputs and predicted outputs. With subscripts we indicate the matrix dimensions and with superscripts the respective layers.

In this case the independent variables are 8 (j) that are the 6 geometric parameters plus Re and C_{LS} while predicted variables were ε and α ($m=2$).
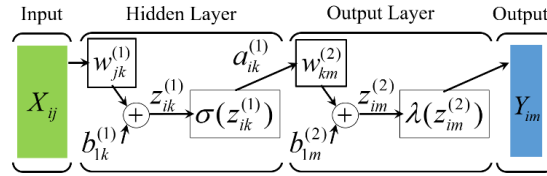
Figure 5 – Adopted neural network structure

Neural network was trained using a Bayesian optimization algorithm randomly initializing weights and biases between 1 and -1. Also Levenberg-Marquardt training algorithm was tested providing less accurate results and higher computational effort. In order to further reduce the probability to converge into a local minimum and detect overfitting the sampling dataset was reorganized into 5 different datasets. Each dataset is then split in order to create two sub-datasets: a *"training dataset"* containing 80% of the total samples and a *"test dataset"* that contains the remaining samples. In this way, five datasets are needed in order to have each point at least once in each sub-datasets. The ANN is then trained on each dataset and the accuracy is evaluated by means of the coefficient of determination R^2 calculated above the entire normalized prevision set: ε^* and α^*. During training, the overfitting was monitored and non-compliant nets were discarded.

Optimization framework

According to the working style classification proposed by Jin [37] and Manríquez [17], a Direct Fitness Replacement (DFR) method and an Indirect Fitness Replacement (IFR) method have been adopted in the surrogate-based optimization. In particular, the adopted DFR method is usually classified as No Evolution Control (NEC), a simple-level framework (see Figure 3) where MOEAs calculate their solutions in the SMs exclusively. NEC have provided good results only in problem with low dimensionality in both decision and objective space, while unreliable solutions [17], [10] can be produced in more challenging problems.

In the second method adopted, namely the IFR, the original fitness function is used during the EA process, while one or more components of the MOEA (typically the variation operators) are assessed in the SM. In so doing, a number of solutions are produced, evaluated and compared using the SM. After a stop condition, n best solutions are delivered to the parent approach and evaluated with the real function. By indirectly using the approximated fitness, it is expected to keep the optimization towards the true Pareto front and at the same time to reduce the risk of false optimum convergence [38], [12]. Most of the existing works in this category use the MOEA in a direct coarse grain search, while the SM intervenes in a local search, providing candidate solutions which are then assessed in the real function. Therefore, the IFR approach uses the SM for exploitation purpose, while the MOEA is employed for design space exploration. The IFR method is clearly a two-stage approach (see Figure 4) and represents a viable option to reduce the number of function evaluations required to achieve good results of any MOEA even if it is the most computationally expansive method for surrogated-based multi-objective Evolutionary Algorithm.

OPTIMIZATION RESULTS

This paragraph reports results obtained with the listed optimization techniques starting from the benchmark approach consisting with the standard MOEA. Following this, are presented results with different SMs used in two different approaches.

MOEA

The fitness function selected to assign objective functions ε and α to the individuals created during NSGA II algorithm was XFoil. This software was selected as it is known to give a reasonable estimate of aerofoil lift and drag polars [22, 23]. On the other side, it is also consolidated that the use of XFoil data for fan performance prediction provides inaccurate results since the objective functions are deeply affected by the cascade characteristics (solidity and pitch). Angelini et al. [18] described how prediction accuracy of a quasi-3D axisymmetric code can be improved thanks to cascade numerical simulation in respect of directly using XFoil data. One of the outcomes of their research is that solidity and pitch configuration of the cascade have relevant effects on the aerodynamic performance even for cascade configurations typical of axial flow fans. The present study wants to focus on how a surrogate model is incorporated into MOEA's evolutionary process. XFoil has been selected not as a quick and valid alternative to CFD, but to virtually reproduce typical problems related to computationally expensive techniques such as noisy landscape of the function to optimize. Noise created by complex numerical modeling techniques like CFD were in the past implied to turbulence models, incomplete convergence, discontinuous variations in calculating objective functions and discretization as reported by Giunta et al. [30] and Madsen et al. [31].
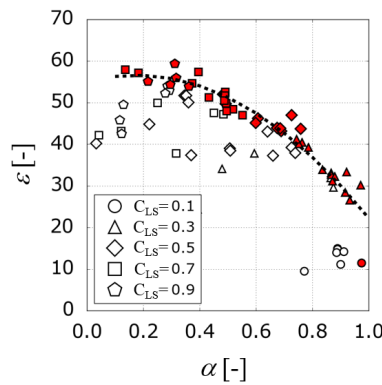
Figure 6 – Different values of objective functions ε and α for Re 1.05×10⁶ and different values of C_{LS}. Full markers are used to interpolate a technological frontier (dotted line) for the baseline aerofoil geometries.

A preliminary analysis with XFoil of the initial set of geometries provides the results plotted in Figure 6 which shows objective function values of the initial population P_t at the intermediate value of Re range and at different C_{LS}. Full markers form the Pareto front of this initial population, sketched by the dotted line. The Pareto individuals have been sorted according to fast non-dominated sorting algorithm (FNDS) suggested by Deb [12]. This, according to XFoil analysis, represents the state of the art and any optimization technique should move this imaginary frontier towards higher efficiencies and stall margins. As expected a clear trend can be reconstructed; the increase in aerodynamic load, requested to the aerofoil, brings to an increased efficiency at the cost of a reduced stall margin.
Figure 7 reports results for all *Re* and C_{LS} combinations of the MOEA test matrix after 20 generations. In each graph, it is reported the initial frontier (dotted line) for the specified *Re* and the final frontier obtained by a selection of elements on the calculated Pareto fronts. In all configurations, the frontier movement was evident resulting in a major improvement of efficiency at lower stall margin.
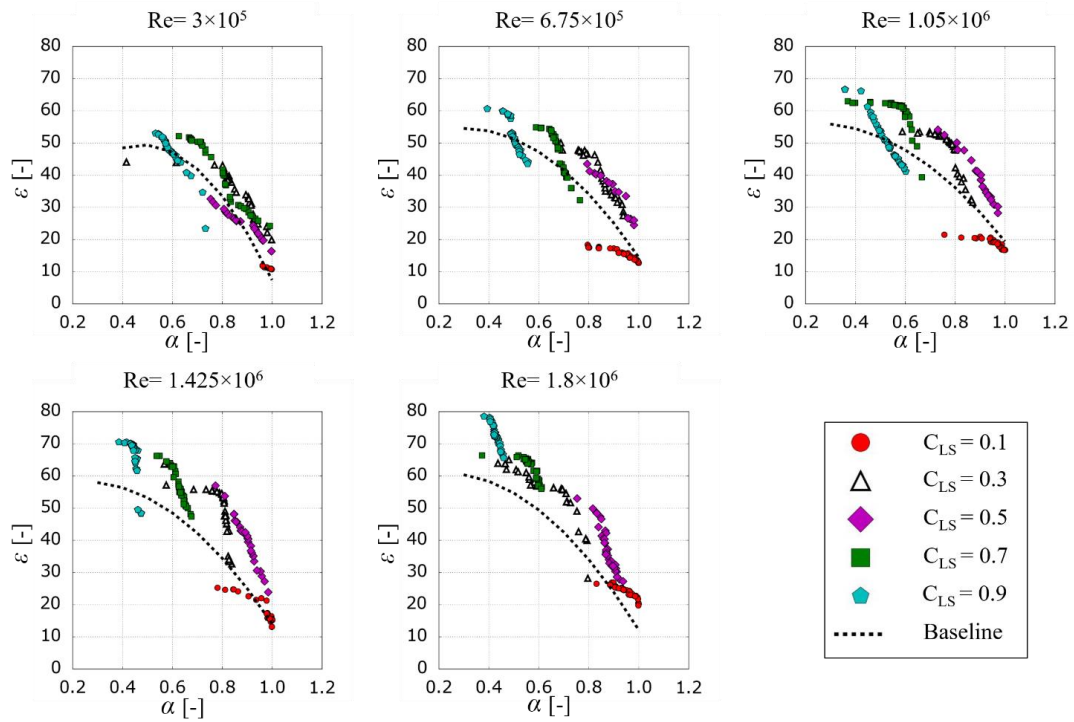
Figure 7 - **Pareto fronts performed at *Re* from 3×10^5 to 1.8×10^6 and *C_{LS}* from 0.1 to 0.9**

Geometrical figures of merit of the geometries produced by the MOEA were analysed to asses that the optimization process was physically reliable. Figure 8 and Figure 9 depict, respectively, the position Y_{a1}, non-dimensional distance from the leading edge x_s and the maximum aerofoil thickness s as functions of ε and α for a specified *Re* 1.425×10^6 for three different Pareto fronts, namely *C_{LS}* values of 0.3, 0.5 and 0.7. As expected for all loading conditions aerofoil thickness s and Y_{a1} result to be directly proportional to the stall margin and inversely to aerodynamic efficiency. Conversely, maximum thickness closer to the leading edge seems to decrease α and increase ε. Some distributions, especially when the ε correlation is expressed, feature relevant scatter. Noisy distributions can be ascribed to an non-converged Pareto front or that the selected parameter is not determinant by itself to completely drive the objective function value. Another important observation is that for both objective functions, clear and common trends for all loading conditions *C_{LS}* can be identified.
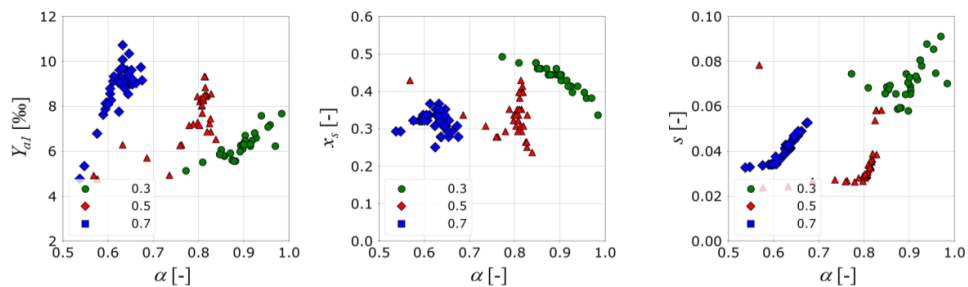
Figure 8 - **Influence of the selection of geometrical parameters on aerodynamic efficiency for a Re of 1.425×10^6 and three different target values for C_{LS} 0.3, 0.5 and 0.7**

9
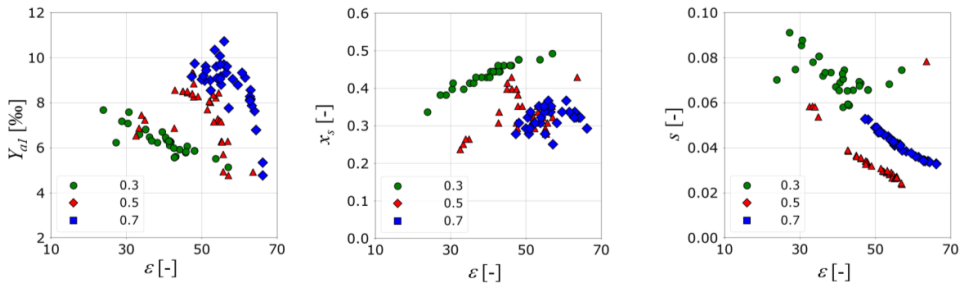
Figure 9 - Influence of the selection of geometrical parameters on aerodynamic efficiency for a *Re* of 1.425×10⁶ and three different target values for *C_LS* 0.3, 0.5 and 0.7

No Evolution Control

MOOP was again solved using at this time NSGA II algorithm assisted by developed meta-models. SMs accuracy in terms of coefficient of determination R^2 for polynomial response surface and artificial neural network is reported in Table 3.

Table 3 – Coefficient of determination for different surrogate model selected for NEC approach.

	R^2	
Output	*LSM*	*ANN*
ε	0.9620	0. 9656
α	0.9480	0.9865
Global	-	0. 9906

Since in this method there is no call to the expensive true function, optimization was simply stopped after 20 generations and final elements were retested with XFoil assessing their objective functions. The entire optimization process was extremely quick: the entire matrix was simulated on a 4 cores i7 laptop in less than 1 hour for each meta-model. When Pareto fronts obtained by means of surrogated models assisted optimization were retested with XFoil a consistent discrepancy between predicted and meta-model estimated objective functions emerged, as depicted in Figure 10 that well represents the common trend of simulations. These discrepancies are present in both surrogate models.
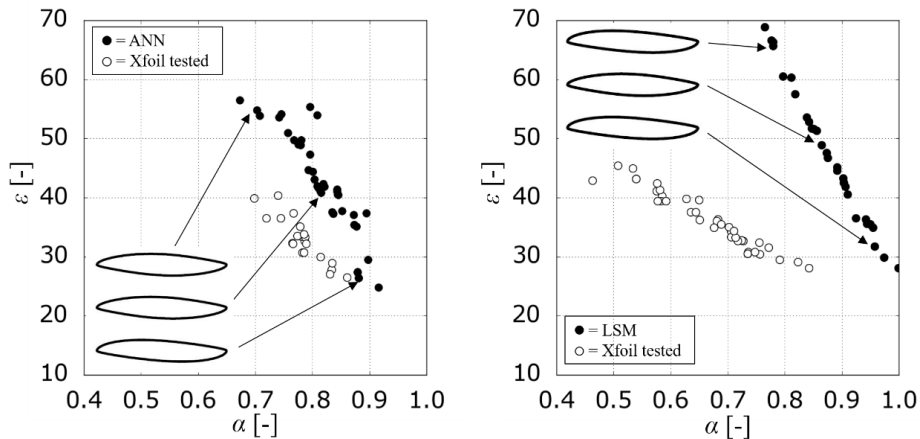
Figure 10 – Final iteration (in black dots) and its XFoil verification (white dots) for NEC approach for artificial neural network (left) and polynomial response surface (right) for *Re* 1.05×10⁶ and *C_LS* 0.5

In Figure 11 the evolution of SMs prediction capability (P_C) for a selected case (Re=1.05×10^6, C_{LS}=0.5) is reported. The prediction capability is an index formally identical to the coefficient of determination R^2. For the case reported in Figure 10, each Pareto front generated during iterative process was tested by means of XFoil and results were used to calculate P_C. This index was based only on elements of which XFoil could give a prediction of objective functions. In Figure 11 are reported trends for both SMs in terms of P_C for objective functions and the number of elements that effectively converged in Xfoil. Generation after generation in both SMs the P_C for both ε and α decreases. While in the ANN case the number of elements that effectively can be simulated by XFoil quickly decreases, the polynomial response surface methods appear to be extremely conservative, unfortunately with no beneficial effects on P_C. Trends reported in Figure 11 suggest that despite the good prediction metric reached during meta-models training, the genetic algorithm tends to emphasize SMs defects that generation by generation bring the optimization algorithm to generate distorted or unrealistic geometries that are hard or impossible to simulate by means of XFoil and therefore, to unreliable SMs predictions.

A geometrical analysis made on few geometries of the SMs Pareto fronts, confirms that the geometrical trends, previously found with MOEA, are not reproduced. As described in Figure 10 each of the Pareto fronts estimated by SMs provide similar aerofoil shape in contrast with the problem physics.

The inability of developed meta-models to replicate the behaviour of aerofoils is strongly connected to the incorrect prediction of elements in the intermediate regions of the sampled design space for SMs instruction. This issue was already detected by other researchers in high dimensionality problems that adopted a NEC approach [39, 40]. In this case the selected aerofoil parametrization determined a high problem dimensionality.
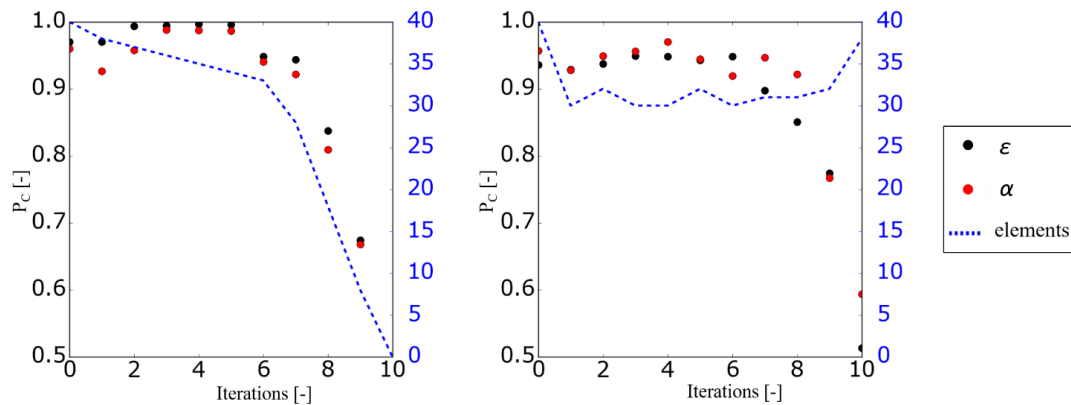
Figure 11 – Prediction capability progression and optimized elements generated during the first 10 generations for both objective functions for Re=1.05×10^6 and C_{LS}=0.5. Left: ANN; Right: LSM.

Indirect Fitness Replacement

The issues connected with NEC approach show the need of another optimization framework with a better balance between exploitation and exploration of the design space that, in a NEC approach, is totally favourable to the exploitation part. The use of an IFR approach was justified by an additional analysis of Figure 11. Prediction capability P_C for both objective functions during the first generations keeps an acceptable value (more than 90% for the first 5 generations) effectively generating optimized elements in proximity of the current Pareto front. With this perspective, the IFR framework as reported in Figure 8 was implemented for the solution of MOOP. In this case the initial sampling was used to train the first iteration meta-models. Then meta-model assisted NSGA II was invoked for 5 generations. Nothing of the GA was modified from the original formulation used in the MOEA. After the NSAG-II is completed, the 40 best new members are evaluated with the true objective function and are added to the memory storage. SMs are trained again and the loop is repeated until the number of calls to the true objective function reaches the prescribed limit. In this case a limit of 10 calls to the objecti**v**e function was set, in order to see if it was possible to substantially reduce the optimization burden.

11
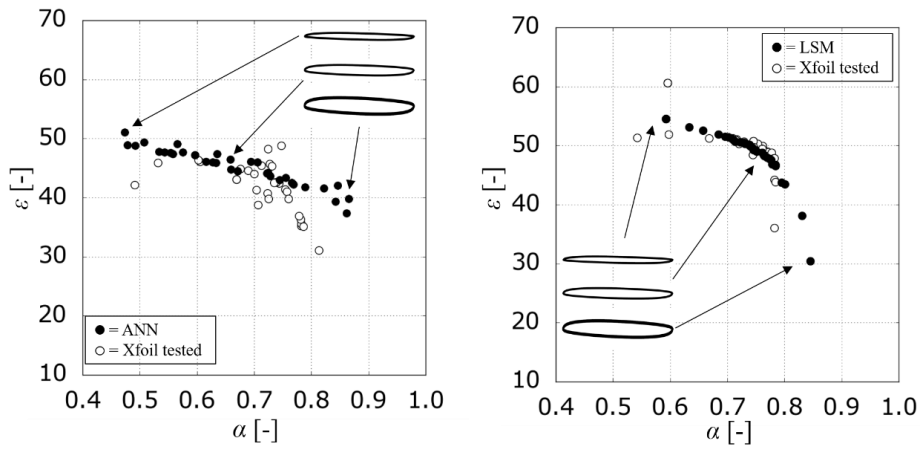
Figure 12 – Final iteration (in black dots) and its XFoil verification (white dots) for IFR approach for artificial neural network (left) and polynomial response surface (right) for *Re*=1.05×10⁶ and *C$_{LS}$*=0.5

In Figure 12 is reported the final iteration loop for the same case reported in Figure 10. In the IFR approach aerodynamic performance predictions are in good agreement with XFoil predictions, and the gap between the meta-model estimated Pareto front and the XFoil prediction is minimized. The physics of the problem is well represented by different thickness aerofoils. Thinner aerofoils populate the upper left region of Pareto front where the efficiency increases to the detriment of stall margin as expected and confirmed by MOEA analysis.

Figure 13 shows 5 different configurations of the test matrix where are reported all results both from the standard MOEA approach and the SMs assisted optimization. Figure 13 also includes a dotted line that represents the state of the art for the specified *Re* and *C$_{LS}$* values for the initial set of aerofoils showing significant improvements in both objective functions.

These results give a good overview of all results obtained with the IFR technique. An additional test was performed using a reduced complexity level artificial neural network with equivalent to the one previously described but with 10 neurons in the hidden layer. Globally, results show that SMs assisted optimization produced good results using half of the computational effort required by the MOEA. In particular in all cases described by the test matrix, SMs produced an improved Pareto front with respect to the MOEA.

In order to further assess the quality of results calculated from SMs assisted multi-objective optimization a comparison between the different results obtained was performed.

Usually, the quality of a Pareto-optimal set can be assessed from three aspects: (i) the number of Pareto optimal solution in the set, (ii) the accuracy of the solution in the set i.e. the closeness of the solutions to the theoretical Pareto-front and finally (iii) the distribution and spread of the solutions [41]. Several performance indices were computed in order to have a metric to evaluate the quality of Pareto solution set observed in Figure 13.

ONVGR is a cardinality-based index derived from the one defined in [41] and it relates to the number of non-dominated solutions in the Pareto front. To compute this index, all the elements that populate the optimized solution sets (from all optimization framework: MOEA and SMs assisted optimizations) were combined in an overall Pareto front for each matrix case. We sorted the overall front according with the non-dominated sorting algorithm. Referring to the elements of the highest domination class, *ONVGR* defines the percentage of elements that are generated from metamodel-assisted optimization or using XFoil as fitness function. Hyperarea (*H*) identifies the area of objective space subtended by the Pareto solution set. Max Sum (*MS*) is the sum of the highest objective values obtained in each Pareto set. Overall Pareto Spread (*OS*) quantifies how widely the optimized solution set spreads over the objective space. In a two objectives optimization, it is computed as the ratio of the rectangle that is defined selecting the good and bad points (according to each objective functions) and the rectangle that has two vertices on the Pareto front extreme points. A solution set presenting higher *OS* value is characterized by wider spread. Spacing (*Sp*) identifies the distance between the elements

that populate the solution set. Table 4 reports values for calculated indexes. In each column the best value is identified in bold, while the worst in italic.

According to the values of *ONVGR* listed in the table, the SMs assisted optimization produces the major number of non-dominated elements in the solution set if compared to MOEA optimization. The only exception regards the matrix case central point (Re=105000, C_{LS}=0.5) where MOEA optimization reaches the 33.3 % of non-dominated elements. However, we can obtain the same result using LSM as fitness function. The highest domination class does not contain elements from MOEA for Re=1425000.

Referring to *H*, the use of ANN determines wider domination areas in the objective space, although LSM has very close values for the same test cases. As observed above, also in this case, worse results have been obtained using the MOEA approach. The values of *OS* tend to confirm that ANN Pareto sets present wider spread over the objective space, in line with the *H* values observed above. Concerning *SP* values the analysis shows that ANN 10n Pareto fronts are characterized by the minor distance between the elements that populate the solution set even if in one case (Re = 1425000, C_{LS}=0.3) this result was obtained concurrently with the lowest values of OS.

As a final result it is impossible to say that the overall quality of solution sets for MOOP cannot be accounted by means of a single performance index, especially if the shape of Pareto front is extremely different. In the end, since in this preliminary study the declared final objective was to move as much as possible the technological frontier on the α-ε chart, the effectiveness was assessed by means of *ONGVR* index concluding that SMs assisted optimization can be equivalent or even better in this case.
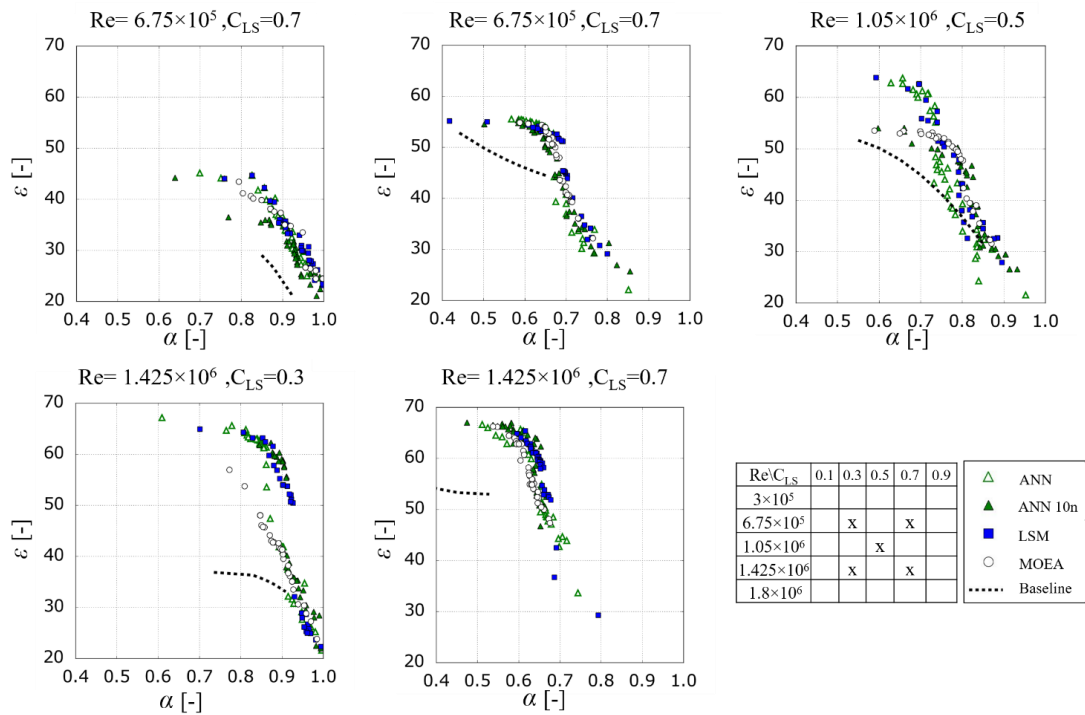
Figure 13 – Final Pareto fronts for five different test matrix configurations reported in figure bottom right. Dotted line rapresents the initial Pareto fronts.

Table 4 – Pareto Fronts quality indexes for different optimizations techniques

Re	*C_LS*	*Fitness*	*ONVGR*	*H*	*MS*	*OS*	*Sp*
675000	**0.3**	*ANN*	28.6	**43.0**	**46.2**	0.29	0.57
		ANN 10n	*10.7*	41.7	45.7	**0.32**	**0.28**
		LSM	**46.4**	42.4	45.7	0.20	**0.28**
		MOEA	14.3	*41.6*	*44.4*	*0.15*	*0.40*
	0.7	*ANN*	**43.8**	42.8	**56.4**	0.36	*1.62*
		ANN 10n	10.4	**43.0**	56.2	0.31	**0.26**
		LSM	37.5	41.8	55.9	**0.38**	0.66
		MOEA	8.3	*40.4*	*55.6*	*0.15*	0.60
1050000	**0.5**	*ANN*	11.9	**53.3**	64.7	**0.51**	*0.80*
		ANN 10n	21.4	47.1	55.0	0.35	0.27
		LSM	**33.3**	53.1	**64.8**	0.42	0.72
		MOEA	**33.3**	45.2	54.4	*0.24*	**0.24**
1425000	**0.3**	*ANN*	18.4	**62.1**	**68.2**	**0.68**	*1.28*
		ANN 10n	**52.6**	58.8	63.2	*0.23*	**0.29**
		LSM	28.9	61.3	65.9	0.48	0.62
		MOEA	0.0	53.0	64.5	0.27	0.97
	0.7	*ANN*	32.0	45.8	67.4	**0.31**	0.62
		ANN 10n	28.0	44.1	**67.7**	0.15	**0.06**
		LSM	**40.0**	**47.8**	66.2	0.27	*1.65*
		MOEA	0.0	43.8	66.9	*0.10*	0.30

CONCLUSIONS

This paper presents a preliminary investigation of surrogate-based optimization of truly reversible profile family for axial fans. The Multi-Objective Optimization Problem (MOOP) is based on the NSGA-II, an Evolutionary Algorithm able to find multiple Pareto-optimal solutions in one simulation run. The MOOP has been firstly solved by using the XFoil software as true function, avoiding the modelling and use of any SM. These results have been compared with those obtained by implementing different SMs in the MOOP, considering two different optimization frameworks, namely NEC and IFR.

The use of SMs to assist MOEAs is a complex matter which requires an exhaustive analysis of the entire optimization framework and how the SMs are embedded in the considered optimization algorithm.

This work has shown that, in this benchmark problem, an IFR approach has to be preferred to a NEC approach. A simple-level framework in which the MOEAs calculate the solutions only in the SMs has produced false Pareto-fronts in all the tested configurations. In particular, the NEC has proven several criticisms; even if both the considered SMs were satisfactory modelled according the selected metrics, the optimization has been not able to explore the entire design space in between the sampling points. The genetic algorithm led the optimizer to candidate solutions that were, during every iteration, more and more distant from the corresponding true value. This interpretation was suggested by the decreasing value of prediction capability during iterations, bringing to consider only unrealistic geometry and thick profiles.

An IFR approach has produced more reliable results, providing a good prediction capability during the iterations and, hence, reducing the distance between estimated and true Pareto fronts. The optimization was able to consider the entire design space, providing a geometry along the Pareto fronts similar to those experienced by the true function based optimization. The IFR method has required a more complex and computationally expensive optimization framework based on a bi-level approach, with the infill criterion based on the results of the GA.

An analysis of the ONVGR index have shown that, in most cases, the IFR-based optimization was able to produce better results (individuals) than the XFoil-based optimization.

Regarding the SMs used in this work (a LSM and ANN with different number of neurons) IFR results show the independence of the MOEA to the SM considered. This is considered an important outcome being a LSM easier and faster to model if compared to an ANN. From the other side, NEC approach results do not present any relevant differences between the two SMs, even though different prediction accuracies, estimated by the coefficient of determination, were reached.

The different reliability of the results obtained adopting a NEC and IFR approach, scales down the role and importance of the initial sampling in SMs based optimization. In fact, it is evident that a NEC approach is totally favourable to

exploitation, being, on the contrary, not able to correctly explore the design space. An IFR approach, which clearly involve an infill criterion, overcomes the difficulties and limitations related to the correct initial sampling creation, by iteratively adding optimized solutions evaluated with the true function to the initial sampling. This approach ensures a better balance between exploration and exploitation of the design space.

Results shown for the IFR approach demonstrated that, in the selected cases, a consistent reduction of MOOP computational cost is possible. In the specific case, according to the metric selected to judge the Pareto frontiers, the calls to the expensive objective function were reduced of 50% producing in all cases a reliable set of better solutions in comparison with the standard MOEA approach.

In conclusions, this preliminary study clarified the strong impact of the optimization framework on the reliability of the obtained Pareto fronts in a SM-based design optimization for an industrial fan benchmark problem. With an IFR approach, the use of the considered SMs can significantly reduce the computational time needed to solve the MOOP by reducing the call of the true function, while ensuring the creation of the same of even better Pareto fronts if compared to those obtained by using only the true function. Further work on this topic will be focused on the use of a different and decisively more time-consuming true function (as a CFD simulation) to overcome simplifying assumptions used in this preliminary work.

NOMENCLATURE

Acronyms

ANN	Artificial Neural Network
CCD	Central Composite Design
CCI	Central Composite Inscribed
CFD	Computational Fluid Dynamic
DFR	Direct Fitness Replacement
EAs	Evolutionary Algorithms
FNDS	Fast non dominated sorting algorithm
GAs	Genetic Algorithms
H	Dominated Space or Hyperarea
IFR	Indirect Fitness Replacement
MOEA	Multi-Objectives Evolutionary Algorithms
MOOPs	Multi-Objectives Optimization Problems
MS	Max Sum
NSGAII	Non-dominated sorting genetic algorithm
NEC	No Evolution Control
ONVGR	Overall Non-dominated Vector Generation Ratio
Q_t	Offspring population
OS	Overall Pareto Spread
P_C	Prediction capability
P_t	Initial population
PRS	Polynomial Response Surface
R_t	Global population
SMs	Surrogate Models
SP	Spacing

Latin

a, z	Synapse activity	[-]
AoA	Angle of attack	[deg]
C_D	Drag coefficient	[-]
C_L	Lift coefficient	[-]
C_{LS}	Specified lift coefficient	[-]
g	Aerofoil geometry	[-]
k	Neuron number	[-]
m	Number of predicted dependent variables	[-]
q	PRS associated error	[-]
Re	Reynolds number	[-]
s	PRS number of factors	[-]
W	Relative velocity	[m/s]
X	Neural network input	[-]
Y	Neural Network predicted output	[-]

Symbols

α	Stall margin	[-]
β	Flow angle	[deg]
γ	Aerofoil stagger	[deg]
ε	Aerodynamic efficiency	[-]
ζ	PRS regressors	[-]
θ	Deflection	[deg]
λ	Linear activation function	[-]
ν	Star point distance	[-]
σ	Sigmoid activation function	[-]

REFERENCES

1. G. Sheard and K. Daneshkhah, "The Conceptual Design of High Pressure Reversible Axial Tunnel Ventilation Fans," Advances in Acoustics and Vibration, vol. 2012, Article ID 562309, 11 pages, 2012. doi:10.1155/2012/562309

2. Bullock, R. O., and I. A. Johnsen. "Aerodynamic design of axial flow compressors." (1965).

3. Cory, William. Fans and ventilation: a practical guide. Elsevier, 2010.

4. Herrig, L. Joseph; Emery, James C.; Erwin, John R. Systematic two-dimensional cascade tests of NACA 65-series compressor blades at low speeds. 1957.

5. Lieblein, Seymour; Ackley, Richard H. Secondary flows in annular cascades and effects on flow in inlet guide vanes. 1951.

6. Marler, R. Timothy, and Jasbir S. Arora. "Survey of multi-objective optimization methods for engineering." Structural and multidisciplinary optimization 26.6 (2004): 369-395.

7. Forrester, Alexander IJ; Keane, Andy J. Recent advances in surrogate-based optimization. Progress in Aerospace Sciences, 2009, 45.1: 50-79.

8. Queipo, Nestor V., et al. Surrogate-based analysis and optimization. Progress in aerospace sciences, 2005, 41.1: 1-28.

9. Bamberger, Konrad; Carolus, Thomas. Performance Prediction of Axial Fans by CFD-Trained Meta-Models. Proc. ASME TurboExpo 2014, 2014.

10. Gonzalez, Luis F., et al. A generic framework for the design optimisation of multidisciplinary uav intelligent systems using evolutionary computing. In: Proceedings of the 44th AIAA Aerospace Sciences Meeting and Exhibit. 2006. p. 1-19.

11. Goel, Tushar, et al. Response surface approximation of Pareto optimal front in multi-objective optimization. Computer methods in applied mechanics and engineering, 2007, 196.4: 879-893.

12. Deb, Kalyanmoy, et al. "A fast and elitist multiobjective genetic algorithm: NSGA-II." IEEE transactions on evolutionary computation 6.2 (2002): 182-197.

13. Drela, Mark, and H. Youngren. 'X-Foil 6.96' Software December (2001).

14. Arias-Montano, Alfredo; Coello, Carlos A. Coello; Mezura-Montes, Efrén. Multi-objective airfoil shape optimization using a multiple-surrogate approach. In: Evolutionary Computation (CEC), 2012 IEEE Congress on. IEEE, 2012. p. 1-8.

15. Tenne, Yoel. Initial sampling methods in metamodel-assisted optimization. Engineering with Computers, 2015, 31.4: 661-680.

16. Jin, Ruichen; Chen, Wei; Sudjianto, Agus. An efficient algorithm for constructing optimal design of computer experiments. Journal of Statistical Planning and Inference, 2005, 134.1: 268-287.

17. Díaz-Manríquez, Alan, et al. A review of surrogate assisted multiobjective evolutionary algorithms. Computational intelligence and neuroscience, 2016, 2016.

18. Angelini, G., Bonanni, T., Corsini, A., Delibra, G., Tieghi, L., and Volponi, D. (2018). A Meta-Model for Aerodynamic Properties of a Reversible Profile in Cascade with Variable Stagger and Solidity. Proceedings of ASME Turbo Expo 2018.

19. Cardillo, Lucio, et al. "A numerical investigation into the aerodynamic effect of pressure pulses on a tunnel ventilation fan." Proceedings of the Institution of Mechanical Engineers, Part A: Journal of Power and

Energy 228.3 (2014): 285-299.Daly, B. B. Woods practical guide to fan engineering. Woods of Colchester Limited, 1978.

20. Drela, M. "An analysis and design system for low Reynolds number airfoil aerodynamics." Conference on Low Reynolds Number Airfoil Aerodynamics, University of Notre Dame. 1989.

21. Dixon, S. Larry, and Cesare Hall. Fluid mechanics and thermodynamics of turbomachinery. Butterworth-Heinemann, 2013.

22. Cencelli, N.A. (2006). Aerodynamic optimisation of a small-scale wind turbine blade for low windspeed conditions. Master's thesis, Stellenbosch: Stellenbosch University.

23. van der Spuy, S.J. and von Backström, T.W. (2015). An evaluation of simplified cfd models applied to perimeter fans in air-cooled steam condensers. Proceedings of the Institution of Mechanical Engineers, Part A: Journal of Power and Energy, vol. 229, no. 8, pp. 948_967.

24. Wang, G. Gary, and Songqing Shan. "Review of metamodeling techniques in support of engineering design optimization." Journal of Mechanical design129.4 (2007): 370-380.24

25. Wu, H.Y., Yang, S.C., Liu, F. and Tsai, H.M., 2003. Comparison of three geometric representations of airfoils for aerodynamic optimization, AIAA 2003-4095, 16th AIAA CFD Conference, June 23–26, Orlando, FL.(1)

26. Kulfan, Brenda M., and John E. Bussoletti. "Fundamental parametric geometry representations for aircraft component shapes." 11th AIAA/ISSMO multidisciplinary analysis and optimization conference. Vol. 1. sn, 2006.

27. Samareh, Jamshid A. "Survey of shape parameterization techniques for high-fidelity multidisciplinary shape optimization." AIAA journal 39.5 (2001): 877-884.

28. H. Sobieczky, Parametric airfoils and wings, Notes on Numerical Fluid Mechanics, vol. 68, Vieweg Verlag, Wiesbaden(1998), pp. 71-78

29. Schneider, Philip J. "An algorithm for automatically fitting digitized curves." Graphics gems. Academic Press Professional, Inc., 1990.

30. Giunta, Anthony A., et al. Noisy aerodynamic response and smooth approximations in HSCT design. In: Proc. 5-th AIAA/USAF/NASA/ISSMO Symp. on Multidisciplinary and Structural Optimization. 1994. p. 1117-1128.

31. Madsen, Jens I.; Shyy, Wei; Haftka, Raphael T. Response surface techniques for diffuser shape optimization. AIAA journal, 2000, 38.9: 1512-1518.

32. Montgomery, D.C. Design and Analysis of Experiments; John Wiley & Sons, Inc.: Hoboken, NJ, USA, 2001; p. 456.

33. Box, G.E.P.; Hunter, J.S.; Hunter, W.G. Statistics for Experimenters: Design, Innovation, and Discovery; Wiley-Interscience: Hoboken, NJ, USA, 2005; pp. 47, 455.

34. Jin, Ruichen; Chen, Wei; Simpson, Timothy W. Comparative studies of metamodelling techniques under multiple modelling criteria. Structural and multidisciplinary optimization, 2001, 23.1: 1-13.

35. Jin, Ruichen; Du, Xiaoping; Chen, Wei. The use of metamodeling techniques for optimization under uncertainty. Structural and Multidisciplinary Optimization, 2003, 25.2: 99-116.

36. Hagan, Martin T.; Demuth, Howard B.; Beale, M. H. Neural network design, 1996. Boston, PWS Pub, 1996.

37. Jin, Yaochu. A comprehensive survey of fitness approximation in evolutionary computation. Soft Computing-A Fusion of Foundations, Methodologies and Applications, 2005, 9.1: 3-12.

38. Adra, Salem Fawaz; Griffin, Ian; Fleming, Peter J. An informed convergence accelerator for evolutionary multiobjective optimiser. In: Proceedings of the 9th annual conference on Genetic and evolutionary computation. ACM, 2007. p. 734-740.

39. Choi, Seongim, Juan J. Alonso, and Hyoung S. Chung. "Design of a low-boom supersonic business jet using evolutionary algorithms and an adaptive unstructured mesh method." AIAA paper 1758 (2004): 2004.

40. Gonzalez, Luis F., et al. "A generic framework for the design optimisation of multidisciplinary uav intelligent systems using evolutionary computing." Proceedings of the 44th AIAA Aerospace Sciences Meeting and Exhibit. 2006.

41. Okabe, Tatsuya; Jin, Yaochu; Sendhoff, Bernhard. A critical survey of performance indices for multi-objective optimisation. In: Evolutionary Computation, 2003. CEC'03. The 2003 Congress on. IEEE, 2003. p. 878-885.

Bibliography

[1] G. Angelini, T. Bonanni, A. Corsini, G. Delibra, L. Tieghi, and D. Volponi, "A preliminary investigation on surrogate-based optimization of truly reversible profile family for axial fans", *Currently under review on: Journal of Power and Energy*,

[2] G. Angelini, T. Bonanni, A. Corsini, G. Delibra, L. Tieghi, and D. Volponi, "A metamodel for deviation in 2d cascade with variable stagger, solidity and reversible profiles", in *ASME Turbo Expo 2018: Turbomachinery Technical Conference and Exposition*, American Society of Mechanical Engineers, 2018.

[3] ——, "Effects of fan inflow distortion on heat exchange in air-cooled condenser. unsteady computations with synthetic blade mode", in *ASME Turbo Expo 2018: Turbomachinery Technical Conference and Exposition*, American Society of Mechanical Engineers, 2018.

[4] T. Bonanni, A. Corsini, G. Delibra, D. Volponi, A. G. Sheard, and M. Bublitz, "Design of a single stage variable pitch axial fan", in *ASME Turbo Expo 2017: Turbomachinery Technical Conference and Exposition*, American Society of Mechanical Engineers, 2017, V001T09A011–V001T09A011.

[5] G. Angelini, T. Bonanni, A. Corsini, G. Delibra, L. Tieghi, and D. Volponi, "Optimization of an axial fan for air cooled condensers", *Energy Procedia*, vol. 126, no. Supplement C, pp. 754 –761, 2017, ATI 2017 - 72nd Conference of the Italian Thermal Machines Engineering Association, ISSN: 1876-6102.

[6] T. Bonanni, A. Corsini, G. Delibra, D. Volponi, and A. G. Sheard, "Modelling of axial fan and anti-stall ring on a virtual test rig for air performance evaluation", in *ASME Turbo Expo 2016: Turbomachinery Technical Conference and Exposition*, American Society of Mechanical Engineers, 2016, V001T09A005–V001T09A005.

[7] T. Bonanni, L. Cardillo, A. Corsini, G. Delibra, A. G. Sheard, and D. Volponi, "Derivative design of axial fan range: From academia to industry", V006T07A006–V006T07A006, 2016.

[8] R. Lewis, *Turbomachinery performance analysis*. Butterworth-Heinemann, 1996.

[9] S. L. Dixon and C. Hall, *Fluid mechanics and thermodynamics of turbomachinery*. Butterworth-Heinemann, 2013.

[10] I. H. Abbott and A. E. Von Doenhoff, *Theory of wing sections, including a summary of airfoil data*. Courier Corporation, 1959.

[11] J. Bagley, N. Kirby, and P. Marcer, *A method of calculating the velocity distribution on annular aerofoils in incompressible flow*. Citeseer, 1961.

[12] S. Lieblein, "Aerodynamic design of axial-flow compressors. vi-experimental flow in two-dimensional cascades", 1955.

[13] A. Howell, "The present basis of axial flow compressor design.", 1942.

[14] J. Horlock, *Axial Flow Compressors-Fluid Mechanics and Thermodynamics*. Butterworth Scientific Publications, 1958.

[15] J. Vad, "Radial fluid migration and endwall blockage in axial flow rotors", 2010.

[16]   J Vad, "Radial fluid migration and endwall blockage in axial flow rotors", *Proceedings of the Institution of Mechanical Engineers, Part A: Journal of Power and Energy*, vol. 224, no. 3, pp. 399–417, 2010. DOI: 10.1243/09576509JPE832. eprint: https://doi.org/10.1243/09576509JPE832. [Online]. Available: https://doi.org/10.1243/09576509JPE832.

[17]   F. Szlivka and I. Molnár, "Measured and non-free vortex design results of axial flow fans", *Journal of mechanical science and technology*, vol. 22, no. 10, pp. 1902–1907, 2008.

[18]   B. Lakshminarayana, *Fluid dynamics and heat transfer of turbomachinery*. John Wiley & Sons, 1995.

[19]   R. Downie, M. Thompson, and R. Wallis, "An engineering approach to blade designs for low to medium pressure rise rotor-only axial fans", *Experimental thermal and fluid science*, vol. 6, no. 4, pp. 376–401, 1993.

[20]   A. Carter and H. P. Hughes, "A theoretical investigation into the effect of profile shape on the performance of aerofoils in cascade, r. & m. 2384", *British ARC*, 1946.

[21]   G. L. Mellor, "The aerodynamic performance of axial compressor cascades with application to machine design", PhD thesis, Massachusetts Institute of Technology, Department of Mechanical Engineering, 1957.

[22]   J. H. Horlock, "Actuator disk theory-discontinuities in thermo-fluid dynamics", *New York, McGraw-Hill International Book Co., 1978. 256 p.*, vol. 1, 1978.

[23]   A. J. Gannon and T. W. von Backstrom, "Comparison of streamline throughflow and streamline curvature methods", *International Journal of Turbo and Jet Engines*, vol. 17, no. 2, pp. 161–170, 2000.

[24]   J. R. Bredell, D. Kröger, and G. Thiart, "Numerical investigation of fan performance in a forced draft air-cooled steam condenser", *Applied Thermal Engineering*, vol. 26, no. 8, pp. 846–852, 2006.

[25]   K. A. Pericleous, M. Patel, *et al.*, "The modelling of tangential and axial agitators in chemical reactors", *Physicochemical hydrodynamics*, vol. 8, no. 2, pp. 105–123, 1987.

[26]   C. Meyer and D. Kröger, "Numerical simulation of the flow field in the vicinity of an axial flow fan", *International Journal for Numerical Methods in Fluids*, vol. 36, no. 8, pp. 947–969, 2001.

[27]   M. H. Vavra, "Aero-thermodynamics and flows in turbomachines", 1960.

[28]   H. G. Weller, G Tabor, H. Jasak, and C Fureby, "A tensorial approach to computational continuum mechanics using object-oriented techniques", *Computers in physics*, vol. 12, no. 6, pp. 620–631, 1998.

[29]   D. C. Montgomery, "Design and analysis of experiments, john wiley & sons", *New York*, pp. 64–65, 2001.

[30]   R. A. Fisher, *Statistical methods for research workers*. Genesis Publishing Pvt Ltd, 1925.

[31]   . W.K. B. Box G. E. P., "Experimental attainment of optimum conditions", *Journal of the Royal Statistical Society*, 1951.

[32]   G Taguchi and Y Wu, "Introduction to off-line quality control (nagaya, japan, central japan quality control association)", *TaguchiIntroduction to Off-Line Quality Control1980*, 1980.

[33]   S. Shan and G. G. Wang, "Survey of modeling and optimization strategies to solve high-dimensional design problems with computationally-expensive black-box functions", *Structural and Multidisciplinary Optimization*, vol. 41, no. 2, pp. 219–241, 2010.

[34]   T. J. Mitchell, "An algorithm for the construction of "d-optimal" experimental designs", *Technometrics*, vol. 16, no. 2, pp. 203–210, 1974.

[35]   A. A. Giunta, V. Balabanov, D. Haim, B. Grossman, W. H. Mason, L. T. Watson, and R. T. Haftka, "Multidisciplinary optimization of a supersonic transport using design of experiments theory and response surface modeling", 1997.

[36]   J. Sacks, W. J. Welch, T. J. Mitchell, and H. P. Wynn, "Design and analysis of computer experiments", *Statistical science*, pp. 409–423, 1989.

[37]   R. Jin, W. Chen, and T. W. Simpson, "Comparative studies of metamodelling techniques under multiple modelling criteria", *Structural and multidisciplinary optimization*, vol. 23, no. 1, pp. 1–13, 2001.

[38]   J. Koehler and A. Owen, "9 computer experiments", *Handbook of statistics*, vol. 13, pp. 261–308, 1996.

[39]   C. Currin, T. Mitchell, M. Morris, and D. Ylvisaker, "Bayesian prediction of deterministic functions, with applications to the design and analysis of computer experiments", *Journal of the American Statistical Association*, vol. 86, no. 416, pp. 953–963, 1991.

[40]   M. E. Johnson, L. M. Moore, and D. Ylvisaker, "Minimax and maximin distance designs", *Journal of statistical planning and inference*, vol. 26, no. 2, pp. 131–148, 1990.

[41]   A. B. Owen, "Orthogonal arrays for computer experiments, integration and visualization", *Statistica Sinica*, pp. 439–452, 1992.

[42]   A. S. Hedayat, N. J. A. Sloane, and J. Stufken, *Orthogonal arrays: theory and applications*. Springer Science & Business Media, 2012.

[43]   M. D. McKay, R. J. Beckman, and W. J. Conover, "A comparison of three methods for selecting values of input variables in the analysis of output from a computer code", *Technometrics*, vol. 42, no. 1, pp. 55–61, 2000.

[44]   R. L. Iman and W. Conover, "Small sample sensitivity analysis techniques for computer models. with an application to risk assessment", *Communications in statistics-theory and methods*, vol. 9, no. 17, pp. 1749–1842, 1980.

[45]   B. Tang, "Orthogonal array-based latin hypercubes", *Journal of the American statistical association*, vol. 88, no. 424, pp. 1392–1397, 1993.

[46]   J.-S. Park, "Optimal latin-hypercube designs for computer experiments", *Journal of statistical planning and inference*, vol. 39, no. 1, pp. 95–111, 1994.

[47]   Q. Y. Kenny, W. Li, and A. Sudjianto, "Algorithmic construction of optimal symmetric latin hypercube designs", *Journal of statistical planning and inference*, vol. 90, no. 1, pp. 145–159, 2000.

[48]   J. R. Kalagnanam and U. M. Diwekar, "An efficient sampling technique for off-line quality control", *Technometrics*, vol. 39, no. 3, pp. 308–319, 1997.

[49]   M. Meckesheimer, A. J. Booker, R. R. Barton, and T. W. Simpson, "Computationally inexpensive metamodel assessment strategies", *AIAA journal*, vol. 40, no. 10, pp. 2053–2060, 2002.

[50] K.-T. Fang, D. K. Lin, P. Winker, and Y. Zhang, "Uniform design: Theory and application", *Technometrics*, vol. 42, no. 3, pp. 237–248, 2000.

[51] T. W. Simpson, D. K. Lin, and W. Chen, "Sampling strategies for computer experiments: Design and analysis", *International Journal of Reliability and Applications*, vol. 2, no. 3, pp. 209–240, 2001.

[52] A. Díaz-Manríquez, G. Toscano, J. H. Barron-Zambrano, and E. Tello-Leal, "A review of surrogate assisted multiobjective evolutionary algorithms", *Computational intelligence and neuroscience*, vol. 2016, 2016.

[53] M. Papadrakakis, N. D. Lagaros, and Y. Tsompanakis, "Structural optimization using evolution strategies and neural networks", *Computer methods in applied mechanics and engineering*, vol. 156, no. 1, pp. 309–333, 1998.

[54] J. Gauss, "Combinationis observationum erroribus minimis obnoxiae", *Gottingen: University of Gottingen*, 1825.

[55] N. Cressie, "Spatial prediction and ordinary kriging", *Mathematical geology*, vol. 20, no. 4, pp. 405–421, 1988.

[56] S. M. Clarke, J. H. Griebsch, and T. W. Simpson, "Analysis of support vector regression for approximation of complex engineering analyses", *Journal of mechanical design*, vol. 127, no. 6, pp. 1077–1087, 2005.

[57] N. Dyn, D. Levin, and S. Rippa, "Numerical procedures for surface fitting of scattered data by radial functions", *SIAM Journal on Scientific and Statistical Computing*, vol. 7, no. 2, pp. 639–659, 1986.

[58] H. Fang and M. F. Horstemeyer, "Global response approximation with radial basis functions", *Engineering Optimization*, vol. 38, no. 04, pp. 407–424, 2006.

[59] R. H. Myers, D. C. Montgomery, and C. M. Anderson-Cook, *Response surface methodology: process and product optimization using designed experiments*. John Wiley & Sons, 2016.

[60] W. Oberkampf and T. Trucano, "Validation methodology in computational fluid dynamics", p. 2549, 2000.

[61] P. J. Roache, "Verification and validation in computational science and engineering", 1998.

[62] M. Meckesheimer, "A framework for metamodel-based design: Subsystem metamodel assessment and implementation issues", 2001.

[63] T. J. Mitchell and M. D. Morris, "Bayesian design and analysis of computer experiments: Two examples", *Statistica Sinica*, pp. 359–379, 1992.

[64] R. J. Brook and G. C. Arnold, *Applied regression analysis and experimental design*. Dekker New York; Basel, 1985.

[65] R. L. Mason, R. F. Gunst, and J. L. Hess, *Statistical design and analysis of experiments: with applications to engineering and science*. John Wiley & Sons, 2003, vol. 474.

[66] A.-S. Richard, "Model comparisons and r2.", *The American Statistician*, vol. 48, 1994.

[67] D. M. Allen, "The relationship between variable selection and data agumentation and a method for prediction", *Technometrics*, vol. 16, no. 1, pp. 125–127, 1974.

[68] C. P. Doncaster and A. J. Davey, *Analysis of variance and covariance: how to choose and construct models for the life sciences*. Cambridge University Press, 2007.

[69] E. E. Rojas Duran, "Staley, kent w. an introduction to the philosophy of science. cambridge introductions to philosophy. cambridge: Cambridge university press, 2014. 297 pp.", *ideas y valores*, vol. 66, no. 163, pp. 381–384, 2017.

[70] N. L. Johnson, A. W. Kemp, and S. Kotz, *Univariate discrete distributions*. John Wiley & Sons, 2005, vol. 444.

[71] R. L. Wasserstein and N. A. Lazar, *The asa's statement on p-values: Context, process, and purpose*, 2016.

[72] G. E. Box, J. S. Hunter, and W. G. Hunter, *Statistics for experimenters: design, innovation, and discovery*. Wiley-Interscience New York, 2005, vol. 2.

[73] J.-F. Barthelemy and R. T. Haftka, "Approximation concepts for optimum structural design—a review", *Structural optimization*, vol. 5, no. 3, pp. 129–144, 1993.

[74] R. T. Haftka, E. P. Scott, and J. R. Cruz, "Optimization and experiments: A survey", *Applied Mechanics Reviews*, vol. 51, no. 7, pp. 435–448, 1998.

[75] T. W. Simpson, J. Poplinski, P. N. Koch, and J. K. Allen, "Metamodels for computer-based engineering design: Survey and recommendations", *Engineering with computers*, vol. 17, no. 2, pp. 129–150, 2001.

[76] G. G. Wang and S. Shan, "Review of metamodeling techniques in support of engineering design optimization", *Journal of Mechanical design*, vol. 129, no. 4, pp. 370–380, 2007.

[77] C. M. Fonseca and P. J. Fleming, "An overview of evolutionary algorithms in multiobjective optimization", *Evolutionary computation*, vol. 3, no. 1, pp. 1–16, 1995.

[78] K. Deb and D. E. Goldberg, "An investigation of niche and species formation in genetic function optimization", in *Proceedings of the 3rd international conference on genetic algorithms*, Morgan Kaufmann Publishers Inc., 1989, pp. 42–50.

[79] C. M. Fonseca and P. J. Fleming, "Multiobjective optimization and multiple constraint handling with evolutionary algorithms. i. a unified formulation", *IEEE Transactions on Systems, Man, and Cybernetics-Part A: Systems and Humans*, vol. 28, no. 1, pp. 26–37, 1998.

[80] K. Deb, A. Pratap, S. Agarwal, and T. Meyarivan, "A fast and elitist multiobjective genetic algorithm: Nsga-ii", *IEEE transactions on evolutionary computation*, vol. 6, no. 2, pp. 182–197, 2002.

[81] K. Deb, *Multi-objective optimization using evolutionary algorithms*. John Wiley & Sons, 2001, vol. 16.

[82] C. M. Fonseca, P. J. Fleming, *et al.*, "Genetic algorithms for multiobjective optimization: Formulationdiscussion and generalization.", in *Icga*, vol. 93, 1993, pp. 416–423.

[83] J. Horn, N. Nafpliotis, and D. E. Goldberg, "A niched pareto genetic algorithm for multiobjective optimization", in *Evolutionary Computation, 1994. IEEE World Congress on Computational Intelligence., Proceedings of the First IEEE Conference on*, Ieee, 1994, pp. 82–87.

[84] N. Srinivas and K. Deb, "Muiltiobjective optimization using nondominated sorting in genetic algorithms", *Evolutionary computation*, vol. 2, no. 3, pp. 221–248, 1994.

[85] E. Zitzler and L. Thiele, "Multiobjective optimization using evolutionary algorithms—a comparative case study", in *international conference on parallel problem solving from nature*, Springer, 1998, pp. 292–301.

[86] A. I. Forrester and A. J. Keane, "Recent advances in surrogate-based optimiza-tion", *Progress in Aerospace Sciences*, vol. 45, no. 1, pp. 50–79, 2009.

[87] N. V. Queipo, R. T. Haftka, W. Shyy, T. Goel, R. Vaidyanathan, and P. K. Tucker, "Surrogate-based analysis and optimization", *Progress in aerospace sciences*, vol. 41, no. 1, pp. 1–28, 2005.

[88] K. Bamberger and T. Carolus, "Performance prediction of axial fans by cfd-trained meta-models", *Proc. ASME TurboExpo 2014*, 2014.

[89] L. F. Gonzalez, J. Periaux, K. Srinivas, and E. J. Whitney, "A generic framework for the design optimisation of multidisciplinary uav intelligent systems using evo-lutionary computing", in *Proceedings of the 44th AIAA Aerospace Sciences Meet-ing and Exhibit*, 2006, pp. 1–19.

[90] T. Goel, R. Vaidyanathan, R. T. Haftka, W. Shyy, N. V. Queipo, and K. Tucker, "Response surface approximation of pareto optimal front in multi-objective op-timization", *Computer methods in applied mechanics and engineering*, vol. 196, no. 4, pp. 879–893, 2007.

[91] D. R. Jones, "A taxonomy of global optimization methods based on response surfaces", *Journal of global optimization*, vol. 21, no. 4, pp. 345–383, 2001.

[92] C. A. C. Coello, G. B. Lamont, D. A. Van Veldhuizen, *et al.*, *Evolutionary algo-rithms for solving multi-objective problems*. Springer, 2007, vol. 5.

[93] L. V. Santana-Quintero, A. A. Montano, and C. A. C. Coello, "A review of tech-niques for handling expensive functions in evolutionary multi-objective optimiza-tion", in *Computational intelligence in expensive optimization problems*, Springer, 2010, pp. 29–59.

[94] R. Landa-Becerra, L. V. Santana-Quintero, and C. A. C. Coello, "Knowledge in-corporation in multi-objective evolutionary algorithms", in *Multi-Objective Evo-lutionary Algorithms for Knowledge Discovery from Databases*, Springer, 2008, pp. 23–46.

[95] Y. Jin, "A comprehensive survey of fitness approximation in evolutionary com-putation", *Soft Computing-A Fusion of Foundations, Methodologies and Applica-tions*, vol. 9, no. 1, pp. 3–12, 2005.

[96] L Shi and K Rasheed, "A survey of fitness approximation methods applied in evolutionary algorithms", *Computational intelligence in expensive optimization problems*, pp. 3–28, 2010.

[97] S. F. Adra, I. Griffin, and P. J. Fleming, "An informed convergence accelerator for evolutionary multiobjective optimiser", in *Proceedings of the 9th annual confer-ence on Genetic and evolutionary computation*, ACM, 2007, pp. 734–740.

[98] A. Arias-Montano, C. A. C. Coello, and E. Mezura-Montes, "Multi-objective air-foil shape optimization using a multiple-surrogate approach", in *Evolutionary Computation (CEC), 2012 IEEE Congress on*, IEEE, 2012, pp. 1–8.

[99] Y. Tenne, "Initial sampling methods in metamodel-assisted optimization", *Engi-neering with Computers*, vol. 31, no. 4, pp. 661–680, 2015.

[100] D. Buche, N. N. Schraudolph, and P. Koumoutsakos, "Accelerating evolutionary algorithms with gaussian process fitness function models", *IEEE Transactions on Systems, Man, and Cybernetics, Part C (Applications and Reviews)*, vol. 35, no. 2, pp. 183–194, 2005.

[101]   R. Jin, W. Chen, and A. Sudjianto, "An efficient algorithm for constructing optimal design of computer experiments", *Journal of Statistical Planning and Inference*, vol. 134, no. 1, pp. 268–287, 2005.